This is a peer-reviewed, author's accepted manuscript of the following research article:
Mularski, J., & Li, J. (2023). A review on biomass ignition: fundamental characteristics, measurements, and predictions. Fuel, 340, [127526].
https://doi.org/10.1016/j.fuel.2023.127526

A review on biomass ignition: Fundamental characteristics, measurements, and predictions

Jakub Mularski [a] *, Jun Li [b] *

[a] Faculty of Mechanical and Power Engineering, Wrocław University of Science and Technology, Wybrzeże Wyspiańskiego 27, 50-370, Poland

[b] Department of Chemical & Process Engineering, University of Strathclyde, James Weir Building, 75 Montrose Street, Glasgow, G1 1XJ, UK

* Corresponding authors

phone: +48 71 3204152 (J. Mularski), +44 (0) 141 5482393 (J. Li)

e-mail addresses: jakub.mularski@pwr.edu.pl, jun.li@strath.ac.uk

Abstract

Exploiting biomass energy is a promising option to reduce CO_2 emissions, owing to its renewability and carbon neutrality. The knowledge of biomass ignition becomes critical for processing fuels with regard to safety control and optimizing their combustion processes. Although there are many papers published in the field that investigate biomass combustion, less research effort was made to focus on the ignition behavior of biomass during the combustion processes. Therefore, this review work aims to investigate in detail the ignition characteristics of biomass dust fuels focusing on the

most critical fuel properties and operating reactor conditions that affect ignition delay and ignition mode. The review also covers biomass combustion modeling methods focusing on the capabilities, similarities, and major drawbacks of the models in terms of ignition prediction.

Highlights:

- The state-of-the-art biomass ignition research is presented.
- Numerical methods for predictions of biomass ignition behavior are summarized.
- Biomass ignition was found to be mainly measured by CH* chemiluminescence.
- CH and OH species used as ignition indicators yielded most exact numerical results.
- Unification of experimental and numerical ignition onset criteria is proposed.

Keywords: Biomass, Ignition, Modeling, Combustion

List of abbreviations

3PM	Three-parallel reaction
C2SM	Competing two-step reaction mechanism
CBK	Carbon burnout kinetics
CBK/E	Carbon burnout kinetics for oxidation
CBK/G	Carbon burnout kinetics for gasification
CCD	Charged-coupled device

CFD	Computational fluid dynamics
CPD	Chemical percolation devolatilization
DAE	Distributed activation energy
DAF	Dry-ash-free
DNS	Direct numerical simulation
DTF	Drop tube furnace
EDC	Eddy dissipation concept
EDM	Eddy dissipation model
FG-DVC	Functional-group, depolymerization, vaporization, and cross-linking model
FPV	Flamelet/progress variable
LES	Large eddy simulation
PDF	Probability density function
PLIF	Planar laser-induced fluorescence
RANS	Reynolds averaged Navier-Stokes
SFOR	Single-step first-order
SLR	Steady laminar flamelet
TCI	Turbulence-chemistry interaction
TGA	Thermogravimetric analyzer
TGA-DSC	thermogravimetric differential scanning calorimetry

Table of contents

1. Introduction

The recent 26th UN Climate Change Conference in Glasgow (COP26) in 2021 has emphasized the original expectations of the Paris Agreement and the global warming limit to 1.5ºC. The driving actions should consider reducing emissions, helping those already impacted by climate change, and enabling countries to deliver on their climate goals. Biomass combustion, in the context of the current world energy crisis and constantly increasing CO_2 constraints, is considered a near-term and low-cost method to reduce carbon emission and increase renewable energy capacity. Recent reports [1] indicate an increasing trend in total bioenergy subsidies across most of the European countries. However, due to specific fuel properties, biomass exhibits different features in terms of fuel handling and processing, and combustion behavior in comparison to coal [2]. For example, the high moisture content in biomass [3] and its fibrous structure typically require more energy for drying and milling, resulting in a decreased conversion efficiency. For instance, for biomass materials with a moisture content of 5-7%, the grinding energy was reported as eight times lower than that with a moisture content of 30% [4]. To address this, a promising solution may be thermal pre-treatment, such as torrefaction, which not only improves biomass grindability [5], but can positively affect the ignition characteristics [6].

From the environmental point of view, replacing coal with biomass as the fuel in combustion furnaces allows for reducing emissions not only of CO_2, but also of SO_x and NO_x, as reported by Demirbas [7], Zhang et al. [8], and Kuo and Wu [9]. Biomass is also characterized by relatively high oxygen and volatile contents [3], resulting in its combustion involving complicated cleavages of a large number of oxygen bonds that could significantly destabilize char oxidation and thus lower the ignition temperature. Another extremely important aspect is biomass fire safety at stages including transport,

storage, and operation which can be related to the risk of self-heating that can develop further to ignition. Biomass fuels tend to exhibit a very high inclination toward self-ignition [10–12].

Ignition, which is generally observed as the process that initiates combustion, has a strong impact on the flame characteristics, such as the flame stability, flame structure, and flame extinction, but also pollutant formation with the consequent impact on the reactor operation, energy efficiency, and emissions. Ignition of biomass fuels is also a result of complex interaction mechanisms which include particle heating, drying, devolatilization, gas-phase oxidation, heterogeneous oxidation, and transport phenomena [13]. Three general ignition modes can be attributed to fuels including biomass: (a) homogeneous ignition, where volatile matters around the particle ignite and a flame envelope is formed. The formed flame prevents oxygen from reaching the particle surface. Therefore, char combustion takes place either at the later phase of devolatilization or afterward; (b) heterogeneous ignition where the fuel particle ignites and is directly exposed to oxygen. Such an ignition can occur under very high heating rates and for small particle sizes, where particle temperature reaches the ignition temperature in the very earliest stage of devolatilization where only a small amount of volatile matter has devolatilized or even before devolatilization. In such a case, the solid is the whole biomass, not just char, and the surface reaction removes the material that would be otherwise devolatilized. One can also observe a transient heterogeneous mechanism which can shift to homogeneous mode due to the increased devolatilization rate, and (c) the ignition process takes place simultaneously at the particle surface and in the surrounding gas. It is referred to as hetero-homogeneous ignition. In particular, biomass, due to the high volatile content, is highly sensitive to the devolatilization and subsequent volatiles combustion in the surrounding gas which

119 makes these sub-mechanisms much more dominant in the biomass
120 ignition/combustion behavior. The characterization of biomass ignition is complicated,
121 similar to coal ignition features, because the ignition parameters, such as the ignition
122 temperature or ignition delay, are not fundamental fuel parameters, but instead, they
123 are highly dependent on the fuel properties and operating conditions.

124 The knowledge of biomass ignition becomes critical in fuel processing with respect
125 to safety issues, potential co-firing, reactor operation, pollutant formation, and most
126 importantly, process efficiency. However, much less research effort was made to focus
127 on the biomass ignition behavior. There is still no common consensus regarding the
128 fundamental criteria on how to calculate the ignition onset and the published literature
129 is not definitive in this matter. Some research efforts have attempted to investigate
130 biomass ignition by determining the effect of specific biomass components, such as
131 cellulose, hemicellulose, and lignin content [14]. For a realistic representation of
132 biomass in numerical models that can effectively predict ignition properties, it is also
133 important to consider the biomass fibrous structure as a fundamental step toward the
134 reliable classification of biomass fuels in terms of ignition characteristics.

135 The aim of this review is to summarize the latest developments in biomass dust
136 ignition behavior along with the subsequent combustion process. A particular
137 emphasis is laid on the commonly applied modeling techniques, and the feasibility of
138 the models in terms of ignition prediction will be subjected to critical analysis. As the
139 biomass dust ignition is not extensively reported in the literature and the research
140 related to biomass fuels of larger sizes is almost unavailable, it is thus important to
141 analyze the potential use of modelling approaches developed for coal ignitions for
142 studying biomass ignitions, especially defining the similarities and differences between
143 coal and biomass ignition modeling.

2. Biomass ignition with combustion

Ignition can be perceived as an offshoot of the combustion governing mechanisms [15]. Fig. 1 illustrates the general relationship between biomass combustion steps and ignition. An initial description of physical mechanisms that occur during biomass combustion, such as drying, devolatilization or char combustion is essential from the ignition perspective as the dynamics of these processes directly impact the biomass ignition behavior. The distinctive biomass structure, particle morphology, different physical and thermochemical properties, and reactor operating conditions have a direct impact on the time scale and strength of the aforementioned combustion steps. The ignition occurrence can be estimated by applying specific determination methods of ignition onset which are also depicted in Fig. 1. The literature review has indicated that these methods are widely used both in biomass and coal studies with satisfactory results. Judging by Fig. 1 it is also evident that, apart from ignition criteria, a proper description of the main combustion mechanisms will also be crucial in the accurate estimation of ignition delay as these mechanisms provide the key information of both the evolution of gas species with respect to time and space (e.g. CH, OH, CO/CO_2) and the reaction rate of the given combustion step. Figure 1 clearly illustrates that the ignition may occur during volatile matter combustion, or even before the start of devolatilization.

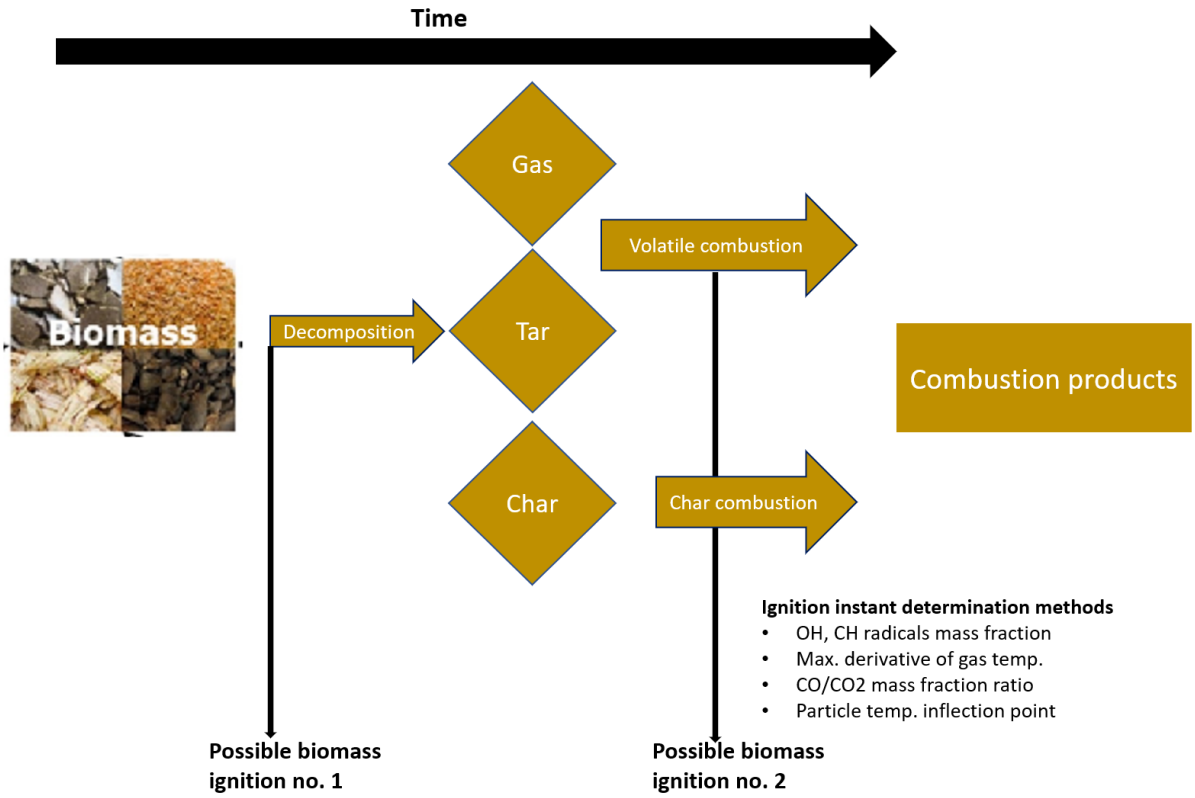

Fig. 1 Relationship between biomass conversion and ignition.

The first important combustion stage when a biomass particle is subjected to high-temperature conditions is drying. Drying is a complex, multiphase process that combines three phases: gas (vapor), liquid (water), and solid through which water and gas migrate to the surface. The process is also strongly dependent on the operating reactor pressure. The amount of biomass moisture depends on the biomass source, storage conditions, and pretreatment. Because of the high biomass moisture content, it is an important step during solid fuel conversion which reduces the gas temperature, affecting the initial particle heating rate [16] and, eventually, ignition. For example, for particle sizes of 230 μm, the drying time was found to be the controlling parameter in the ignition delay time [17] indicating an overlap between drying and devolatilization.

Pyrolysis [18–25] is the next key stage in biomass combustion. It is a breakdown of the structure of main biomass components in the absence of oxygen. The main

177 products are gas species, bio-oil or tar, and fixed carbon. Typically, raw biomass
178 consists of 40-50% cellulose, 25-35% hemicellulose, and 15-30% lignin with some
179 amount of extractives. Hemicellulose decomposes mainly between 220-315^{o}C,
180 cellulose between 315-400^{o}C, whereas lignin has rigid structures resistant to thermal
181 decomposition and it pyrolyzes over a wide range of temperatures (160-900^{o}C) [26].
182 Moreover, strong interactions during decomposition between the components are
183 reported [26]. The process is also extremely sensitive to the particle size, heating rate,
184 and furnace temperature. While at low heating rates, more char is produced, at higher
185 heating rates, depolymerization of biomass compounds to permanent gases and tars
186 is enhanced [27]. The released volatile matter during pyrolysis subsequently reacts
187 with oxygen in the form of homogeneous combustion. The dynamics of the volatile
188 matter release and the instantaneous gas yield with its composition have an enormous
189 impact on the ignition characteristics. As a result of pyrolysis, a char layer is formed
190 that may further react with oxygen in the form of heterogeneous combustion. Char
191 conversion is the final stage of biomass thermochemical conversion. The overall
192 reaction rate depends on the following processes:

193 • Transport of reaction agents from the bulk phase to the particle surface through
194 the boundary layer (film diffusion). The structure of the boundary layer depends
195 on the flow conditions. In the study of Richter et al. [28], it was found that the
196 Stefan flow substantially affects the boundary layer thickness. Concentration
197 gradients of reactive gases can be mostly observed in the boundary layer.
198 • Ash layer diffusion
199 • Transport of reaction agents inside the char porous structure
200 • Intrinsic kinetics which is not influenced by transport processes

Based on which process controls the reaction rate, three regimes can be distinguished for char combustion. Zone I where chemical reactions limit the particle mass loss, Zone II where chemical reactions and pore diffusion effects are equally important, and Zone III where mass loss is governed by oxygen diffusion to the particle surface.

During the combustion process, the biomass particle morphology undergoes substantial changes. The release of moisture and volatiles cause the pores and voids inside the particle to grow and the mass loss and structural reordering can result in the particle swelling or shrinkage. The evolving volatile matter consisting of light hydrocarbons, tars, and permanent gases surrounds the particle surface. Subsequent char reacts differently depending on the temperature conditions. In Regime I, there is an unlimited penetration of char inside by gaseous reagent as kinetics limit the reaction rate and therefore it changes its density with a constant size. In Regime II, both diameter and density decrease, whereas in regime III, the char particle shrinks at a constant density. For example, in the study of Meesri and Moghtaderi [29] where pine sawdust particles were burned in DTF at 1473K, char oxidation reactions occurred in Regime II. Biomass particles may also undergo fragmentation due to collisions, thermal stresses, particle shrinkage, local pressure changes, or loss of structural integrity. This may also affect the combustion behavior as one obtains smaller particles due to fracture. Fragmentation was also found to be important for the char oxidation stage [30]. Figure 2 illustrates the mass loss which can represent the main stages of biomass dust combustion. One can observe that there is a slight overlap between the combustion steps indicating that the processes occur almost sequentially. Moreover, based on the mass loss rate and the time scale of the illustrated stages, it is expected that devolatilization dynamics will affect the biomass ignition characteristics most significantly.

226 The above Section 2 makes one aware of the complexity and the existing
227 interrelations between biomass properties and the reactor operating conditions that
228 overall impact the occurrence of ignition, and these interrelations should be accurately
229 accounted for in the state-of-the-art biomass models. In fact, a reliable classification of
230 biomass fuels in terms of ignition characteristics requires the application of both
231 experimental and numerical methods. Therefore, as part of this review, Section 3
232 investigates the most recently used experimental techniques in biomass ignition
233 studies, whereas Section 4 describes in detail the governing models for the main
234 combustion stages along with their capabilities in ignition prediction.

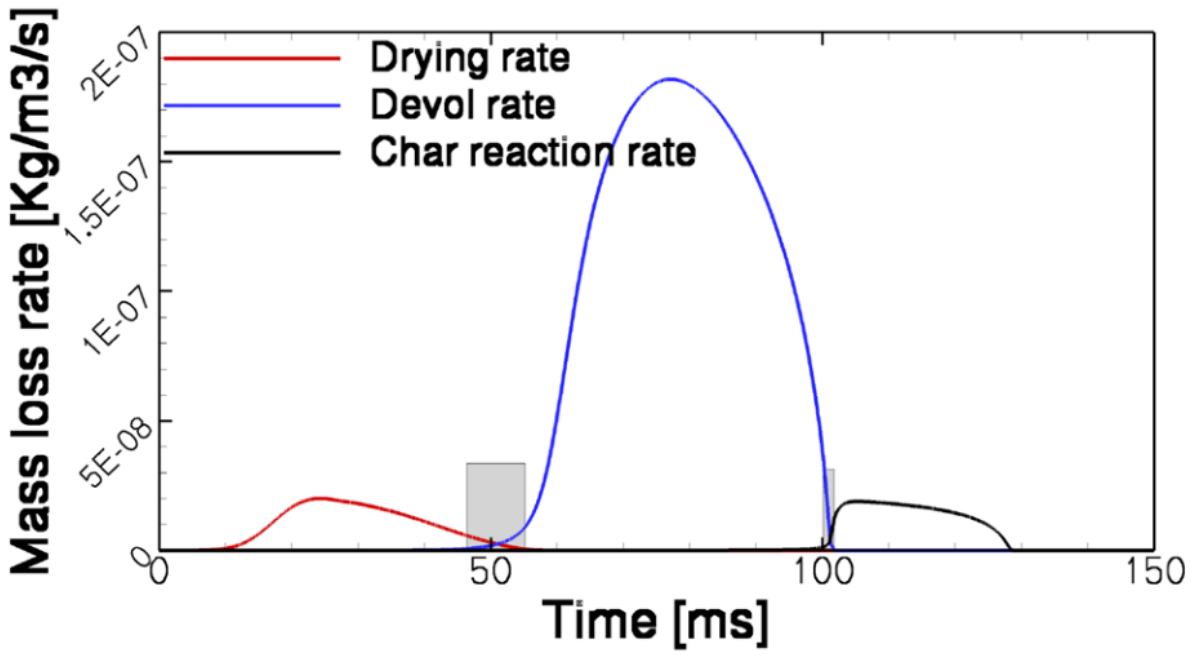

235

236 Fig. 2 Mass loss of 250 μm biomass particle in oxidizing environment. Reprinted with
237 permission from [31].

238 **3. Ignition**

239 Ignition is a critical step of transition from a slow reaction to a high-temperature
240 fast reaction. It is a process of interaction between heat release, heat loss, heat and
241 mass transfer, and chemical kinetics. Fundamental ignition combustion theory [32] has

been mostly derived from experimentally measured ignition properties, which can be further applied to predict ignition characteristics through numerical modelling, where analytical solutions are available.

3.1 Experimental methods of ignition onset determination

From an experimental point of view, the ignition delay definition is ambiguous and strongly depends on the measurement techniques and experimental accuracy. An overview of biomass fuel particle ignition measurement techniques encountered in the literature is summarized in Table 1.

Table 1. Reported biomass particle ignition measurement techniques

Ignition onset indicator	Optical equipment	Operating conditions set for measurements				Ref.
		Fuel type	Particle feeding rate	Atmosphere	Flow conditions	
CH^* emission	ICCD	Biomass, coal	Single particle scale	O_2/N_2 and O_2/CO_2	Laminar, Hencken burner	[33]
CH^* emission	ICCD	Biomass	Single particle scale	CH_4/Air	Laminar, McKenna burner	[34,35]
Onset of luminous combustion	High-speed cinematography	Biomass with coal	Single particle scale	O_2/N_2 and O_2/CO_2	Laminar, Drop tube furnace	[36–38]
12% of max. luminosity	High-speed imaging	Biomass with coal	1.2g/min	Air	Laminar, Drop tube furnace	[39]
10% of max. luminosity	High-speed imaging	Biomass with coal	Single particle scale	$CH_4/O_2/N_2$,O_2 – 3.5, 5.1, 6.5%	Laminar, McKenna burner	[40]

As shown in Table 1, there are scarce publications that investigate experimentally biomass ignition. It is mainly measured through the chemiluminescence of excited CH^* radicals although high-speed imaging was also investigated in some publications,

where using the fraction of maximum visible light served as an ignition indicator.

Köser et al. [41,42] emphasized that the CH^*- chemiluminescence signal, which can be utilized as an indicator of ignition, was found to be a better indicator than blackbody emission from soot or hot char [43]. However, the CH^* signal is considered weak and has a strong spectral overlap with broadband blackbody emission. For example, it is possible that CO_2^* chemiluminescent emission, obtained from CO oxidation may extend over a broad spectral range and overlap the CH^* emission line [44]. To address this technical challenge, a multi-filter methodology, first suggested by Karnani et al. [45], has been recently extended by Yuan et al. for the application of obtaining pure CH^* signal in coal combustion [46]. However, although CH^* or OH^* emission products may provide reliable and accurate ignition characteristics [34], they are extremely difficult to be compared with numerical models where the excited species are not available [47]. Lately, a high-speed OH planar laser-induced fluorescence (PLIF) method was used, but in coal combustion research [41,42,48,49]. This technique allows obtaining pure CH or OH radicals, also exempting the interference in sooting flames [41]. Spatial distributions of relative OH-LIF signals can be more easily compared with simulations by locating the zones of the reactions [42]. In the study of Köser et al. [42], the goal was to record OH-fluorescence, while suppressing the impact of flame luminosity and OH^*- chemiluminescence. This technique is recommended for biomass ignition research as it would allow a direct confrontation of experimental data with numerical results based on non-excited species, such as CH or OH radicals.

3.2 Experimental determination of ignition mechanisms

Because of the impact of ignition on the combustion efficiency and reactors stability, it is critical to identify different ignition steps and the early stages of biomass particle combustion and to distinguish the most important factors affecting the ignition

mechanism. So far, research attempts have been made to use high-speed imaging techniques to capture either the visible light signal of single particle ignition [21,38,40,50] or chemiluminescence emission [43,46] of diluted particle streams. In high-speed imaging techniques where visible light is captured, a homogeneous ignition is typically defined as the time at which the first flash of volatile is observed near the particle boundary layer, whereas heterogeneous ignition considers the instant at which bright flame and strong luminance are observed on the biomass particle. The observation of spontaneous emission is an effective way to investigate the release of different species which also can provide detailed information about the ignition characteristics. For example, temporally resolved CH* chemiluminescence images with corresponding signal intensity profiles, apart from being an accurate ignition indicator, were also utilized in the determination of ignition mode where local signal minima reasonably differentiated specific combustion stages [33–35].

Simões et al. [40] investigated the effect of temperature and oxygen concentration on the ignition behavior of different pulverized biomass fuels. A high-speed imaging system was applied to record the image of single particles in a laminar flame burner where ignition delay was defined with a criterion of 15% of the maximum signal intensity – Fig. 3a. Fig. 3b depicts the gas-phase ignition of kiwi branches particles with the key combustion steps illustrated in the sub-figures, such as initial heating, ignition, volatiles cloud burning and char oxidation indicating a dual ignition mode with homogeneous ignition followed by the heterogeneous char oxidation. Fig. 3c illustrates the surface ignition of elongated vine branch particles with no visible volatile cloud indicating that burning occurred in one heterogeneous phase. The ignition mode was identified to strongly correspond with biomass shape and size. The surface temperature was found to be a more dominant parameter in the occurrence of a

heterogeneous ignition mode than the volatile matter content as the volatile matter content of kiwi branches and vine branches was almost the same. Very high surface temperatures result in very fast heating rates increasing the particle temperature that induce surface ignition before any substantial amount of volatile matter is released.

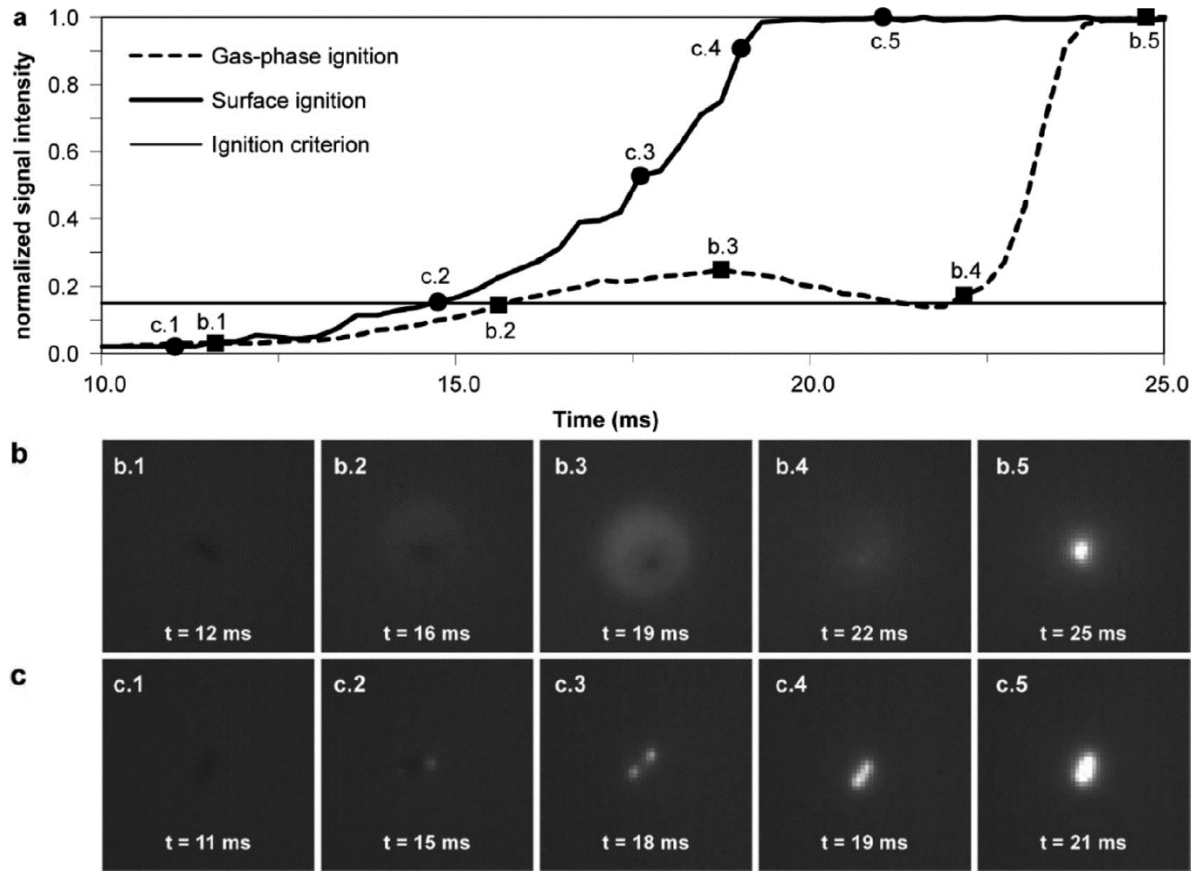

Fig. 3 Signal intensity profiles and images of ignition process. (a) maximum visible light signal intensity , (b) gas-phase ignition of a particle kiwi branches, (c) surface ignition of a particle vine branches. Particle sizes: 212-224 μm. Reprinted with permission from [40].

Magalhães et al. [51] compared the ignition behaviors of different biomass fuels at low and high heating rates. Fig. 4 illustrates the frames of typical combustion events for the investigated fuels under high heating rate conditions. Fig. 4b and Fig. 4d show the surface ignition of small size almond shell and olive residue particles. Fig. 4c and

Fig. 4e illustrate the gas-phase ignition of larger size almond shell and olive residue particles. In Fig. 4e, where the gas-phase ignition occurs, one can clearly observe that sub-figure e.1 corresponds to the initial heat-up stage, sub-figure e.2 illustrates the ignition onset, sub-figure e.3 depicts the maximum visible light during the combustion of volatiles, sub-figure e.4 indicates the last phase of volatiles combustion and sub-figure e.5 illustrates char oxidation. For Fig. 4b and Fig. 4d, it is not possible to clearly differentiate between the combustion stages, and due to intense char oxidation luminosity which worsens the visibility, it is hard to identify if it is a heterogeneous or hetero-homogeneous ignition mode. It indicates that, in some situations, high-speed imaging may be inconclusive in the determination of the ignition mechanism.

Under low heating rate conditions, the fuels were investigated in TGA. The ignition mode was determined based on the procedure applied by Chen et al. [52]. Eventually, both biomass fuels ignited homogeneously. Under high heating rate conditions, smaller biomass particles (80-90 μm) tended to ignite heterogeneously, while larger particles (224-250 μm) tended to ignite homogeneously.

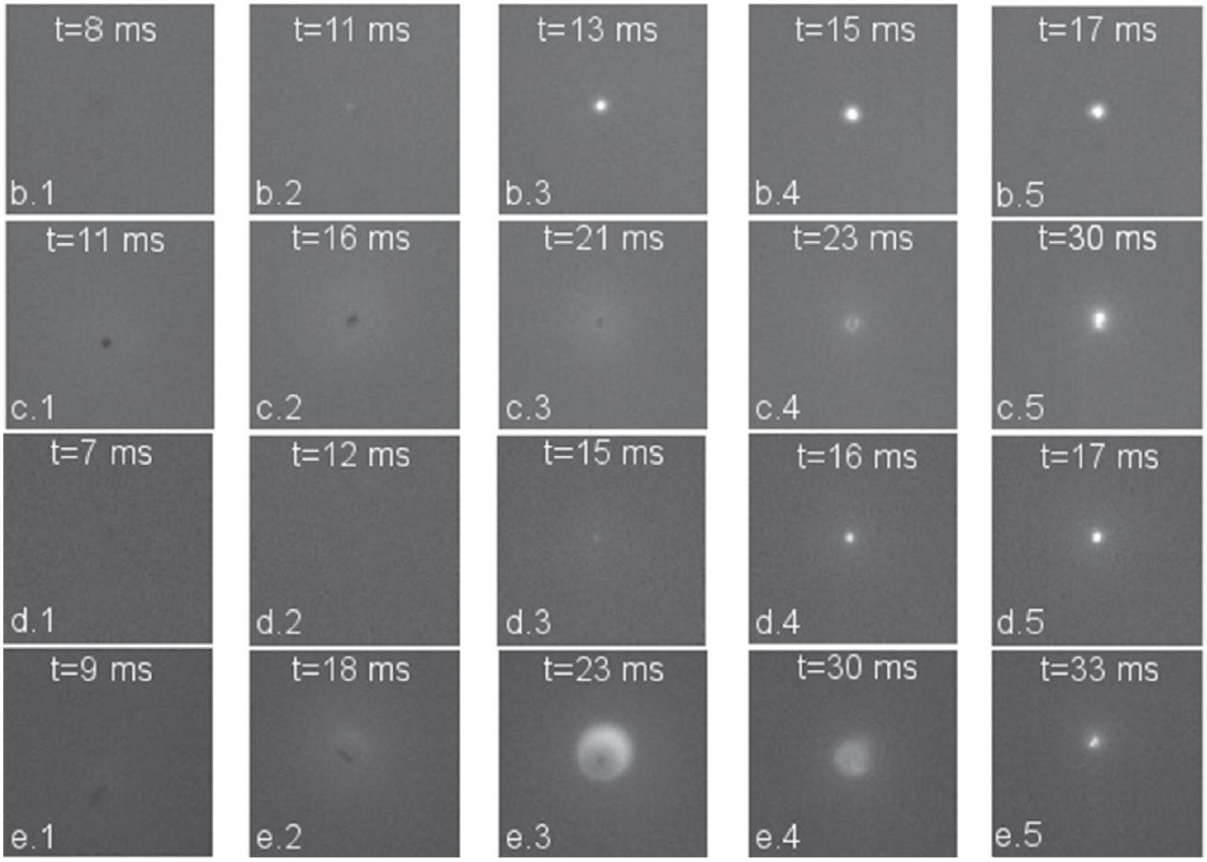

Fig. 4. Ignition events during entrained flow reactor experiments. (b) surface ignition of almond shell particle with size of 80-90 μm, (c) gas-phase ignition of almond shell particle with size of 224-250 μm, (d) surface ignition of olive residue with size of 80-90 μm, (e) gas-phase ignition of olive residue particle with size of 224-250 μm. Reprinted with permission from [51].

Magalhães et al. [53] investigated combustion behaviors of single raw and torrefied biomass particles in a drop tube furnace (DTF) at 1400K using high-speed cinematography. The fuels were sieved to a size 212-300 μm. It was reported that all biomass fuels (raw and torrefied) ignited homogeneously forming large and circular volatile matter envelope flames, followed by a char combustion phase indicating a dual ignition mode. The released volatile matter ignited first, while the devolatilizing particle still remained dark at the envelope flame center. Non-overlapping effect of the volatile matter combustion and char combustion was observed. This effect could be attributed

to the low aspect ratio of biomass particles.

Weng et al. [17,35] applied an ICCD camera with different band filters – 430, 515, 589, and 766 nm to capture the chemiluminescence from CH*, C_2*, Na*, and K*, respectively. The research was carried out for pulverized single biomass particles in a flat flame McKenna burner. Eventually, the reported information was used to identify the homogeneous ignition, volatile combustion, and alkali species release. The CH* and thermal radiation signals also indicated that all studied biomass char particles underwent heterogeneous oxidation at or immediately after the extinction of volatile matter combustion. For one fuel out of four, there was a slight overlap between the two stages.

Qi et al. [33] studied the ignition and combustion of single pulverized biomass and coal particles in N_2/O_2 and CO_2/O_2 atmospheres in a Hencken burner. Fig. 5 illustrates CH* chemiluminescence images and signal intensity profiles for wheat straw (WS) and corn straw (CS). One can observe a spherical flame surrounding the CS particle between 12 and 20 ms. The figure actually indicates that both biomass fuels (CS) and (WS) undergo similar ignition and combustion processes. They ignite homogeneously and devolatilize rapidly. The local minimum at 25-30ms in Fig. 5b and the less pronounced intensity image from Fig. 5a suggest the end of intense volatile matter combustion and the beginning of char heterogeneous oxidation.

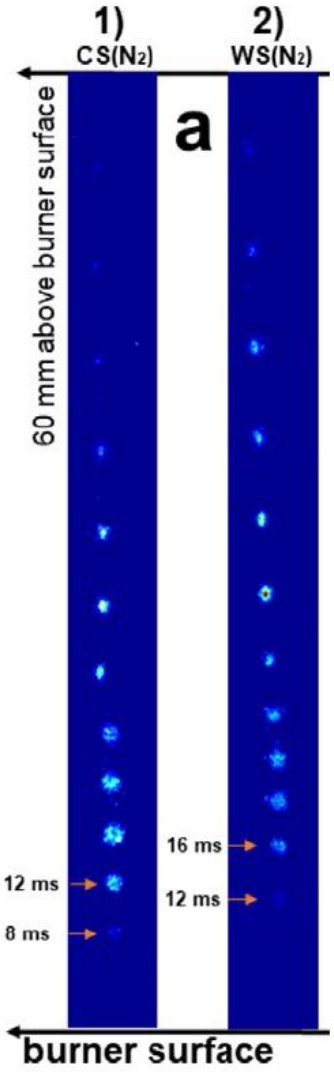
1)
CS(N2)
2)
WS(N2)
a
60 mm above burner surface
16 ms
12 ms
12 ms
8 ms
burner surface

367

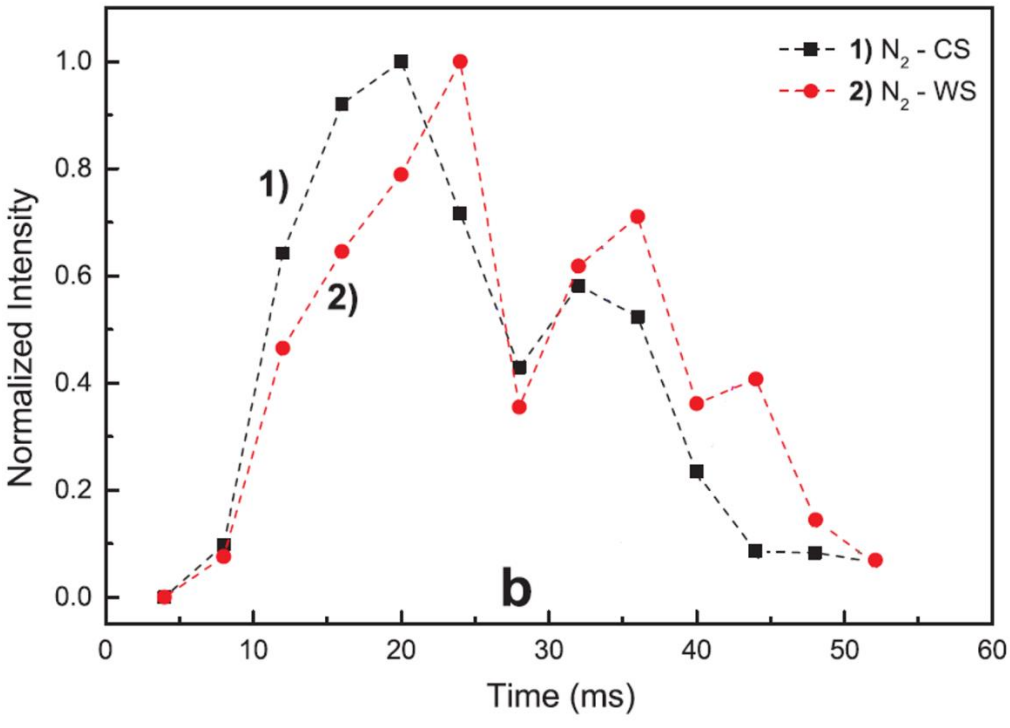
1) N2 - CS
2) N2 - WS
1)
2)
b
Normalized Intensity
Time (ms)
0.0
0.2
0.4
0.6
0.8
1.0
0
10
20
30
40
50
60

368

Fig. 5 (a) chemiluminescence images of single biomass particles in N_2/O_2 atmosphere, (b) normalized CH* signal intensity profile in N_2/O_2 atmosphere. Adapted from [33].

3.3 Impact of fuel properties and operating conditions on ignition

It must be emphasized that, as regards the ignition delay time (i.e. ignition onset), there are different determination methods as aforementioned. The lack of a commonly accepted method makes any direct comparisons of the results from works defining the onset of ignition differently, unreasonable. Therefore, the discussion in this work will not be focused on the absolute result values, but focusing on the general impact of different processes and the parameters of interest on the ignition properties.

3.3.1 Impact of temperature

The most obvious observation considers the decrease of ignition delay with respect to the increasing temperature [3,13,17,40,51,54,55]. Rybak et al. [3] studied the ignition delay of different pulverized biomass fuels with respect to the furnace temperature, by recording the moment of the ignition appearance indicated by the change of illuminance that is detected using two photo elements. Their results, summarized in Fig. 6, shows that in addition to the temperature impact, fuel type has also a strong influence on the ignition onset. Among the illustrated fuels, it shows that the highest ignition delay time is characterized by the smallest amount of volatile matter. However, the ignition mode was not determined as this would require the use of additional sophisticated tools, such as cameras with the high filming speed, pyrometry etc. Therefore, the direct impact of temperature on ignition mode could not be investigated. When temperatures are sufficiently high, e.g., over 800^{o}C, the absolute difference of ignition delays diminishes substantially, and thus the impact of

393 fuel composition becomes less dominant. The obvious relation of decreasing ignition
394 delay with increasing temperature can also be directly linked to pyrolysis behavior, as
395 higher temperatures result in higher heating rates which cause more dynamic
396 devolatilization and higher instantaneous yield of permanent gases. Of course, the
397 local gas temperature in the particle's vicinity which contributes to the governing
398 particle heating rate is strongly affected by the gas composition and particle size and
399 may differ from the global reactor temperature [49].

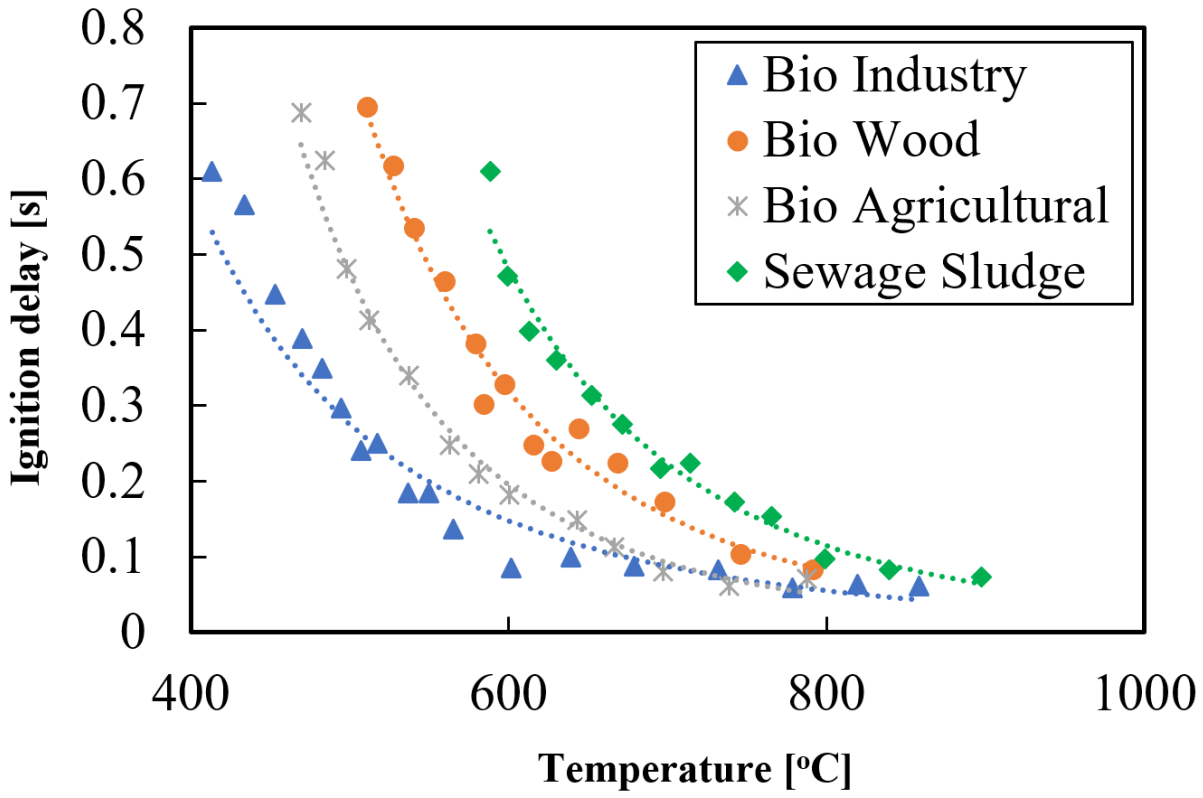

400

401 Fig. 6 Ignition characteristics of different biomass fuels. Adapted from [3].

402 Simões et al. [40] suggested that the ignition of their investigated biomass fuels
403 occurred mostly in the gas phase with few exceptions where surface ignition took
404 place. As opposed to pine bark which ignited homogeneously, for wheat straw particles
405 under low temperature conditions, in spite of high amount of volatiles, the surface
406 ignition occurred. However, the investigated wheat straw was characterized with sharp

edges and hot spots with a non-spherical structure. This could explain the occurrence of the heterogeneous ignition mode. The critical diameters for the ignition mode mechanism transition was found to vary with the fuel type. Accounting for the fact that volatile matter is the main component in biomass fuels, it is expected that devolatilization and volatile combustion dominate in the form of homogeneous combustion although particle shape also plays an important role over the ignition mechanism. It was eventually observed that the ignition delay was found to be highly dependent on the biomass type and particle size in the temperature range between (1500 – 1650 K), whereas for the temperatures higher than 1650 K, it was governed mainly by the particle size. Fig. 7 depicts ignition delay times for different biomass fuels from the study of Simões et al. [40] and Magalhães et al. [51]. The results clearly indicate a strong effect of biomass composition and particle size for lower temperatures, whereas, for higher temperatures, the fuel composition does not play a dominant role.

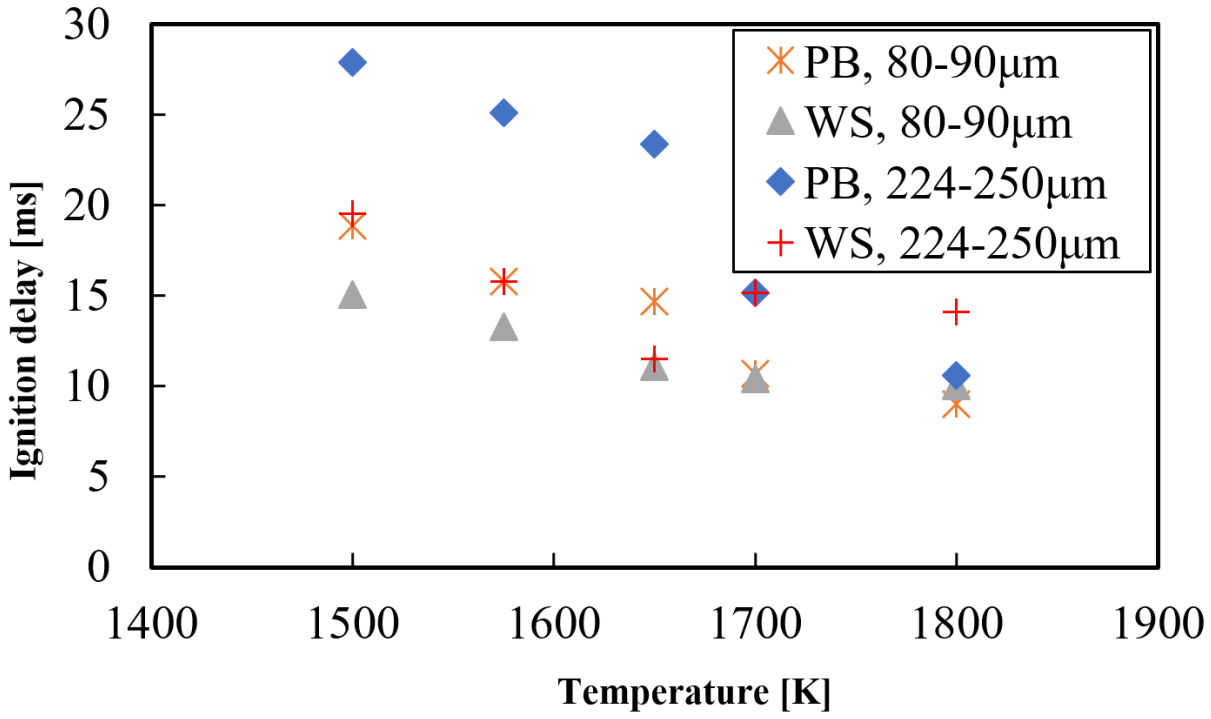

a)

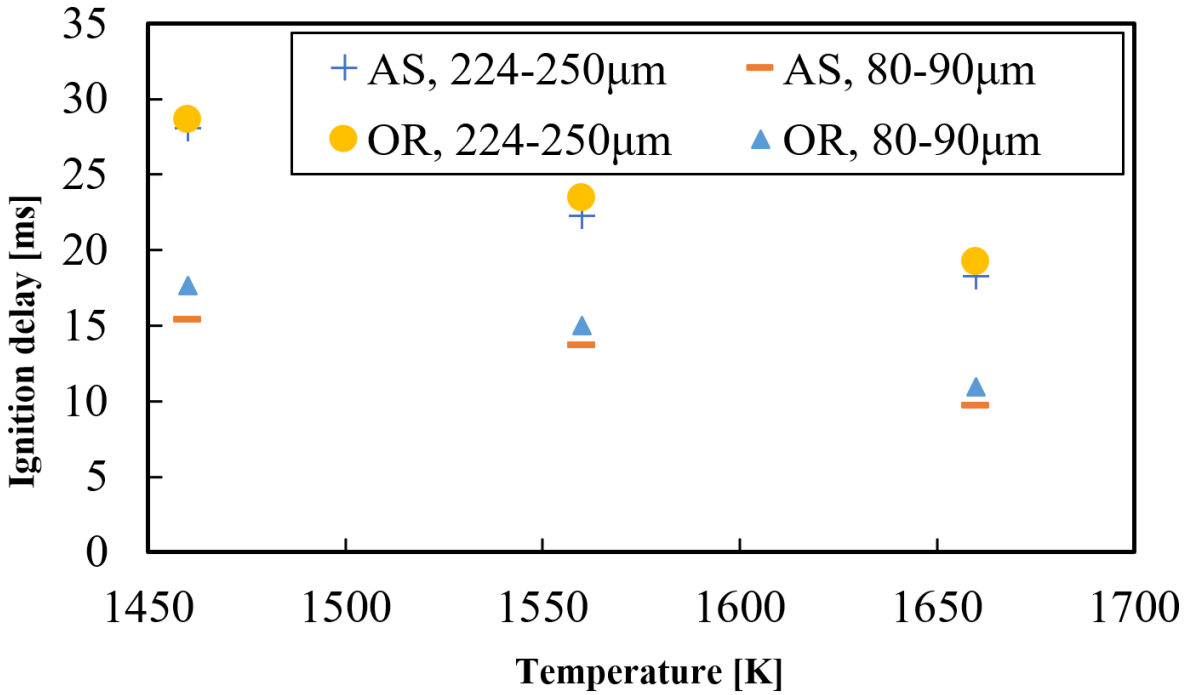

b)

Fig. 7 Ignition delay times of single biomass particles for a) pine bark (PB), wheat straw (WS) b) almond shell (AS), olive residue (OR). Adapted from [40,51].

3.3.2 Impact of particle size and shape

Particle size has a substantial impact on the ignition delay and ignition mechanism [13,17,40,51]. It is obvious that ignition delay is greater for larger particles [13,40,51]. Simões et al. [40] and Magalhães et al. [51] also observed that smaller biomass particles tended to ignite heterogeneously while larger particles ignited homogeneously. It is also reasonable since the heating rate is much greater for smaller particles. A recent study by Fatehi et al. [17] considered the analysis of critical radius with respect to the ignition mechanism for wheat straw and pine bark for particle size of 80 µm for different shapes, as shown in Fig. 8. The particle critical size is defined as the smallest size at which the volatile flux can prevent the oxidant from reaching the particle surface. Figure 8 depicts a strong dependence of the particle shape and type

438 on the ignition mode. Figure 8a clearly indicates that 80 μm spherical particles (aspect
439 ratio of 1) always undergo a homogeneous ignition mechanism. This considers the
440 case when the critical radius is below the actual particle size during the entire
441 devolatilization. For particles with an aspect ratio of 4 (cylindrical particles), particles
442 can undergo a heterogeneous ignition mechanism – wheat straw. One can observe
443 that in spite of the fact that ignition occurs at first in the heterogeneous mode, it can
444 shift to a homogeneous mode when the rate of devolatilization increases – Fig. 8b.
445 Since devolatilization is not uniform and the devolatilization intensity is not constant,
446 the ignition mechanism may change during the process. It especially considers non-
447 spherical particles, where the heating rate acting on a particle is highly non-uniform As
448 for pine bark, in each investigated case, it ignited homogeneously. The results can be
449 justified by the fact that pine bark had a much higher volatile yield than wheat straw.
450 This directly affects devolatilization dynamics and ignition. In comparison with coal,
451 biomass has a higher moisture and content, larger particle sizes, and is composed of
452 cellulose, hemicellulose and lignin which have different pyrolysis characteristics. This
453 resulted in an uneven devolatilization throughout the particle and significant changes
454 of particle critical size. Moreover, the inherent differences between biomass and coal
455 as regards the volatile content and surface-to-volume ratio result in a considerably
456 smaller biomass critical size.

457 With respect to particle size impact, one also has to consider the possible effect of
458 particle shrinkage during devolatilization [56] as it is reported to have a strong effect
459 on the intraparticle heat and mass transfers and thus the rate of devolatilization [57].
460 The shrinking effect refers to both diameter and density changes that also affect the
461 heating rate acting on a particle. On the basis of the observations, one can conclude
462 that particle critical size is a key parameter when estimating ignition mechanism.

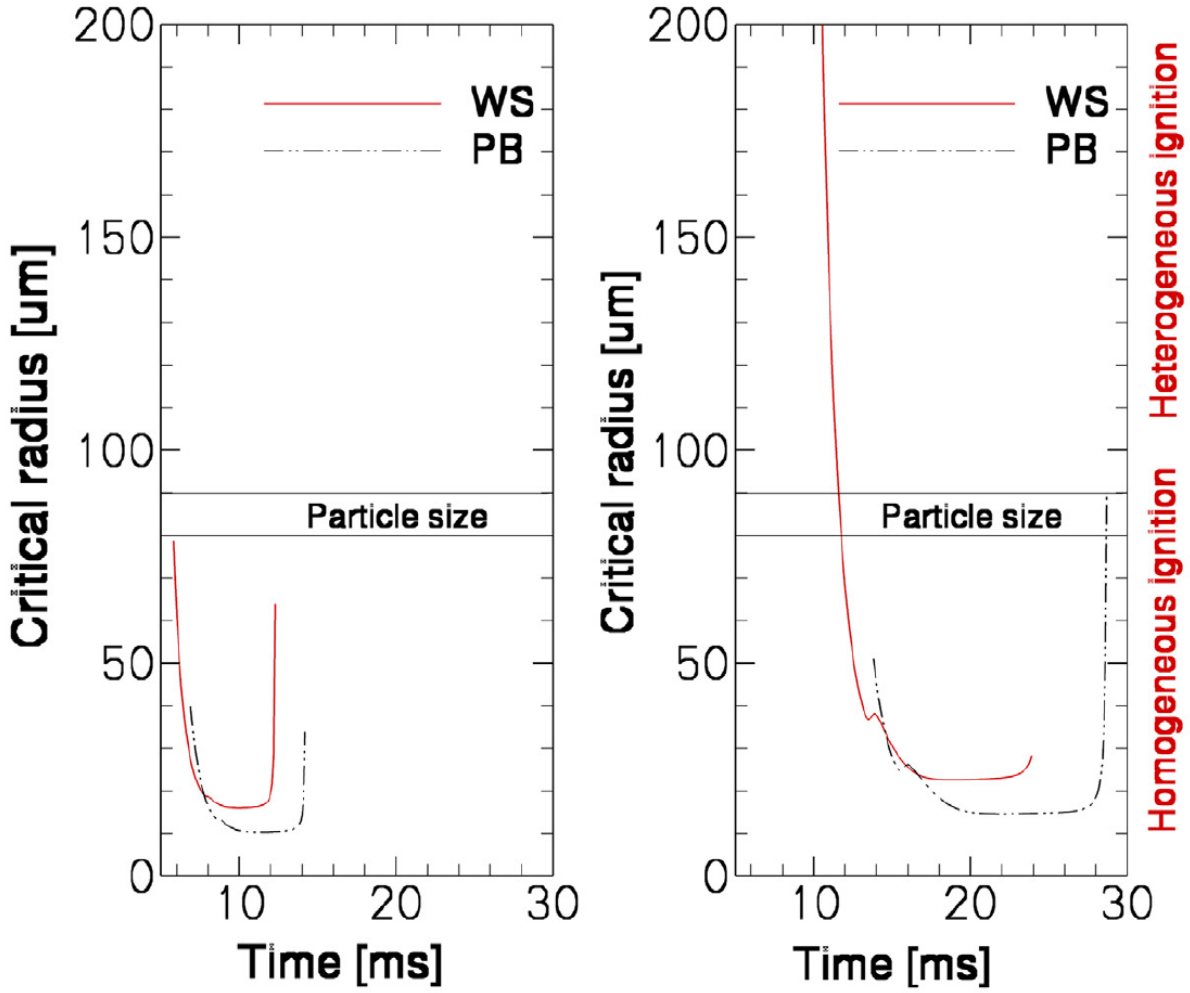

Fig. 8 Critical radius of different biomass particles during devolatilization. WS – wheat straw, PB – pine bark (a) radius = 40 μm, aspect ratio = 1, T = 1500 K, (b) radius = 40 μm, aspect ratio = 4, T = 1500 K. Adapted from [17].

Elfasakhany et al. [58] reported uneven wood ignition and conversion. Fig. 9 illustrates wood particle burning. The thin short bar illustrates the burning particle whereas the thick tail illustrates the flame. Devolatilized gases oxidize forming a diffusion flame attached to the particles. A long bright tail is a result of particle acceleration. In the left bottom corner, one can observe a nearly spherical flame indicating that the particle is not accelerated by the moisture/volatiles release. The

474 acceleration depends on the fiber orientation and the uneven volatiles/moisture release
475 generating a propulsion force.


476

477 Fig. 9 Experimental photo of impact of moisture and volatile release on particle motion
478 at approximate time 20 ms. Most of particles are in the range between 0.2 mm and 0.7
479 mm in diameter and 1 mm in length. Furnace diameter is equal to 0.25 m. Reprinted
480 with permission from [58].

481 In terms of particle size and shape, an important biomass feature is also biomass
482 morphology which dictates the macroscopic parameters such as density, porosity,
483 conductivity, and diffusivity which can eventually affect ignition. Fiber orientation is an
484 important parameter in biomass thermochemical conversion due to the anisotropic
485 structure. In Fig. 9, for example, fiber orientation was found to be an impactful
486 parameter in the occurrence of particle acceleration acting as a propulsion force during
487 moisture/volatile release. In [49], it has been shown that the higher slip velocity
488 accelerates the heat convection between the gas phase and the particle eventually
489 reducing ignition delay.

490 The situation becomes more complicated for thermally thick particles where
491 intraparticle heat transfer cannot be neglected [25] and where particle temperature
492 gradients play a key role in the ignition. Moreover, a strong overlap between the

493 governing combustion stages (drying, devolatilization, and char combustion) is
494 observed [17]. An important non-dimensional number representing the ratio of the
495 resistance to heat transfer from the body inside to the surface is the Biot number. Biot
496 number values (>0.1) indicate a thermally thick regime. Under such conditions,
497 biomass particle microstructure gains enormous significance as dynamic
498 morphological changes affect ignition characteristics. An extensive review considering
499 the advances of multiscale modelling of lignocellulosic biomass structure has been
500 reported by Ciesielski et al. [59] [60,61], from which the modeling approach concerning
501 the impact of biomass structure is believed to be useful in future ignition studies.
502 Unfortunately, the literature on biomass ignition that falls into the category of thermally
503 thick particles is extremely rare and it is mostly devoted to experimental investigation
504 [54,62–64]. For a representative review in this field, further research is required.

505 For example, Momeni et al. [54] studied experimentally the effects of particle shape
506 (employing the aspect ratios 1, 2, 4, 6, 8) on combustion characteristics of single
507 biomass particles. Two shapes were analyzed – a sphere (3mm) and a cylinder (length
508 from 4 to 18mm). It was concluded that particles with a larger aspect ratio will be heated
509 faster due to radiation and convection resulting in a shorter burnout time and
510 devolatilization time. It is because spherical particles have the smallest surface to
511 volume ratio, resulting in a slower rate of heat and mass transfer and higher conversion
512 time with respect to aspherical particles. For ignition, the trend is the same, however,
513 the differences with respect to the studied aspect ratios (from 1 to 8) are less
514 remarkable.

515 *3.3.3 Impact of volatile matter and devolatilization*

516 In the study of Rybak et al. [3], the minimum ignition temperature was investigated
517 based on the volatile content of the fuel. By way of exception, the authors have decided

518 to include also coal fuels in this analysis, as an interesting observation can be made
519 from Fig. 10. The content of volatile matter on a dry-ash-free basis was adopted as a
520 measure of coal rank. It is evident that for coals, the minimum ignition temperature
521 strongly depends on a coal rank. For biomass and waste, on the other hand, the
522 ignition temperature increases with the increase of volatile matter content. Large
523 differences in ignition temperature (150^{o}C) can also be observed for biomass fuels with
524 very similar volatile matter content. At the same time, fuels with lower volatile content
525 (60-65 %) have the lowest ignition temperature (400-450^{o}C) which:

526 • creates the highest possibility of fire explosions
527 • these fuels are also characterized by the best flame stability

528 Takigawa and Yoshizaki [65] performed similar studies of six fuels (three coals and
529 three biomasses) and observed the lowest ignition temperature for rice husk containing
530 62% of volatile matter. No correlation was found between the ash fuel content and
531 ignition which could be linked to the above observation.

532 The reason for the non-instinctive relation of ignition temperature with respect to dry-
533 ash-free volatile content (V^{daf}) was attributed to the ignition mechanism. It was
534 concluded that under experimental conditions, volatiles were ignited in the gaseous
535 environment - a homogeneous ignition of a dilute cloud. The ignition of a dilute dust
536 cloud, which can be compared to the single particle combustion, was probably favored
537 by high volatile content, high devolatilization rates, Stefan flow, and low relative speeds
538 between the gas and particles. It resulted in a dust cloud dilution and insignificant
539 particle-to-particle interaction. Eq. (1) defines the critical value of volatile content in the
540 fuel above which a homogeneous ignition occurs: [3]

$$V_{cr}^{\infty} = \frac{RT_{i,\infty}^2}{E} \frac{3\lambda}{r_s^2 \rho_s \beta q_v k_{0,v} e^{-\frac{E_v}{RT_s}}} \quad (1)$$

Where R – universal gas constant, T_∞ - ambient temperature, λ – thermal conductivity, E – activation energy, r_s – solid particle radius, ρ_s – solid particle density, q_v – heat of devolatilization reaction, $k_{0,v}$ – reaction rate constant of devolatilization. For the derivation of Eq. (1) refer to [3].

The above equation indicates that for fuel with the volatile matter content $V^{\infty} < V_{cr}^{\infty}$, the flame associated with the volatile matter ignition will not detach from the particle surface, indicating either heterogeneous ignition, or hetero-homogeneous ignition. The Eq.(1) also indicates that the smaller the particle size or the smaller the devolatilization reaction rate, the higher the critical value of volatile content above which a homogeneous ignition mechanism occurs. It means that smaller particles with a lower devolatilization rate under higher temperatures will tend to ignite heterogeneously. Unfortunately, the ignition mechanisms were not investigated experimentally, therefore, it is impossible to verify the theoretical conclusions. Further research would be desirable in this field.

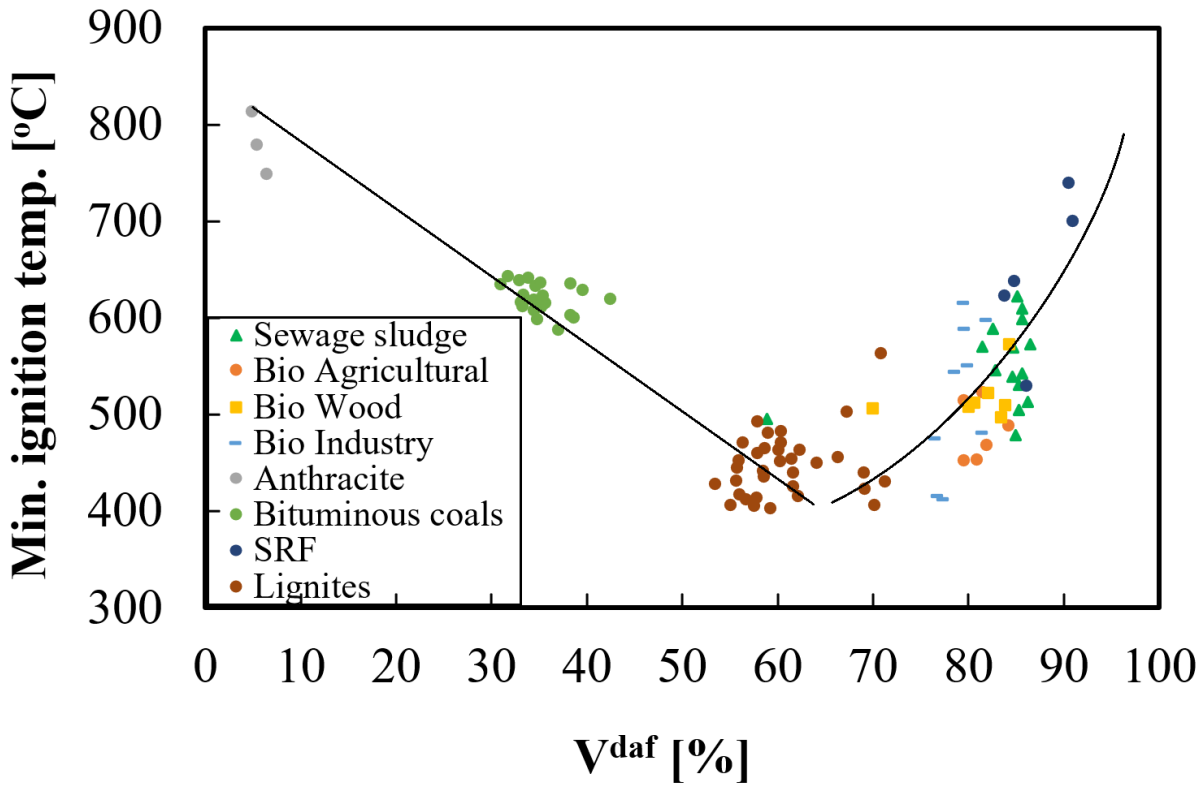

Fig. 10 Minimum ignition temperature with respect to volatile matter content (dry-ash-free). Adapted from [3].

Li et al. [13] studied the ignition behavior of wheat straw and softwood particles in a down-fire reactor and connected the ignition characteristics of biomass directly with an extent of devolatilization that are estimated using their dynamic-mesh single particle model, as shown in Fig. 11. One can observe that biomass at low furnace temperatures requires a higher degree of devolatilization for the ignition onset to occur. It confirms the sensitivity of ignition to devolatilization dynamics which is determined by the furnace temperature. A conclusion can be drawn that at certain temperatures, biomass can ignite before devolatilization, indicating a heterogeneous ignition mechanism [13]. Therefore, the degree of devolatilization with respect to the furnace temperature can be an important modeling criterion when defining the ignition mechanism.

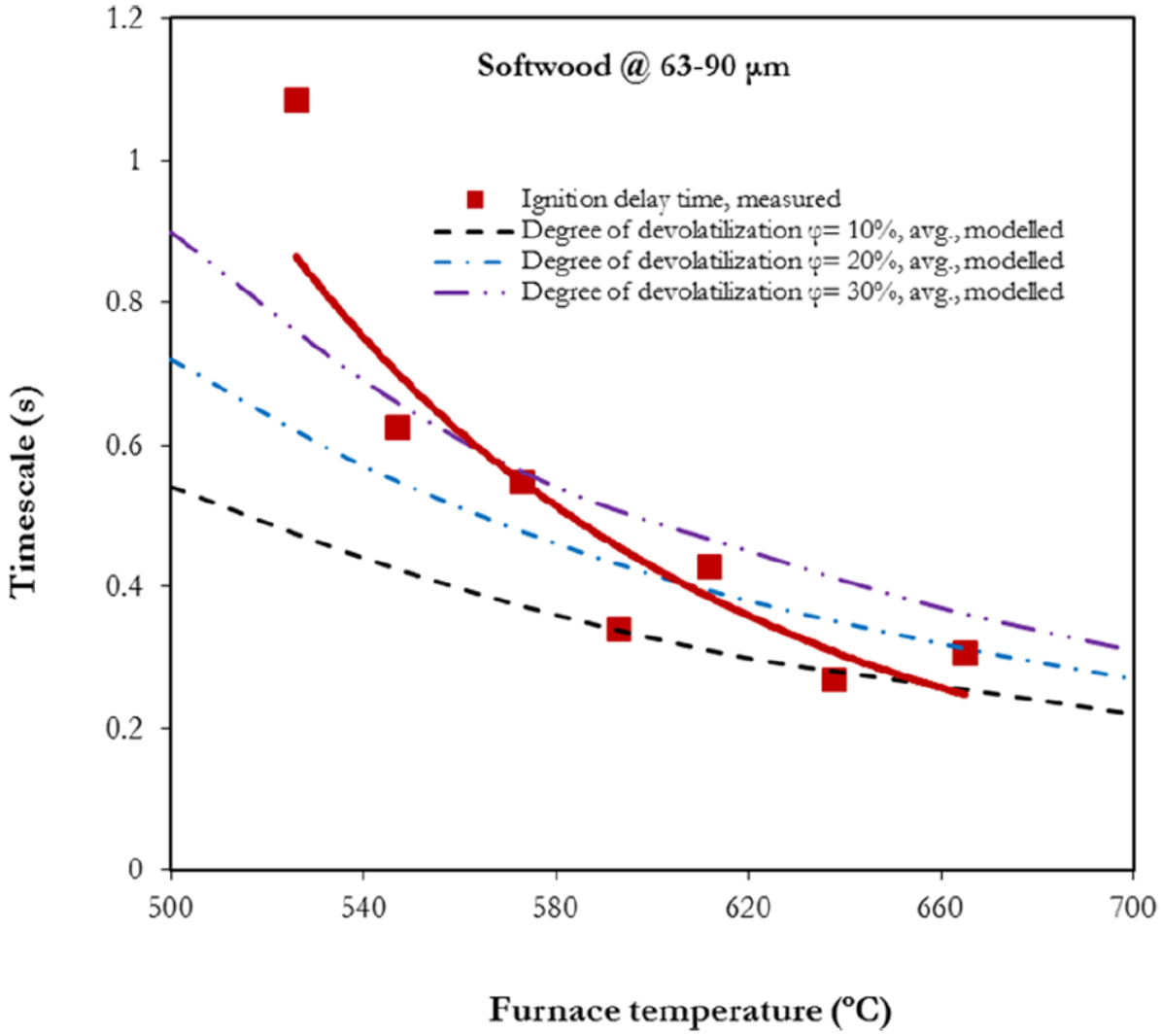

Fig. 11 Measured ignition delay times of softwood with respect to extent of devolatilization. Reprinted with permission from [13].

3.3.4 Impact of cellulose, hemicellulose, and lignin

One of the important aspects of lignocellulosic biomass ignition regards the impact of specific biomass components, such as cellulose, hemicellulose, and lignin. Despite biomass has composition similar to coal [66], it varies in the content of constituents such as holocellulose and lignin. Moreover, there are structure and density differences which, overall, substantially impact the pyrolysis mechanism. To date, the ignition and combustion behavior of cellulose, hemicellulose and lignin were widely studied mostly with TGA [67–73]. The main results indicate that the decomposition temperature of

lignin is lower than that of hemicellulose, whereas decomposition temperature of hemicellulose is lower than the cellulose temperature. Moreover, lignin decomposes in a wider range of temperatures (423 – 1173 K), while hemicellulose decomposes in the range of (493 – 588 K), and cellulose (588 – 673 K). It means that even though lignin starts to devolatilize before hemicellulose and cellulose, the complete devolatilization is achieved by hemicellulose and cellulose first. Chen et al. [74] demonstrated that cellulose had the highest yield of CO at high temperatures (above 550^{o}C), whereas below 550^{o}C, similar share of CO and CO_2 was observed. Hemicellulose had the highest CO_2 yield for all studied temperatures (400-800^{o}C), whereas lignin had the highest CH_4 yield, although CO and CO_2 yields were also comparable. High CH_4 content could be attributed to aromatic rings and methoxy groups in the structure of lignin. As a result, different share of the biomass main components, results in a different yield of pyrolysis permanent gases which has a direct effect on ignition. It must be emphasized, however, that in TGA experiments, the mass of the fuel is typically given in mg or grams. Moreover, the heating rate is limited to 5-100^{o}C/min, whereas in real-life reactors, the heating rate is as high as 10^3-10^5 C/s. High heating rates conditions favor greater weight loss thereby yielding more volatile species and less char. Therefore, the TGA experiment does not directly correspond to the real combustion scenario in an industrial reactor, but it can be used as an indication for the ignition performance. Burhenne et al. [75] reported that herbaceous biomass containing higher cellulose and hemicellulose content decomposed faster and produced larger amount of gas products than woody biomass containing larger lignin content. Zhang et al. [76] found that melted lignin can delay the volatiles release during devolatilization due to the created barrier. Pang et al. [77] reported that lignocellulosic composition strongly correlate with char reactivity and char morphology. Ma et al. [78]

604 revealed that lignin char was characterized by higher energy and mass yield than
605 hemicellulose and cellulose chars due to enhanced thermal stability, and pore
606 structure. Yan et al. [64] studied the effect of the three main biomass components with
607 TGA and a fixed bed and reported that the higher lignin content, the higher ignition
608 delay. Lignin was also found to be the least reactive component which inhibited the
609 combustion different stages. It requires a longer time and broader temperature range
610 to decompose. The lignin's low reactivity could also be linked to a large amount of
611 benzene rings which are thermally stable.

612 In contrast to previous studies which considered mainly TGA, Wang et al. [14]
613 investigated the effect of these three components on the ignition behavior of biomass
614 in a drop tube furnace (DTF) at 1273K under fast heating rate conditions. The biomass
615 particle size was in the range of 500 μm, whereas the size of cellulose, hemicellulose,
616 and lignin representatives was between 70-150 μm. It was ultimately reported that the
617 lignin content strongly affected the biomass ignition characteristics. The ignition
618 mechanism was strongly correlated with the lignin content. Biomass particles with very
619 high lignin content exhibited hetero-homogeneous ignition, whereas particles with high
620 and moderate content showed a homogeneous type of ignition. After homogeneous
621 ignition, biomass char ignition with higher lignin content occurred earlier. Biomass with
622 a very low lignin content also exhibited a hetero-homogeneous type of ignition.
623 Cellulose was reported to ignite hetero-homogeneously. A similar ignition behavior was
624 observed for hemicellulose. A substantial difference could be observed for lignin
625 ignition behavior which ignited homogeneously. The homogeneous ignition of lignin
626 and hetero-homogeneous ignition of holocellulose is hard to explain and therefore
627 further research is recommended in this field, especially, as this is the only study found
628 under high-temperature conditions. As regards the ignition temperature, it was

reported to depend strongly on the cellulose content regardless of whether the ignition mode is hetero-homogeneous or homogeneous. Shan et al. [79] studied the combustion behavior of three different fuel samples in DTF. It was reported that each fuel had two combustion phases: volatile combustion in an envelope flame, and subsequent char combustion with high luminance. Additionally, two peak values in the flame size profile and the average luminous intensity during volatiles combustion were observed which were corresponded to the cellulose and hemicellulose devolatilization.

3.3.5 Impact of presence of alkali metals

The alkali metals like sodium (Na) and potassium (K) along with chlorine (Cl) are the most important elements inherent in biomass fuels that can generate operational issues. The presence of these aggressive alkali species in ash [80] can lead to problems of heat exchanging surfaces related to slagging and fouling [81], but also affect biomass ignition characteristics. Fahmi et al. [82] report a strong catalytic effect of alkali metals, especially, potassium in both devolatilization and combustion. The same catalytic effect was demonstrated by Jones et al. [83] under high heating rate and temperature conditions. Moreover, the proportion of potassium released to the gas phase to that retained in the ash is correlated to the initial potassium content. However, this relationship varied between wood and herbaceous materials. Carvalho et al. [84] investigated the effects of potassium and calcium on single grape pomace biomass particles. The ignitions were recorded with a CMOS high-speed camera, and ignition delay was determined based on image post-processing. It was ultimately demonstrated that the ignition delay time increased with the demineralization process confirming a catalytic effect, as shown in Fig. 12.

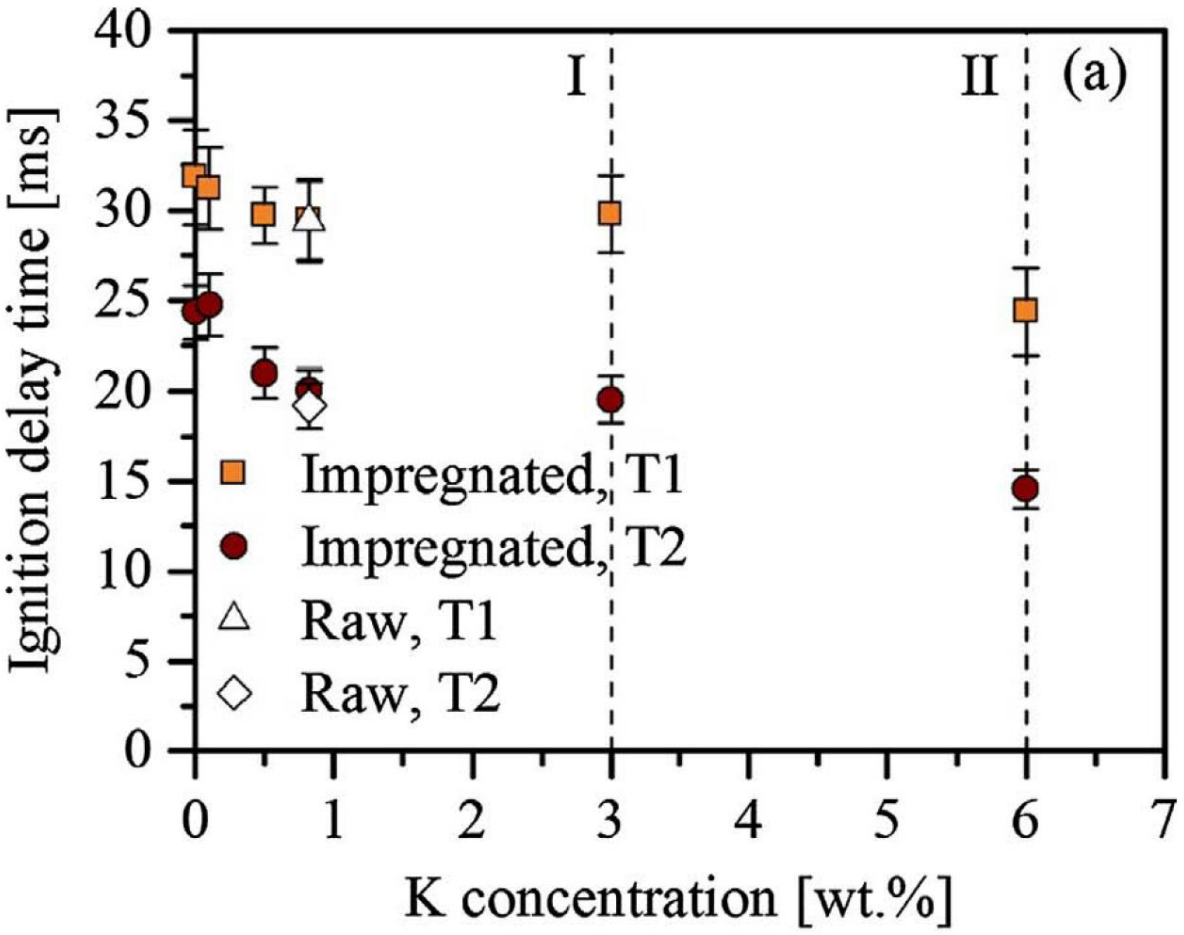
Ignition delay time [ms]
K concentration [wt.%]
I
II
(a)
Impregnated, T1
Impregnated, T2
Raw, T1
Raw, T2
0
5
10
15
20
25
30
35
40
0
1
2
3
4
5
6
7

652

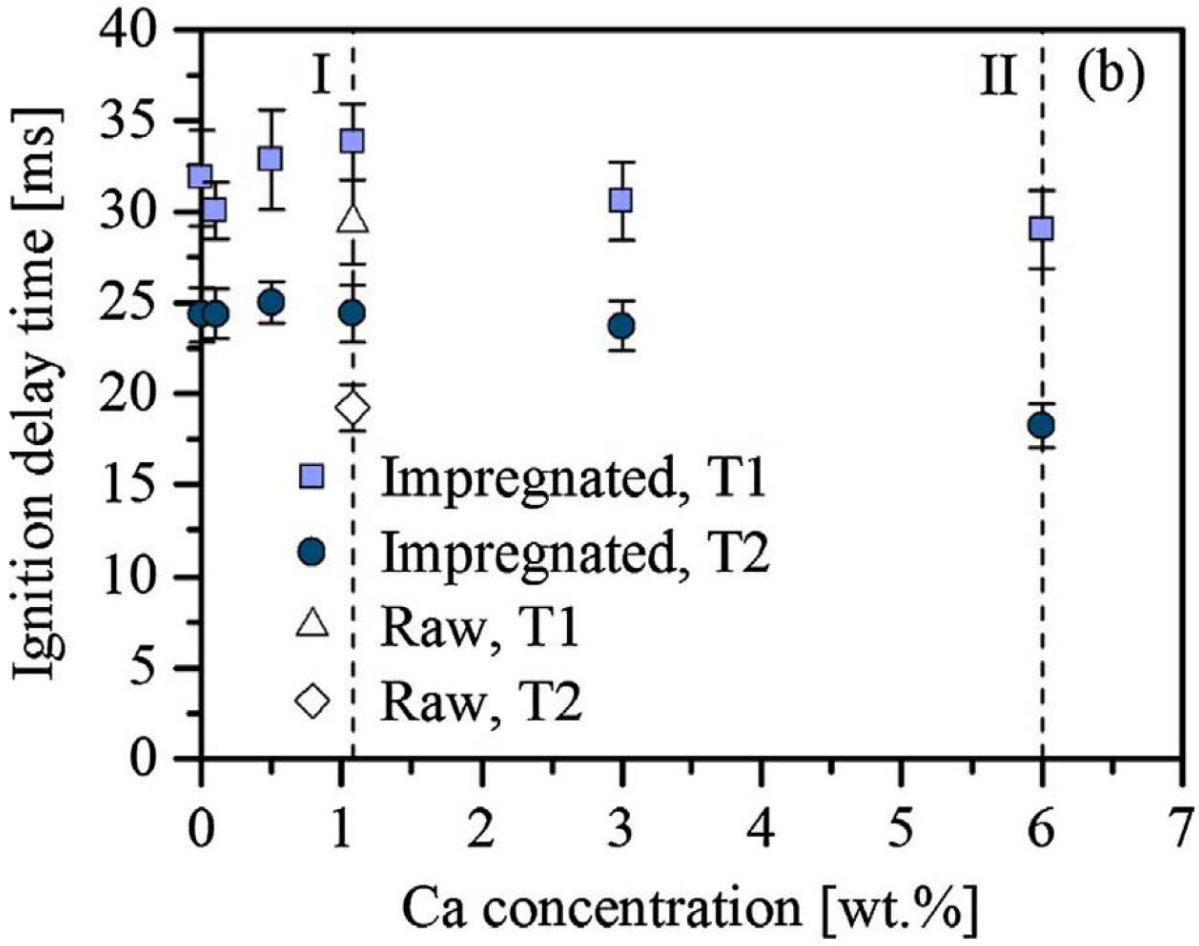

Fig. 12 Ignition delay time of grape pomace versus a) K concentration, b) Ca concentration. Hollow symbols represent raw biomass, whereas zero concentration represents demineralized samples. Reprinted with permission from [84].

The literature clearly indicates a noticeable dependence of the investigated elements on the ignition characteristics. It is, therefore, important to effectively predict the yield of these species, by means of, e.g., a reaction mechanism [85,86] but also experimental methods such as chemical fractionation [87–89]. The method is a stepwise leaching procedure. The fuels are leached in three steps, water, ammonium acetate and hydrochloric acid. Chemical fractionation has been used extensively for determination of ash forming matter distribution in coal and biomass fuels.

With respect to ignition, there can be many intricacies. For example, the release

665 of K is highly dependent on other elements present in biomass. Sulfur and chlorine, for
666 example, can facilitate K release, while the presence of aluminum and silicate promote
667 formation of stable compounds that remain in the ash structure. As a result, accurate
668 experimental measurements are required to better understand the chemistry involved
669 [90,91] and the actual impact of trace elements on the ignition behavior.

670 Qu et al. [91] utilized a robust wavelength-multiplexed TDLAS spectrometer for
671 simultaneous time-resolved potassium detection. The experimental method allowed
672 obtaining precise measurements of K during devolatilization and char conversion of
673 four different biomass fuels: softwood from spruce, wheat straw, and two energy crops
674 – Salix and Miscanthus. The experimental results were compared with the proposed
675 model yielding a good agreement. In the K release sub-model, which was developed
676 over the years [92–94], the interaction between K/S/Cl is determined through a set of
677 elementary reactions. Potassium was divided into an organic and inorganic part in the
678 following way:

$$Inorganic\ K(K^+) \rightarrow \phi_1 KCl + \phi_2 K_2SO_4 + \phi_3 K_2CO_3 \quad \text{(R1)}$$

679

680 Inorganic potassium forms crystallized salts during drying. The organic potassium is
681 transformed to char-bonded K during temperature increase and to carboxyl groups,
682 releasing K in the gas phase.

$$Organic\ K(R-COOK) \rightarrow Char-K \quad \text{(R2)}$$

683

$$Organic\ K(R-COOK) \rightarrow R-COOH(carboxyl\ groups) + CO_2 + K(g) \quad \text{(R3)}$$

684

The model is also coupled with a CFD solver, where the chemistry of the K/Cl/S system can be investigated using different chemical mechanisms for these species. In spite of some model limits and assumptions, it is a first attempt to model the release rate of important trace element species from biomass fuels that can affect the ignition characteristics. For further details regarding the model refer to [91–94].

3.3.6 Impact of atmosphere composition

The literature regarding the effect of combustion atmosphere on ignition regards, above all, O_2/N_2, O_2/CO_2, and O_2/H_2O concentrations, and oxygen concentration. Riaza et al. [38] investigated the combustion of four pulverized biomasses at 1400K in DTF in air and O_2/CO_2 atmosphere containing different O_2 mole fractions. It was reported that under the same O_2 concentration, when N_2 was replaced by CO_2, the ignition delay, ignition temperature and volatiles combustion time increased. Such an outcome can be justified by the difference in specific molar heats of N_2 and CO_2. The same result was obtained by [37,38,95–97]. Biomass also released large amount of volatiles that burned in the form of spherical envelope flames. The subsequent car combustion produced stronger pyrometric signals. The increase in O_2 also allowed more stable combustion and shorter volatile flame. Both the volatile combustion time and burnout time decreased [37,38,95]. It was also reported that, unlike coal, the combustion behavior of biomass from four different sources appeared unified. Riaza et al. [96] investigated oxy-fuel combustion of coal and biomass blends in DTF at 1273K. It was reported that the addition of biomass improved the ignition temperatures and the burnout values in both air and oxy-fuel combustion atmospheres. The application of biomass turned out to have more substantial effect on the ignition temperature than on burnout. Zhou et al. [98] investigated experimentally the ignition and combustion characteristics of single biomass corn stalk particles in O_2/N_2 and

O_2/H_2O atmospheres in an electrically heated single particle reactor at 1073K. The ignition was recorded with a CCD camera, while two-color pyrometry was used to estimate the volatile flame temperature. It was reported that the ignition delay time was lower in O_2/H_2O atmosphere than in O_2/N_2. Moreover, for O_2/N_2 atmosphere, in higher O_2 concentrations, a shift from homogeneous to heterogeneous ignition mode was observed, whereas in O_2/H_2O atmosphere, a homogeneous ignition was observed for the entire O_2 range. The reason for the obtained shift from homogeneous to heterogeneous mode for O_2/N_2 atmosphere is sensible as this entails better access to oxygen and more intensified oxidation reactions where particle temperature reaches the ignition temperature faster even before devolatilization properly develops. An interesting aspect may consider O_2/H_2O atmosphere where for the entire investigated O_2 range 21-50%, a homogeneous ignition mode was observed. It should be noted that replacing N_2 with H_2O enhances two reactions: ($C + H_2O \rightarrow CO + H_2$ and $CO + H_2 \rightarrow CO_2 + H_2$). This supports CO and H_2 production which is beneficial to reducing ignition delay as well as promoting homogeneous ignition mode. Borrego et al. [99] obtained chars from different pulverized biomasses by pyrolysis in oxy-fuel and air conditions in DTF at 1200K. They reported no substantial changes between char characteristics, namely pore volume, morphology, reactivity.

3.3.7 Impact of biomass pretreatment – torrefaction, pyrolysis, and water leaching

Pretreatment technologies, such as torrefaction, pyrolysis and water leaching, are commonly applied to improve the quality of biomass fuels, in terms of reactivity, grindability, and uniformity, etc. Botelho et al. [100] compared the combustion characteristics of raw and torrefied grape pomace and concluded that the burnout values of torrefied biomass were lower than for the raw one, due to the lower volatile content and higher fixed carbon content. Gürel et al. [6] investigated the effect of

735 torrefaction, slow, and fast pyrolysis on the single particle combustion of agricultural
736 biomass at high heating rate conditions, and observed that all studied raw and torrefied
737 fuels were ignited in the gas phase, while chars produced from slow or fast pyrolysis
738 underwent a heterogeneous ignition which is reasonable as the lack of volatiles should
739 always result in a surface-type ignition. Fig. 13 illustrates the ignition delay time of olive
740 residue and almond shell before and after pretreatments. It can be observed that the
741 impact of torrefaction on ignition delay is different for olive residues and almond shells.
742 It also shows that slow pyrolysis increased the ignition delay time substantially among
743 all pretreatment methods. During slow pyrolysis, the volatiles escape slowly while the
744 particle withstands cooling and heating cycles which may result in cross-linking of the
745 char and a more stable carbon structure and higher carbon content. This may cause
746 an increase in ignition delay. As regards the fast pyrolysis, there is a rapid temperature
747 increase and there is an intense release of volatiles. This may result in macropores
748 creation. Owing to insufficient resident time, char cross-linking did not occur after
749 bridge breaking, as opposed to slow pyrolysis, which affects the particle reactivity. As
750 a result, one obtains a highly porous and reactive particle which has a much lower
751 ignition delay. The ignition delay of fast pyrolyzed olive residue and almond shell is
752 comparable to that of raw biomass fuels. Even though a heterogeneous ignition was
753 observed for fast pyrolysis chars, such a low ignition delay may result from the
754 presence of a volatile cloud attached to the surface as the volatile content was around
755 20 wt.% on a dry basis.

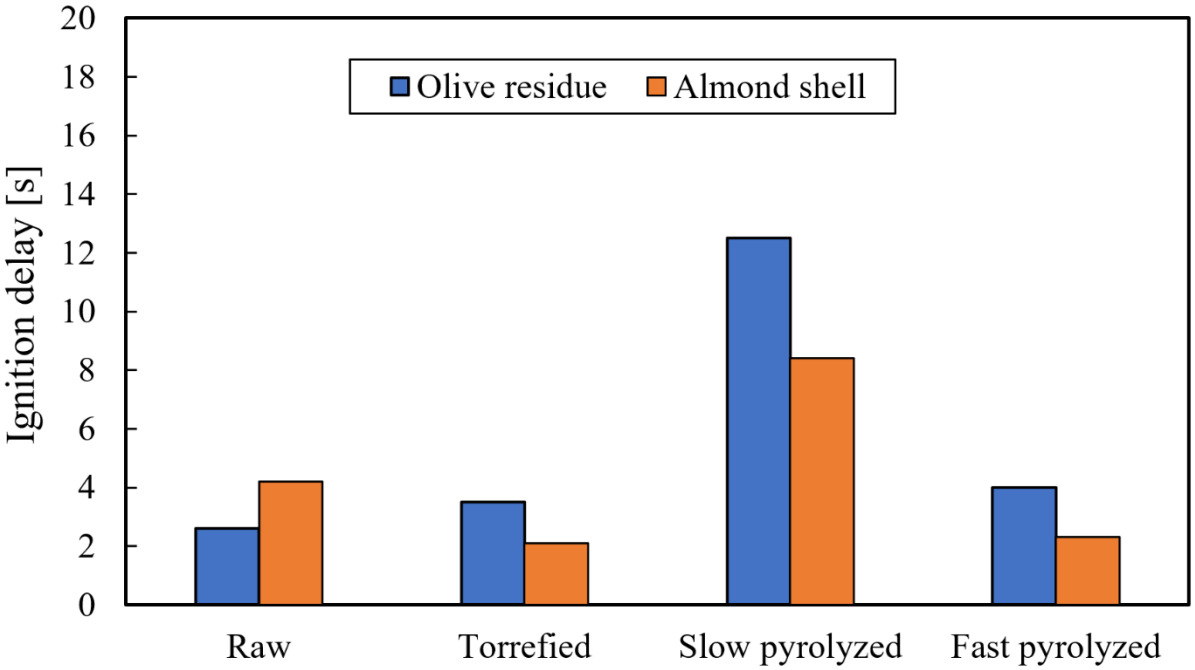

Fig. 13 Ignition delay times for olive residue and almond shell. Adapted from [6].

Wang et al. [101] studied the effect of feedstock water leaching on ignition during wheat straw combustion in a flat-flame burner reactor. Water leaching removes 90% of the K and all the Cl, whereas the less soluble minerals like Si, Ca, Mg, P, and Fe minerals were found to be hard to remove by water leaching. As regards the biomass particles properties, it was observed that water leaching increases the surface area and pore volume. Fig. 14 indicates a lower ignition delay at 1300^{o}C than at 1000^{o}C. Moreover, after water leaching, the ignition at 1000^{o}C is delayed (from 20 ms to 24 ms), whereas for 1300^{o}C it is delayed from 9.2 ms to 10.2 ms. It is evident that at higher temperatures, water leaching has a smaller impact on ignition. Additionally, as seen in Fig. 14b, burnout finishes sooner after water leaching.. Eventually, the results obtained from the flat-flame burner are in a good agreement with the results obtained generally from TGA. It is a noteworthy observation since in TGA studies, the heating rate is limited to 5-100^{o}C/min, whereas in real-life reactors, the heating rate is as high as 10^{5} ^{o}C/s.

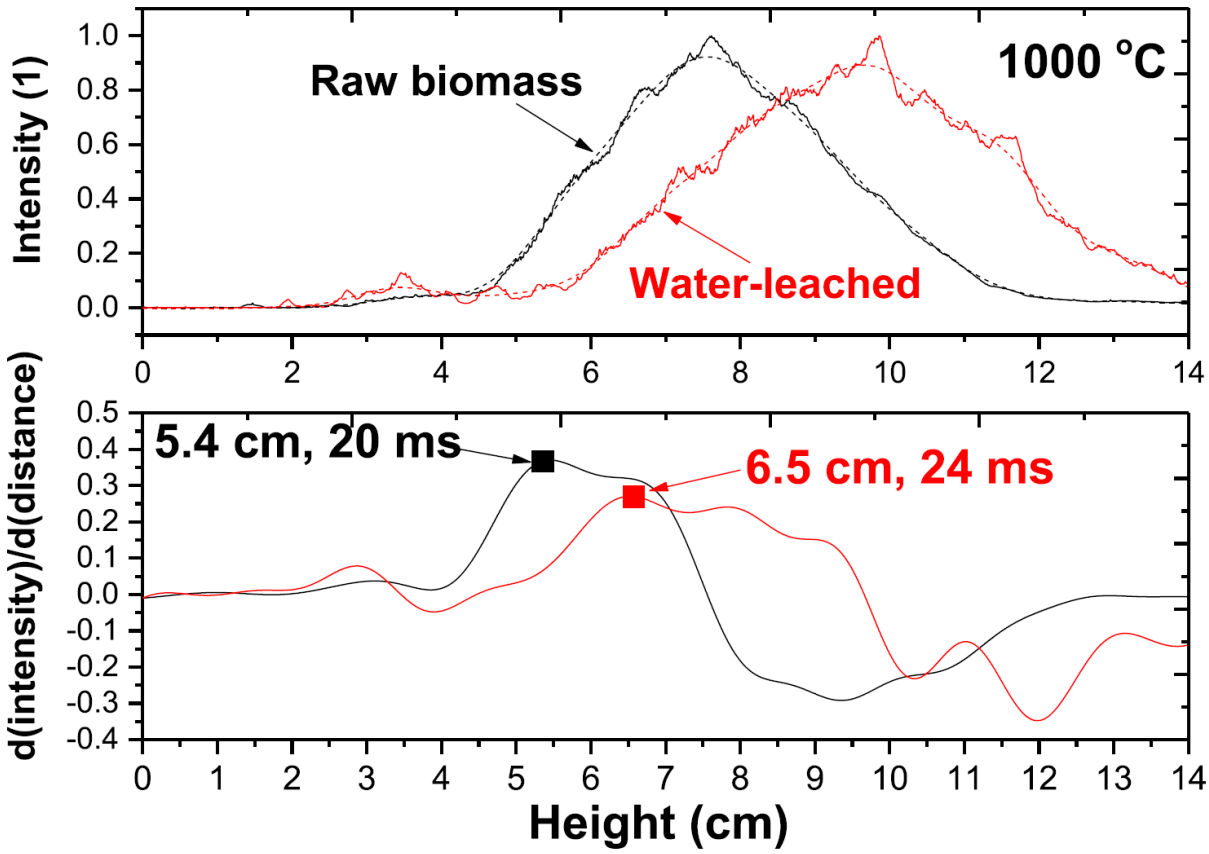
Raw biomass
1000 °C
Water-leached
Intensity (1)
5.4 cm, 20 ms
6.5 cm, 24 ms
d(intensity)/d(distance)
Height (cm)

(a)

772

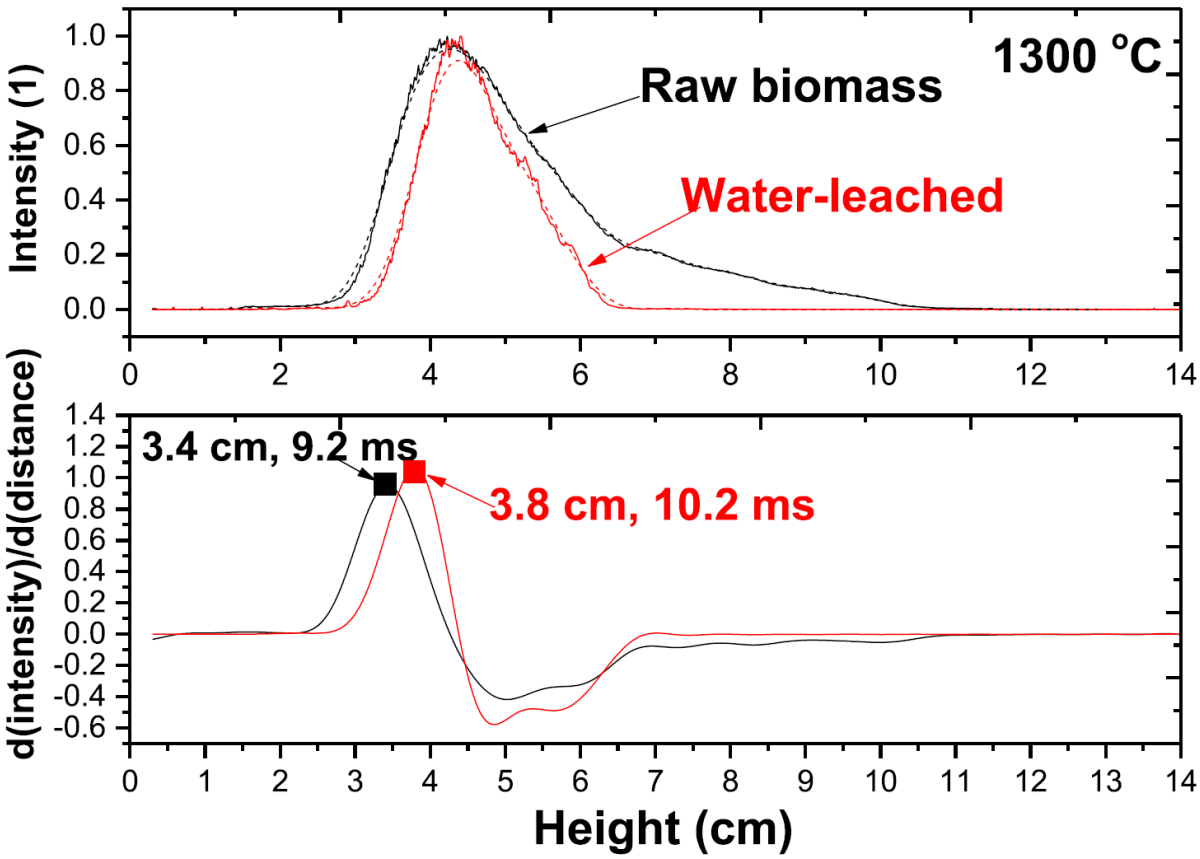

Figure 14. Ignition time of biomass wheat straw particles a) at 1000ºC, b) at 1300ºC. Reprinted with permission from [101].

3.4 Applied reactors

Reactors play a key role in combustion technology of biomass where the specific working conditions such as combustion atmosphere, pressure or heat transfer affect the biomass thermochemical conversion process. Currently, most of world-wide reactors fall into the category of entrained flow reactors, fluidized bed reactors and fixed-bed reactors. These reactors differ in terms of operating conditions and fuel requirements which will directly affect the ignition. However, most studies on biomass ignition have been performed in drop tube furnaces (DTFs) [3,13,14,29,36–39,53,58,77,79,101] and entrained flow reactors (EFRs) [17,33,35,40,51,84,96] with

785 feedstocks of dust biomass particles. DTFs and EFRs reactors have similar working
786 principle, although temperatures obtained in EFRs are slightly higher (1800K) than in
787 DTFs (1400-1500K) but the operating conditions for both reactors are close to the
788 conditions of large-scale boilers as cold particles are injected into the very hot
789 atmosphere. The typical residence times in DTFs, EFRs are in the order of
790 seconds/milliseconds. As a result, such facilities are considered appropriate to
791 investigate the early stages of particle combustion, especially the ignition behavior,
792 provided that experimental techniques allow for a sufficient time resolution. The recent
793 development in experimental research concerning ignition was achieved mainly thanks
794 to significant advances in nonintrusive optical diagnostics. However, most of the
795 current knowledge from ignition-related studies is based on laminar flow conditions and
796 single particle scale. Large-scale combustors operate under fully turbulent flow with
797 high mass flow rates of the fuel where the ignition characteristics can deviate from
798 those obtained under simplified reactor conditions. For example, in contrast to single
799 particle ignition, ignition in a stream or particle cluster is much more complex, and the
800 ignition mechanism would be additionally influenced by, for instance, the dust
801 concentration or the size of the dust cloud. Under such conditions, it would be important
802 to determine whether the ignition occurs around individual particles or in a gas mixture
803 away from particles. The turbulence effect should also not be neglected as in the study
804 carried out by Tufano et al. [102], the increased turbulent intensity was found to delay
805 the ignition.

806 Due to the complexity of the ignition process, there are still many uncertainties.
807 Future biomass ignition research should incorporate the strength and advantages of
808 both experimental and numerical methods to allow proper classification of biomass
809 fuels in terms of ignition delay and ignition mechanism. This would be a huge step

forward for the optimum selection of process conditions, fuel selection, designing or retrofitting reactors.

3.5 Incorporated numerical definitions of biomass ignition onset

The experimental measurement techniques of ignition onset have been discussed in section 3.1. However, the determination of ignition onset by experiments is often time consuming and restricted by the access to specific facilities and equipment. Nowadays, numerical simulations are constantly utilized in the field of thermochemical conversion of solid fuels [103–105]. They provide insight on design and process optimization and can be a reliable and time saving alternative to experiments. A complex simulation, by means of e.g. DNS or LES can provide fundamental information related to ignition, such as local instabilities, unsteadiness, instantaneous species concentration, temperature, and heat exchange which can help to further understand the occurring phenomena before the actual ignition. The literature devoted to numerical investigation of biomass ignition is, however, extremely limited [17,106–108].

3.5.1 Biomass ignition

Fatehi et al. [17] analyzed different criteria for ignition onset of pulverized wheat straw and pine bark particles with respect to the ignition delay. The normalized CO and CH mass fractions, the time derivative of the particle temperature at the surface, and time derivate of the gas temperature at 3 particle locations were investigated. For example, the application of the definition based on 10% of maximum CH results in the

834 ignition delay of 47.9 ms, while the calculation based on the CO mass fraction results
835 in 55.3 ms. The 10% of maximum CH concentration yielded the most accurate ignition
836 delay results against the experimental measurements. A comparison between
837 numerical and experimental data is illustrated in Fig. 15.

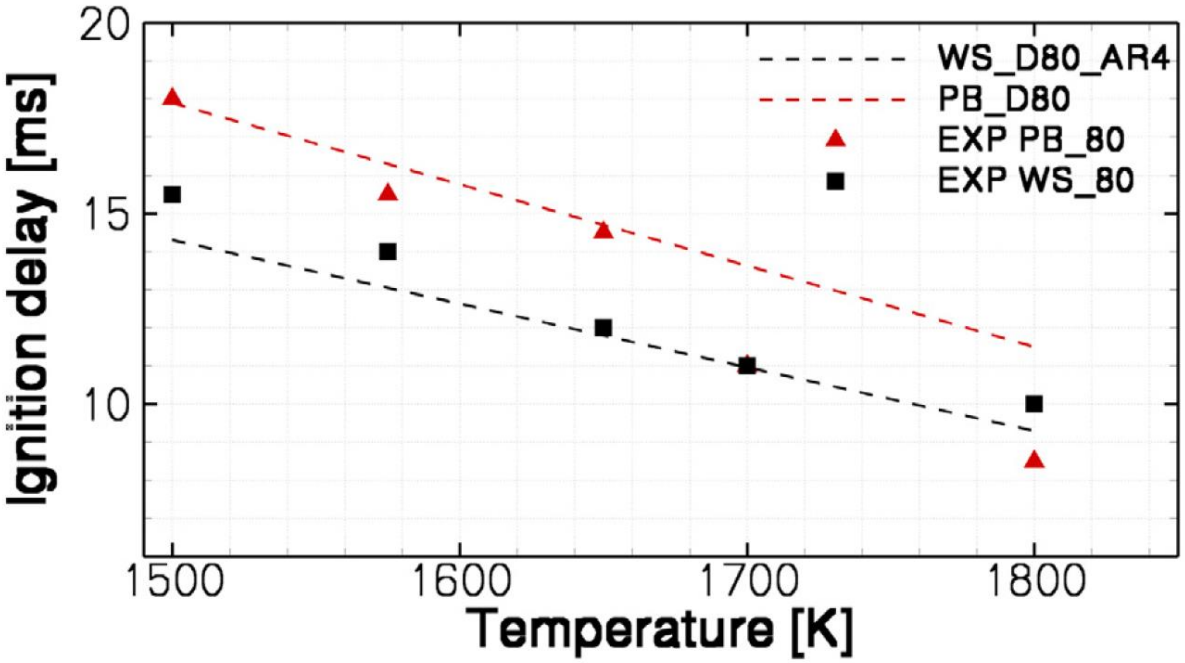

838

839 Fig. 15 Ignition delay of wheat straw (WS) and pine bark (PB) for 80 μm particles.
840 Reprinted with permission from [17].

841 Niksa [108] studied the macroscopic combustion characteristics of different
842 biomass forms in pulverized fuel furnaces by means of bio-FLASHCHAIN
843 devolatilization model in combination with the detailed carbon burnout kinetic model
844 for oxidation - CBK/E given only proximate and ultimate analyses. This work defined
845 ignition delay as the time to reach 5 daf wt.% of volatiles and the resulting data were
846 in good agreement with experimental data – Fig. 16. The ignition delay definition was
847 considered plausible as the temperatures at the end of the assigned ignition delay were
848 beyond the temperature point for gas fuel mixtures combustion.

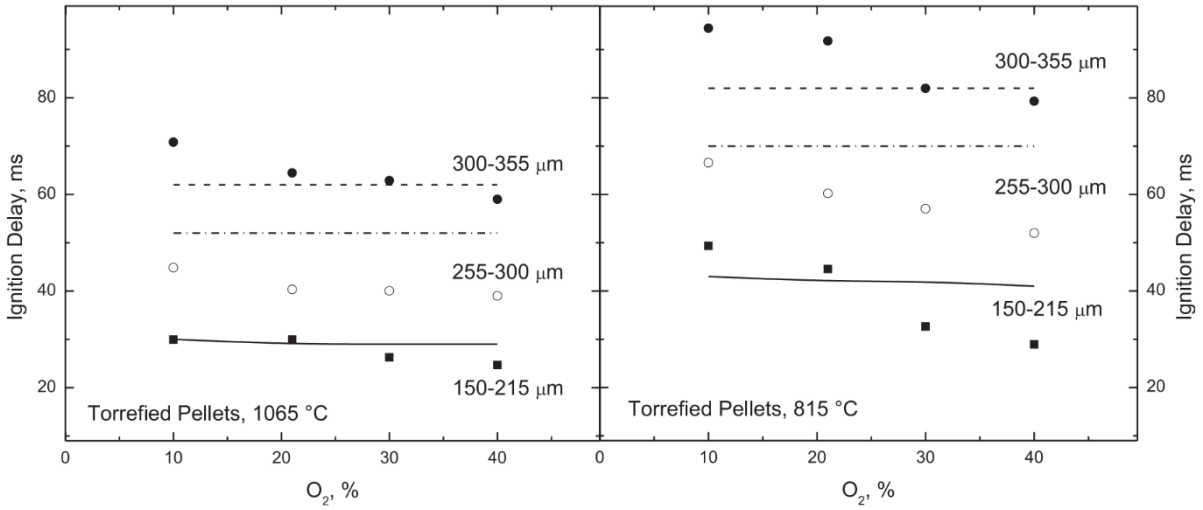

849

850 Fig. 16 Ignition delays for torrefied wood pellets, left: 1065ºC, right: 815ºC for different
851 particle sizes. Reprinted with permission from [108].

852 Rieth et al. [107] performed a direct numerical (DNS) simulation of a 3-D
853 turbulent mixing layer to study the volatile ignition and combustion behavior of biomass.
854 The gas phase was described by a reduced mechanism of 59 species and 462
855 reactions. The ignition delay was measured as the time from the calculation start until
856 the maximum OH radical mass fraction was reached in Cantera batch reactor
857 simulation. There was no reference to experimental data.

858 Table 2 summarizes the numerical ignition onset definitions that were
859 incorporated in solid fuel combustion research under high heating rate conditions.

860 Table 2. Summary of numerical ignition determination methods.

Numerical ignition delay indicator	Fuel	Operating conditions	Modeling methods	Ref.

CO mass fraction, CH mass fraction, $\left(\frac{\partial T_p}{\partial t}\right)_{min}$, $\left(\frac{\partial T_g}{\partial t}\right)_{max}$	Biomass	Single pulverized particles, CH_4/air	CFD and 1-D model ,Ranzi model [109–111], GRI3.0	[17]
OH mass fraction	Biomass	Pulverized fuel	In-house LES/DNS code, Reduced gas-phase mechanism	[112]
5 dry-ash-free wt.% of volatile matter	Biomass	Pulverized fuel, O_2/N_2	CBK/E [113], bio-FC [114–117]	[108]

In summary, the definition of ignition delay time to reach 5% daf wt. of volatile matter adopted by Niksa, and the CH mass species temporal evolutions adopted in [17] were found to yield the most accurate biomass ignition characteristics with respect to the experimental measurements. The objective of section 4 is to discuss the most widely applied modeling approaches of the combustion main sub-processes that have an impact on ignition and to assess their efficiency in ignition prediction.

4. Ignition-related biomass conversion modeling

4.1 Biomass combustion process

The models will be described for the following combustion processes:

- Inert heating

- Drying
- Devolatilization
- Gas-phase reactions
- Char conversion

4.1.1 Inert heating

When it comes to inert heating, there are two general modeling approaches. The first approach considers the particle to be spherical and isothermal (the second assumption is valid for pulverized particles and it depends on the Biot number). A simple heat balance is generally applied to relate the change of particle temperature to the convective heat transfer and radiation at the particle surface [118] – Eq. (2). This law is valid when the particle temperature is smaller than the vaporization temperature during which drying begins.

$$m_p c_p \frac{dT_p}{dt} = Q_c + Q_r \quad (2)$$

Where m_p – particle mass, c_p – particle specific heat, Q_c – heat due to convection, Qr – heat due to radiation

The second approach – Eq. (3) considers thermal gradients within particles [119]. For example, Gubba et al. [118] developed the model that combined the effect of conductive heat transfer to and from the particle, where thermal gradients took place only in radial directions.

$$\frac{1}{\alpha}\frac{\partial T}{\partial t} + \frac{q}{k}\frac{\partial \rho_p}{\partial t} = \frac{\partial^2 T}{\partial r^2} + \frac{p}{r}\frac{\partial T}{\partial r} \quad (3)$$

Where: α – thermal emissivity, T – local temperature, t – time, q – heat generation/heat loss, k -thermal conductivity, r -radial coordinate, p – shape factor.

The second component of Eq. (3) can be considered during drying, devolatilization or char conversion as mass losses and heat generation/heat loss are expected.

The effect of particle temperature gradient can have a substantial effect on the ignition delay not only during inert heating, but during the entire combustion process that involves all stages. For instance, thermal behavior using spherical and isothermal particle approximations was found to be inaccurate for non-spherical particles larger than 200-300 μm [120]. Fig. 17 illustrates the temperature profile in a pyrolyzing wet wood cylinder of diameter 25.1 mm, in which a substantial temperature gradient away from the particle center could be observed. This potentially affects the moisture release and pyrolysis dynamics thus resulting in a much different ignition behavior.

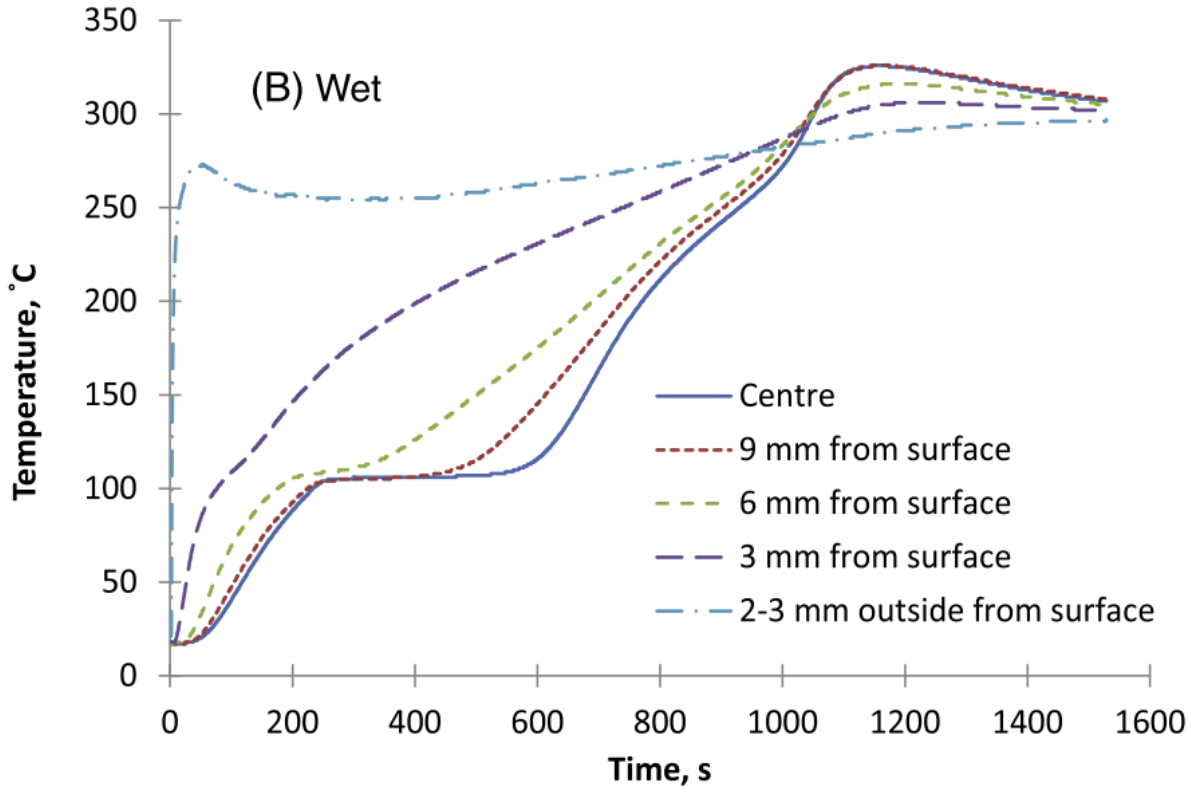

Fig. 17 Temperature profile in a pyrolyzing wet wood cylinder with a diameter of 25.1 mm and a moisture content of 20%. Reprinted with permission from [121].

906 *4.1.2 Particle drying*

907 There are several simple one-step models generally applied in the literature,
908 namely the heat flux model [120,122], the equilibrium model [123], and the chemical
909 reaction model [123]. In the heat flux model, heat transfer to the particle governs the
910 evaporation process. The main assumption of the model is based on the infinitely thin
911 region where evaporation takes place and at the normal water boiling point. Apart from
912 heat transfer to the particle, there is also a mass transfer inside the particle. As regards
913 the chemical reaction model, the drying rate is expressed by applying the temperature-
914 dependent Arrhenius relation. Even though the model is robust and numerically stable,
915 it cannot predict condensation. Moreover, all these models do not take into account
916 the free water movement. Such an assumption limits the validity of the models for initial
917 moisture contents below the free water continuity point [124]. The models prediction
918 capabilities of the evaporation rate have been investigated by Fatehi and Bai [125].
919 For biomass fuels with large moisture content, inaccurately predicted evaporation rate
920 can lead to a misprediction of the particle heating rate at the first stages of combustion.

921 *4.1.3 Devolatilization*

922 Currently, the biomass pyrolysis is generally modeled as the weighted sum of the
923 reference biomass components (cellulose, hemicellulose, lignin) [126] where a
924 hypothesis of noninteraction between the three main biomass components is generally
925 assumed. Recent publications indicate, however, that for low heating rates the
926 interaction did happen to occur [127,128]. For example, lignin reduces char formation
927 and encourages production of light compounds from the decomposition of cellulose.
928 The interaction between organic components and inorganic components is generally
929 neglected as well even in the most comprehensive models [129]. The presence of
930 extractives is very often neglected too. This can be a valid assumption for woody

residues. But for nonwoody residues, the extractives content can be higher than 10% [129] thus making it an impactful component on the final volatile yield. High amounts of inorganic compounds can have an inhibiting or catalytic effect on devolatilization. In general, similarly to coal, biomass devolatilization models can be divided into global and detailed approaches. The summary of the models is presented in Table 3.

Table 3. Summary of widely applied devolatilization models.

Model	Short description
	Global models
Single-step first-order (SFOR) [130–133]	$\frac{dV}{dt} = A \cdot exp\left(-\frac{E}{RT}\right) \cdot (V_\infty - V)$ (4) Volatiles V that evolve during the devolatilization process are related to the difference between the current V and the ultimate yield of V_∞. $biomass \xrightarrow{k_1} (1-\alpha_1)char + \alpha_1 volatiles$ (R4)

Competing two-step (C2SM) - Kobayashi [132]	$biomass \xrightarrow{k_2} (1-\alpha_2)char + \alpha_2 volatiles$	(R5)
	$\frac{dV}{dt} = \left(\alpha_1 A_1\, exp\left(-\frac{E_1}{RT_1}\right) + \alpha_2 A_2\, exp\left(-\frac{E_2}{RT_2}\right)\right) \cdot C$	(5)

Mechanism is based on two competing reactions producing char and volatiles from the fuel. One of the reactions predominates at lower heating rates, whereas the other at higher rates.

Distributed activation energy (DAE) [134]	$\frac{dV}{dt} = A \cdot exp\left(\frac{-E_a - \sigma_E Z}{RT}\right) \cdot (V_\infty - V)$	(6)
	$Z = erfinv\left(1 - 2 \cdot (V_\infty - V)\right)$	(7)

A variable parameter of activation energy is proposed as a function of extent of reaction. E_a - mean activation energy,

σE - standard deviation

A detailed description of the DAE model, including its history, can be found in the work by Cai et al [135].

Three parallel-reaction (3PM) model [136]	$\frac{dm_i}{dt} = k_i(VM_i - V_{g,i})$	(8)

$$VM_i = VM(1 - C_i) \quad (9)$$

	In the 3PM model, biomass is treated as a mixture of cellulose, hemicellulose and lignin. The total weight loss of each component is described by SFOR. For the 3PM model, the volatile matter amount is corrected using the fraction of char produce
	Phenomenological network models
FG-biomass [137]	Modified FG-DVC [138] model making it suitable for pyrolysis modeling of agricultural and forestry feedstocks.
Bio-CPD [127,139]	The biomass chemical percolation devolatilization model is based on the characteristics of a biomass obtained through a 13-C NMR spectroscopy
Bio-FLASHCHAIN [114–117]	Biomass is represented as chain polymers of cellulose and lignin-like polymers. The original chain statistics developed for FLASHCHAIN are also used in bio-FC.
Ranzi's mechanism [109–111]	A mechanist approach based on conventional multistep devolatilization models of lignin, cellulose

	and hemicellulose which predicts the yields and lumped composition of tar, gases and carbonized residue.
Anca-Couce's-Ranzi's mechanism [140]	The model is based on the aforementioned Ranzi's mechanism. The improvement of this mechanism considers the presence of heterogeneous secondary charring reactions during pyrolysis. In these reactions, char is produced with other primary products from biomass pyrolysis. The adapted (RAC) scheme was applied to fixed-bed pyrolysis and torrefaction [141–143].

The global models are easy to implement and have an associated reduced computational cost. The process is represented by an overall reaction rate that determines the yield of lumped products. Kinetic parameters required can be obtained experimentally, using such techniques as TGA, FTIR or MS. However, in order to have specific and precise information regarding the volatiles release rate, volatile yield, and ignition characteristics these models lack extreme accuracy. Classical lumped kinetic models are not able to simulate the structural changes during pyrolysis. These approaches were also found to be less accurate in predicting tar yields, volatile gases and char. Due to specific kinetic parameters, these models are also applicable only to specific data range. Therefore for higher accuracy, detailed mechanisms are required. The global devolatilization model share some specific features that deteriorate the predictive capabilities of ignition: a) final volatile yield and composition. For global models, the yield and composition tend to be provided a priori. They are determined

either on the basis of proximate and ultimate analysis and elemental mass balance, from other literature, from experimental results, or from detailed devolatilization models, b) the global models usually consider only primary devolatilization reactions, whereas secondary reactions are neglected, c) the release rate of volatiles. It is evident that the more adjustable parameters the model has, the more accurate it can be. The most important and the most basic adjustable parameters in global models are the pre-exponential factor and activation energy (e.g. SFOR). In the Kobayashi model, there are two sets of pre-exponential factors and activation energies, but also two stoichiometric coefficients which correspond to the volatile yield at low and high heating rates. Therefore, from the mathematical point of view, the Kobayashi model is expected to be a much more accurate approach, d) with respect to the global models and the release rate of volatiles, the gases are assumed to devolatilize with a constant ratio, but this hypothesis is only reasonable for entrained flow reactors,

Chen et al. [137] developed the FG-biomass model applying the functional-group (FG) model which describes the evolution of the gas species. In contrast with the FG-DVC approach, FG-biomass applies FG sub-mode to describe tar evolution as well. Therefore, the evolution of tars, CH_4, CO, CO_2, or H_2O is described either with one or more FG models. FG model evolution is described with the distributed activation energy (DAEM) approach. Sheng and Azevedo [144] introduced the first version of the bio-CPD model. Chemical structure coefficients were developed for hemicellulose, cellulose, and lignin. Rate coefficients were obtained for bridge breaking, cross-linking, and side-chain release. A correlation was developed that predicted the mass fractions of hemicellulose, cellulose, and lignin on the basis of oxygen to carbon ratio, the hydrogen to carbon ratio, and the volatile matter. The content of hemicellulose is calculated by the difference. This method is referred to as the correlation method.

981 Numerical results were in general agreement with experimental data. Fletcher et al.
982 [127] introduced a different version of the bio-CPD model which is based on the
983 concept of Sheng and Azevedo [144]. Separate devolatilization rates and chemical
984 structures coefficients were obtained for hemicellulose, cellulose, and lignin. Even
985 though percolation lattice structure was applied for each of the three components, a
986 site for cellulose and hemicellulose was defined as anomeric carbon due to no
987 presence of aromatic carbons. Hemicellulose was modeled as an average between
988 glucomannan and xylan. Table 4 and Table 5 present chemical structure parameters
989 and corresponding kinetic constants. Similar to coal, some biomass parameters are
990 obtained directly from nuclear magnetic resonance (NMR) experiments, while some
991 other parameters are determined from the known structures of the main biomass
992 components. During devolatilization, there is a competition between scission and char
993 formation. These reactions are governed by the DAEM model.

994 Table 4. Chemical structure parameters for various biomass fuels [127].

Parameter	Molecular weight per cluster	Molecular weight per side chain	Percent intact bridges	Coordination number
	MW_{cl}	MW_{δ}	P_0	$\sigma + 1$
cellulose	81	22.7	1.0	3.0
Hardwood cellulose	77.5	21.5	1.0	3.0
Softwood cellulose	81	22.7	1.0	3.0
Hardwood lignin	208	39	0.71	3.5
Softwood lignin	186	34	0.71	3.5

Kraft lignin	195	22	0.71	3.5
xylan	85	24	1.0	3.0
glucomannan	96	28	1.0	3.0

995

996 Table 5. CPD kinetic parameters for cellulose, hemicellulose and lignin [127].

Kinetic parameter	Cellulose	Xylan	Glucomannan	lignin
E_b (kcal/mol)	55.4	51.5	51.5	51.5
A_b (s^{-1})	2.0×10^{16}	1.2×10^{20}	55.4	55.4
σ_b (kcal/mol)	4.1	0.1	5.0×10^{19}	5.0×10^{19}
E_g (kcal/mol)	61.2	38.2	7.0×10^{16}	7.0×10^{16}
A_g (s^{-1})	3.0×10^{15}	3.0×10^{15}	1.38	1.38
σ_g (kcal/mol)	8.1	5.0	0.5	0.5
ρ	100	1.08	38.2	38.2
E_{cross} (kcal/mol)	65	65	69	69
A_{cross} (s^{-1})	3.0×10^{15}	3.0×10^{15}	3.0×10^{13}	3.0×10^{13}

997

998 Niksa [117] developed a bio-FLASHCHAIN model which considers biomass to be
999 a mixture of cellulose and a component similar to lignin. The chain macromolecules in
1000 the structure of biomass is described by bridges. They can undergo decomposition by
1001 scission, thus producing a smaller component that can be later released as gas or tars.
1002 Bridges and bridge-scission products can also produce char links that reconnect later
1003 on with the char matrix. The formation of tar is described in analogy to a flash distillation
1004 process. Char devolatilization is accounted for as well. It releases mainly CO and H_2.

The reaction rates for char devolatilization, scission, and condensation were described with distributed activation energy models. Recent publications by Niksa [114–116] utilized bio-FLASHCHAIN theory in validating a modeling framework to accurately predict the total and tar yields from any lignin, the total volatiles yields from any torrefied wood, and the total volatiles yields from torrefied grasses and agricultural residues. Char links replace bridges during torrefaction within macromolecules of both lignin and cellulose. The introduced char links are mainly responsible for volatile yield reduction due to torrefaction. They are estimated based on ultimate analysis. In [145], Niksa developed a phenomenological reaction mechanism for the devolatilization of pure cellulose. Eventually, the goal was to develop a devolatilization mechanism for any form of whole biomass.

Ranzi et al. [109–111] developed the Bio-PoliMi mechanism which is based on conventional multistep pyrolysis models of cellulose, hemicellulose, and lignin, and predicts the yield and lumped composition of the gas, tars, and carbonized residue. 46 representative species are accounted for in the model. Simplified mechanisms are developed for each biomass component. The biomass reference components are evaluated on the basis of the triangulation method. Five different components are taken into account. Cellulose, hemicellulose, and three lignin species (lignin-H, lignin-O, lignin-C). A combination of three components as a representation of lignin is justified by the complexity of its composition. The hydrogen/carbon ratio and oxygen/carbon ratio of three reference fuels are defined as linear combinations of the five aforementioned components, defining a triangle. As a result, any biomass fuel located in the range of carbon and hydrogen encompassed by triangle vertices can be described as a linear combination of the reference fuels. Secondary or successive gas-phase reactions of the released species are also accounted for and are coupled to a

more general pyrolysis kinetic scheme. Eventually, the proposed mechanism provided correct results in micro-TGA experiments and for product composition in fast pyrolysis experiments [146].

The improved Ranzi's mechanism by Anca-Couce [140] accounts for the presence of heterogeneous secondary charring reactions where char is produced along with the gases. The implementation of secondary charring reactions can predict the evolution of the heat of pyrolysis for different conditions. The model was able to describe the heat evolution in micro-TGA-DSC experiments where pyrolysis was endothermic and exothermic.

Most of the described biomass devolatilization models are derived from coal devolatilization models. The main limitation of coal devolatilization models in biomass modeling is the difference in structure between the two fuels. While coal consists mainly of polyaromatic compounds, which is to some extent true for lignin, two biomass other components, namely cellulose and hemicellulose resemble chains. The structure difference will therefore impose greater uncertainty of coal devolatilization models application in biomass modeling.

Rabacal et al. [126] applied two detailed biomass pyrolysis mechanisms, namely the bio-CPD model and the bio-PoliMi model to predict pyrolysis yields of two biomass fuels in high heating rate conditions. On the basis of Figure 18, one can observe differences in terms of the volatiles release rate and the total volatile yield between the two models. The bio-PoliMi approach exhibits the impact of the operating temperature on the final yield. The bio-CPD model, with respect to bio-PoliMi, presents a change in slope of the volatiles release rate which corresponds to the release of hemicellulose. Both correlation and triangulation methods are insensitive to the volatile yield

predictions. The bio-CPD model shows better agreement with experimental data although both approaches underpredict the final yield.

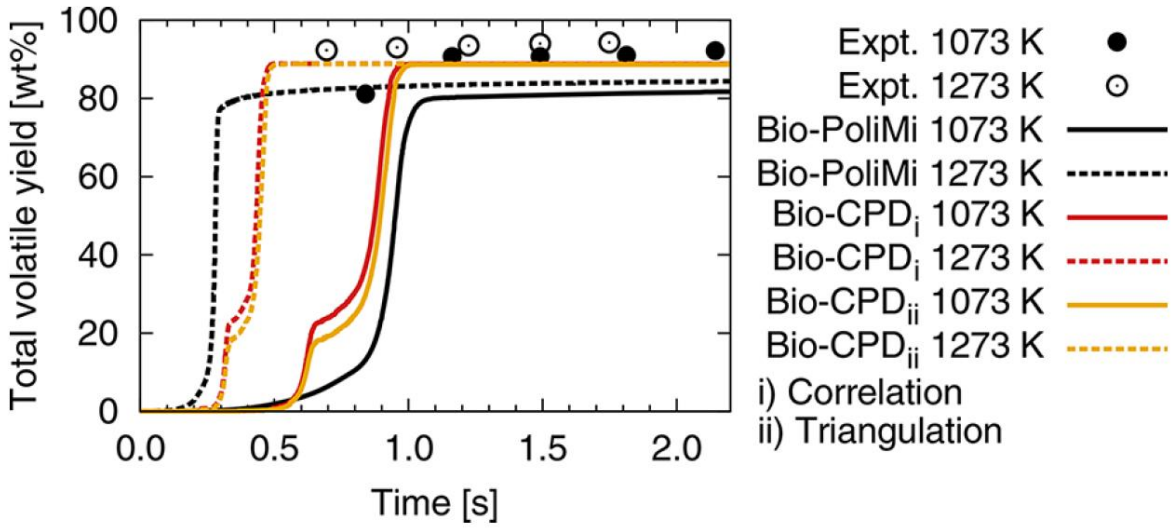

Fig. 18 Total volatile yield of sawdust at 1073 K and 1273 K. Reprinted with permission from [126].

Ferreiro et al. [136] examined the SFOR model and the 3PM model in slow pyrolysis. It turned out that while SFOR captured the general pyrolysis behavior in a reasonable way, the 3PM model was able to predict correctly the maximum devolatilization rates for all of the examined biomass fuels. However, SFOR considered only one biomass component which resulted in three fitting parameters (pre-exponential factor, activation energy, and temperature exponent). In the 3PM model, three biomass components were considered and this resulted in nine fitting parameters. This explains the accuracy of the models.

To sum up, there are not many publications in the field that would thoroughly examine the capabilities and reliability of the models in terms of the biomass ignition. Further research is required.

4.1.4 Gas-phase chemistry

In combustion modeling, as regards the ignition and flame properties, a wide range of coupled issues is involved:

- Detailed chemistry schemes are necessary to assess the fuel consumption rate, combustion products formation, and pollutants. Detailed information about the chemistry is required to predict ignition or extinction, stabilization together with pollutions.
- Fluid mechanical properties are necessary to be able to describe mixing between reactants and, more generally, all transfer phenomena (heat transfer, molecular diffusion, convection, etc.)
- Radiative heat transfer is generated in the flame by carbon particles and some species.

In this review, the main focus will be laid on the first issue. For details regarding fluid mechanical properties refer to [30], whereas for radiative heat transfer details refer to [103]. The most widely applied detailed chemistry schemes are as follows:

- GRI-Mech [147] is an optimized detailed kinetic mechanism designed to model natural gas and air mixture combustion. All the reaction rate constants were obtained empirically. The mechanism consists of radical reactions. The conditions for which GRI-Mech was optimized are approximately 1000 to 2500 K, 10 Torr to 10 atm, and the equivalence ratio of 0.1-5 for premixed systems [47,147].
- Reduced GRI-Mech [148] – two sets of elementary reactions (19-species reaction set and 22-reaction set) developed by truncation of the original GRI-Mech with the aim of developing a smallest reaction set to closely mimic combustion characteristics predicted by the full mechanism.

- CRECK [149–152] – the detailed kinetic mechanism that is provided by the CRECK modeling group at Politecnico de Milano. For instance, there is a C1-C3 mechanism, where the fuel is CH_4. The mechanism is a radical reaction approach which consists of 114 species and 1999 reactions.
- Reduced CRECK mechanism [153,154] –reduced models have been developed in order to closely mimic the combustion behavior of detailed approaches.

The second group of chemistry models constitute global reaction approaches.where kinetic parameters are generally taken from other literature, namely from two global mechanisms: Westbrook and Dryer [155,156] mechanism and Jones and Lindstedt mechanism [157]. Although such an approach can provide a reasonable description of the process, one should not expect to obtain extreme accuracy. It was proven that detailed models were found to provide better agreement with respect to the experimental data. As regards the ignition, all the above gas chemistry models predict the gas species evolution with respect to time and space. For advanced approaches like GRI-Mech or CRECK, it is possible to obtain the yield of CH or OH radicals, whereas global models are only able to provide the yield of e.g. CO or CO_2. Moreover, the effect of neglecting complex chemistry is that the gas temperature tends to be over-predicted. It is because there are no radicals which would carry energy that could be converted to heat. Lysenko et al. [158] carried numerical simulations of the Sandia flame CHNa applying the eddy dissipation concept (EDC) with the detailed GRI-Mech chemistry, the steady laminar flamelet (SLF) model, and the probability density function (PDF). The P-1 radiation model [159] and, in one case, no radiation model was investigated. The Sandia flame CHNa has the advantage over simple geometries,

which makes it possible to focus on the role of chemical kinetics and the role of turbulence in numerical simulations. Fig. 19 illustrates the mean temperature and composition profiles (H_2 and CO_2) along the axis. Several models were analyzed. The FFR model is the mechanism developed by Frassoldati, Faravelli, and Ranzi, specifically for the applications of syngas combustion [160]. The general match between numerical results and experimental data was reasonable and satisfactory. One may also observe that there is a strong interrelation between flame temperature and species prediction. An over-prediction of the flame temperature may be caused by:

- Neglection of the radiative heat losses and under-prediction of the dissipation rate, according to Hewson and Kerstein [161] – possible temp. overprediction (60 – 240 K)
- According to Cuoci et al. [162], the thermal radiation effect should only account for 30-40K of possible peak temperature over-prediction. In [158], the impact of thermal radiation on the peak temperature was more significant – 130K. This could be attributed to the simple P-1 [159] radiation model.

As for the gas composition, even though a satisfactory agreement was obtained no model provided extreme accuracy.

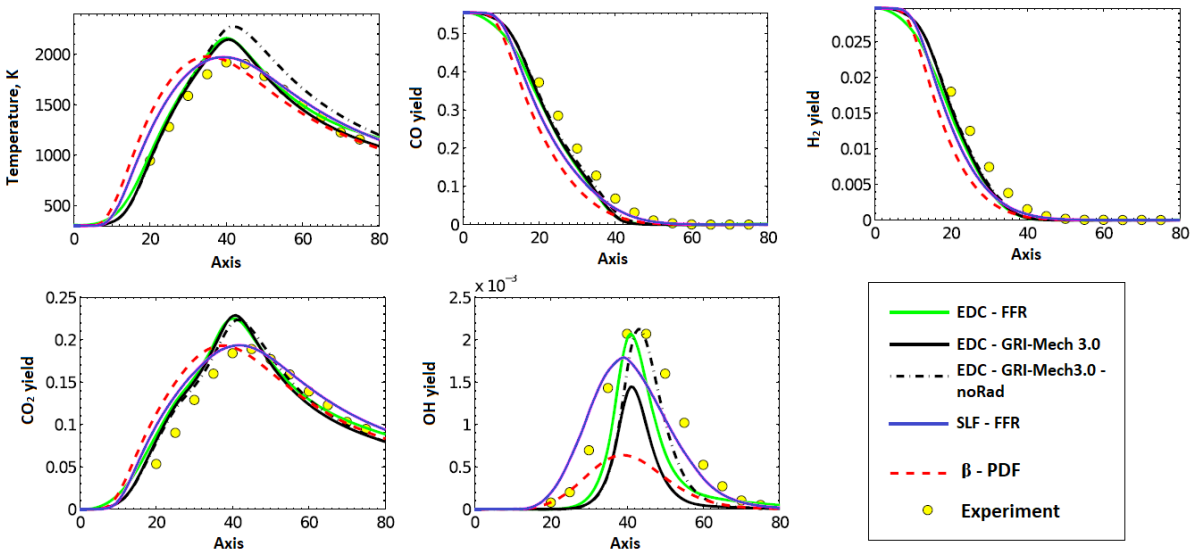

Fig. 19 Exemplary results - mean temperature and composition profiles along the axis for the Sandia flame CHNa. Adapted from [158].

4.1.5 Film diffusion – external transport

In char combustion, external transport processes play a notable role, especially, at very high temperatures, where heterogeneous ignition tends to occur, and where film diffusion limits the reaction rate (Regime III). Film diffusion takes into account the gas transport from the bulk phase to the outer particle surface. The transport takes place via convection and molecular diffusion. While the former dominates in turbulent flows, the latter controls laminar flows. The outer particle surface and the bulk phase are separated from each other by the boundary layer. Therefore, it is important to accurately account for homogeneous reactions in the boundary layer which can have a direct effect on the particle temperature and conversion rate. Generally, there are three widely used modeling approaches of film diffusion:

- Single-film model
- Double-film model
- Continuous-film model

Judging by Fig. 20, one can observe that the single-film model assumes that even though CO and O_2 are present in the boundary layer, there is no chemical interaction, whereas, in the double-film model, CO and O_2 react forming CO_2. This will lead to a different particle temperature prediction. In practice, however, the incorporation of double-film models or continuous-film models into CFD would substantially increase the computational effort as it would require the solution of a system of coupled partial differential equations. Therefore, only the single-film approach is generally applied. For more details regarding the models refer to [105].

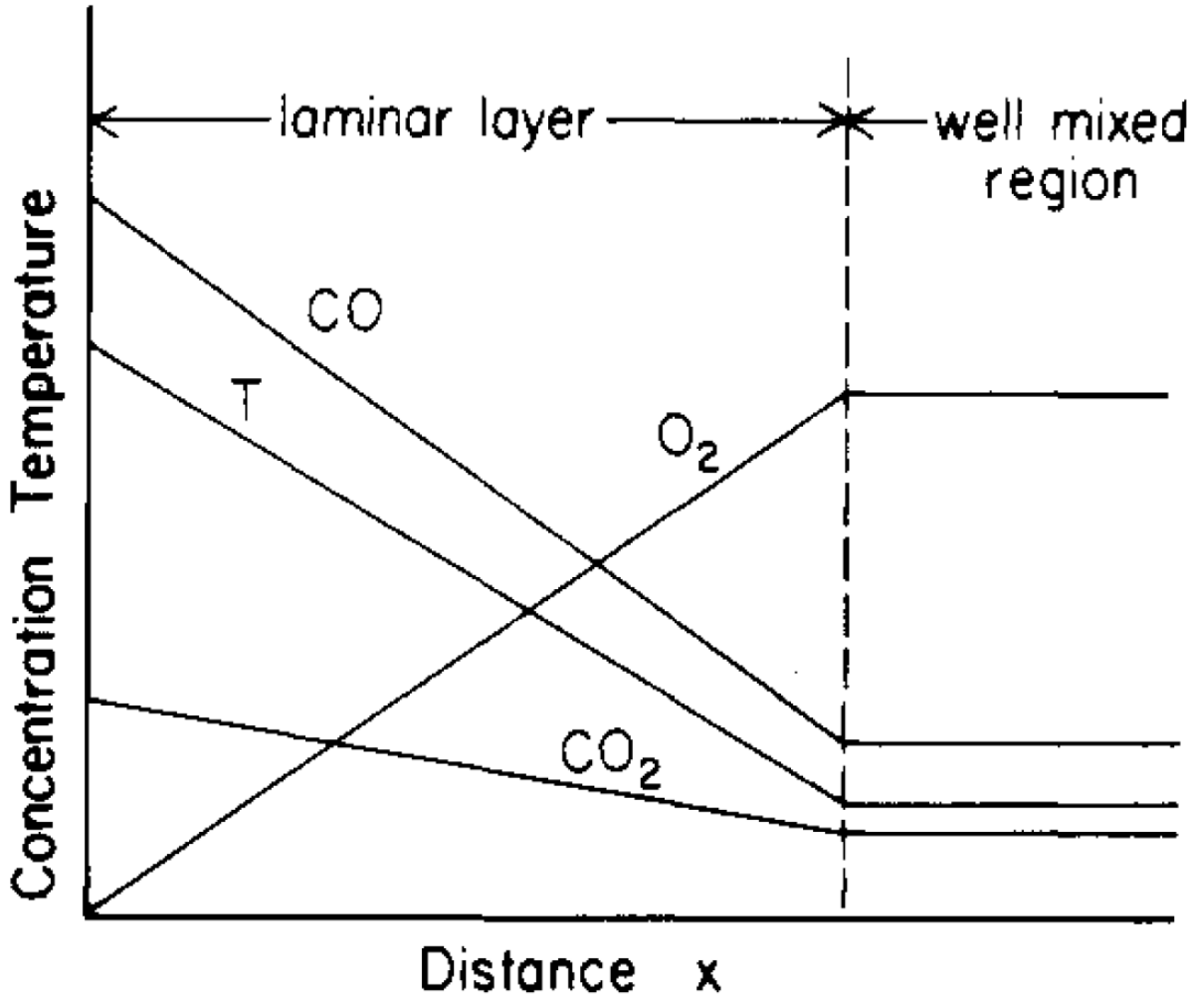

a)

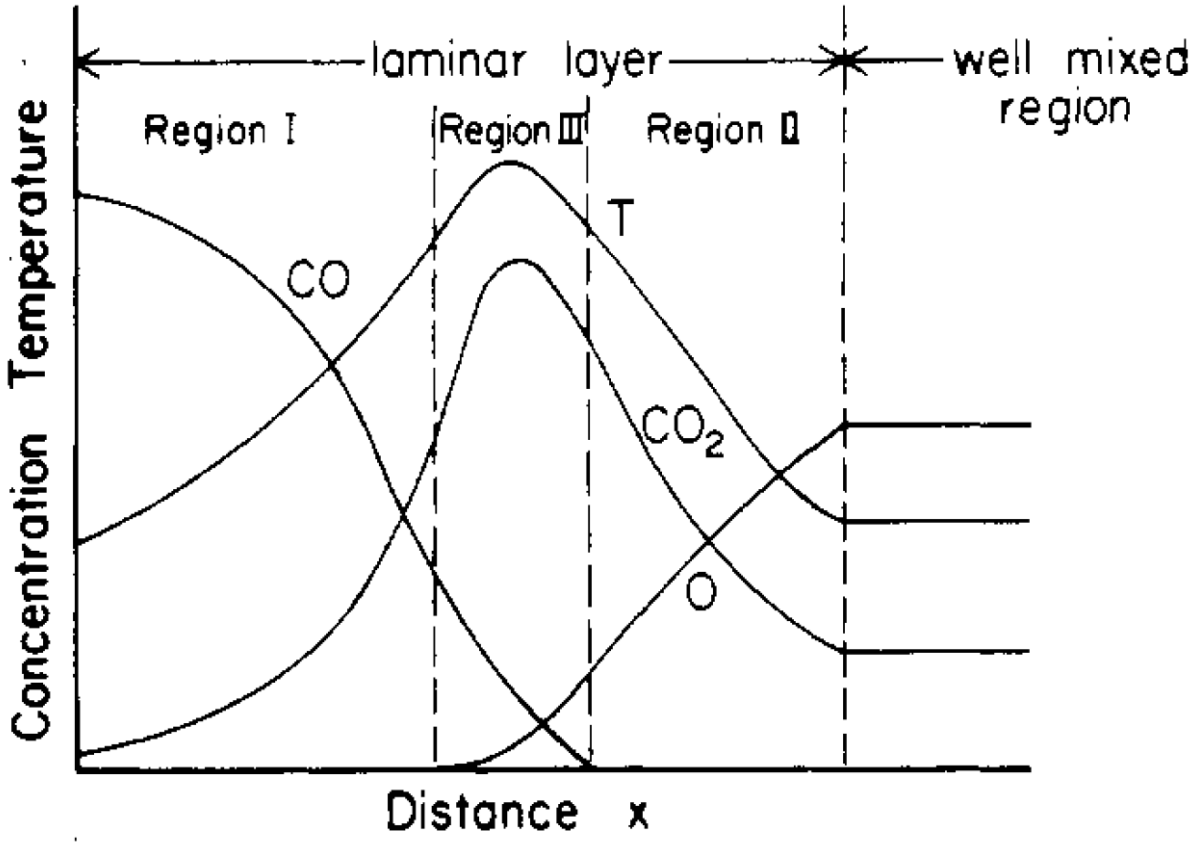

b)

Fig. 20 Schematic concentration of CO, CO_2, O, and temperature profile in laminar layer for a) single-film model, b) double-film model. Reprinted with permission from [163]. Copyright (1977) American Chemical Society.

4.1.6 Char conversion models

Due to high biomass volatile content, a homogeneous ignition is a dominant biomass ignition mechanism [164,165]. However, for specific operating reactor conditions (pulverized biomass particles, high heating rates), biomass can ignite heterogeneously, even before the start of devolatilization. Therefore, even though char conversion does not play a dominant role in homogeneous ignition, it can become impactful during heterogeneous ignition as its reaction rate can directly determine the ignition mechanism. However, it must be emphasized that in the case of a heterogeneous ignition of biomass before devolatilization, instead of the devolatilized

char, non-devolatilized biomass is being ignited and combusted. Therefore, with respect to ignition, the combustion models should account for both devolatilized char combustion and non-devolatilized biomass combustion, depending on the occurrence of ignition. Char conversion of biomass is analogous to that of coal, although biomass reactivity is several orders of magnitude higher, therefore amplifying the effect of gasification reactions. Char combustion from coal has been a subject of research for many years. A detailed review of coal char conversion models can be found in [104,105]. It can be generally assumed that char combustion mechanisms of coal are also applicable for chars originating from lignocellulosic biomass [166]. As for biomass, Di Blasi published a review paper on combustion and gasification rates of lignocellulosic biomass [166]. Among others, the effects of operating conditions (heating rate, pressure, temperature, fuel properties, ash content) on the char reactivity are discussed. The most important aspects influencing the char conversion rate are the char surface area, carbon active sites, the surface accessibility, catalytic effects due to inorganic matter, and the local concentration of the reactant gas species. These char features are extremely difficult to measure via experimental techniques. As a result, the most widely applied approach is based on the global apparent reactivity, where particular char burning characteristics for the given operating conditions are implicitly accounted for. The overall observed reaction rate is measured as:

$$R_{obs} = -\frac{1}{m_c}\frac{dm_c}{dt} = \frac{1}{1-X}\frac{dX}{dt} \quad (10)$$

Where m_c is the current char mass, X is the conversion degree. R is the observed reaction rate and expresses char consumption scaled by the current mass of the remaining char (m). However, char reactivity does not only depend on the kinetics but also on the mass transfer of gases in and out of the biomass particle. The mass transfer

depends on the particle structure which is formed during devolatilization. In this sense, apart from the prediction of gas yield, gas composition, and volatile release rate, devolatilization models should also account for the char structure formation. However, it has been common practice to relate experimental char burning rates to the external char surface area. The model is referred to as the surface-based approach which is based on apparent activation energy and it originates from the Field model [167] and the Baum and Street model [168]. The second approach is a more fundamental one because it utilizes the concept of intrinsic reactivity as set out by Smith [169]. The mathematical formulation of the biomass char conversion models is provided in Table 6. Even though the models were developed in coal combustion studies, they are also widely used for biomass.

Table 6. Summary of biomass char conversion models.

Model	Short description
	Global models
Kinetics/diffusion model	This approach can be represented as a resistance network consisting of kinetic and diffusion resistances. $\frac{dm}{dt} = -\frac{A_p p_{ox}}{\frac{1}{R_{diff}} + \frac{1}{R_{kin}}} \Phi_{en} = -\frac{A_p \rho R T Y_{ox}}{M_{w,ox}} \frac{1}{\frac{1}{R_{diff}} + \frac{1}{R_{kin}}} \Phi_{en}$ (11)

A_p – particle surface area, p_{ox} – partial pressure of oxidant, R_{diff}, R_{kin} – diffusion and kinetic component, respectively. ρ – density, R- universal gas constant, T- temperature, Y_{ox} – oxidant mass fraction, $M_{w,ox}$ – molecular weight of oxidant, Φ_{en} – enhancement factor due to non-sphericity.

Intrinsic model

In the intrinsic model, the observed reaction rate from Eq. (10) can be related with the intrinsic rate in the following way:

$$R_{intr} = \frac{m_c}{\eta m_{c,0} A_s} R_{obs} \tag{12}$$

$\boldsymbol{\eta}$ – effectiveness factor, $m_{c,0}$ – initial char mass, A_s – specific surface area of char particle.

The intrinsic rate can be defined in the following way:

$$R_{intr} = k_s p^n \tag{13}$$

Where k_s is the intrinsic rate coefficient (defined by the Arrhenius expression by means of pre-exponential factor and activation energy), p – partial pressure, n – pressure exponent. Finally, the form for the char consumption rate is as follows:

$$\frac{dm}{dt} = -\eta A_s m_{c,0} k_s p^n \tag{14}$$

Although the oxidation reaction by the intrinsic model through the global nth-order Arrhenius approach, there are more complex methods like the Haynes turnover mechanism [170] where tracking of

	free sites on carbon surface is required, or the semi-global Langmuir-Hinshelwood mechanism [171].
	Phenomenological network models
Carbon burnout kinetics (CBK) [172–175] later modified to CBK/Oxidation (CBK/E) [113] and CBK/Gasification (CBK/G) [176].	The model incorporates the Langmuir-Hinshelwood kinetic approach with random pore model surface area evolution, single film and pore diffusion, thermal annealing, and ash inhibition. As a result, it accurately predicts the low reactivity of unburned carbon, the reactivity loss in the later stages of combustion, inhibition due to mineral matter, and the evolution of the intrinsic surface area. However, the model contains empirical terms for the description of structural development during char conversion of coal which may not be suitable for biomass. Some of the latest studies by Niksa [177,178] extend the application of CBK/G for bio-chars from diverse biomass forms.
Mitchell [179–183] and [184,185]	The char conversion model was developed at Stanford University in the Mitchell group [179–183]. Lately, Tilghman et al. [184,185] extended the model to the conversion of biomass chars in combustion and gasification environments and developed

	reactant-specific effectiveness factor - Thiele modulus relations, along with CO and H_2 inhibition reactions.
CRECK [111,186–191]	In contrast to the models discussed before, devolatilization and char conversion are described in a seamless approach. As regards the model complexity, it resides between the complex network models and the global one-step, two-step, three-step, and DAE models.

5. What one can learn from coal ignition studies?

There are many numerical studies that investigated biomass combustion or biomass co-firing with coal by means of computational fluid dynamics (CFD) [17,125,192–200] or by incorporation of a single-particle approach [20,22,34,120,123,201–208]. Combustion and ignition of particles were also investigated experimentally [38,49,58,164,165,209,210].

Vascellari et al. [211] investigated the ignition of a single coal particle. A comparison was made of time-averaged numerical OH radicals and experimental CH* as a function of particle residence time. The reduced gas-phase mechanism did not include CH species, therefore, OH was applied instead. However, it was reported that additional flamelet simulations with GRI-Mech, which included CH species showed that OH and CH onsets occurred almost instantaneously, but for slightly different values of mixture fraction. As shown in Fig. 21a, in which the grey area stands for the experimentally observed ignition delay, one can conclude that OH concentration yields a reasonable

1229 agreement. Fig. 21b indicates that the temperature increase at 0.034s as the ignition
1230 criterion yields poor agreement with respect to the experimentally determined ignition
1231 and it should not be used in numerical simulations as the ignition onset indicator.

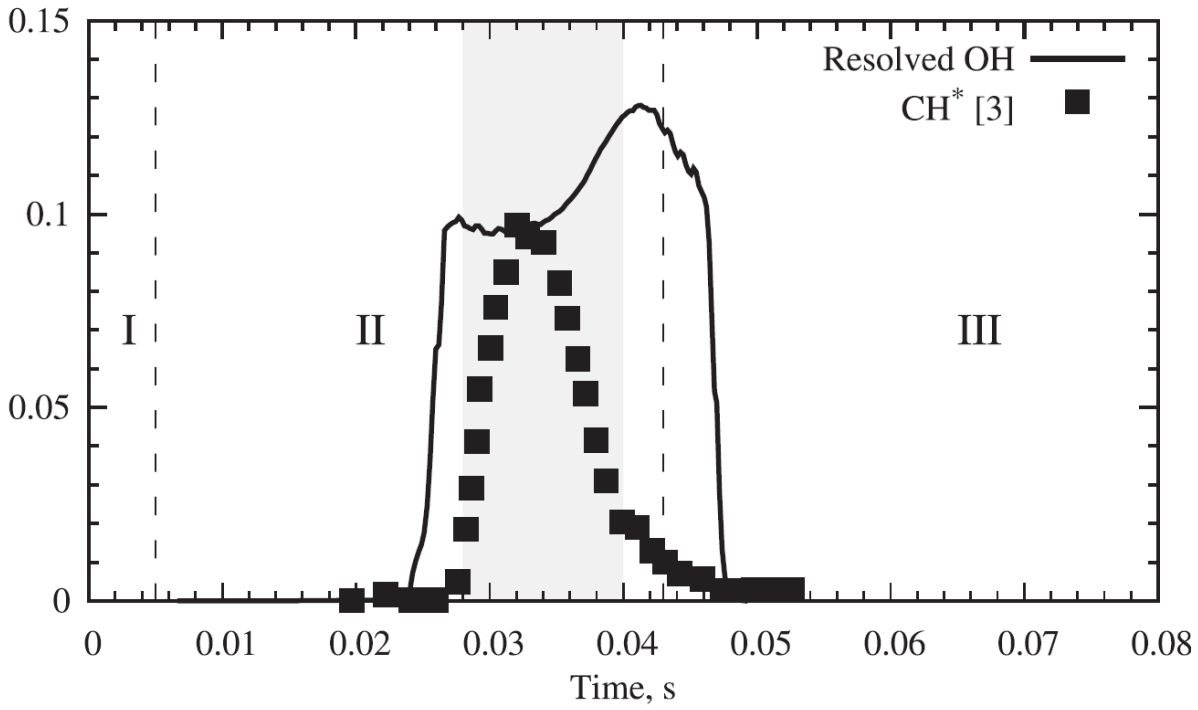

1232

a)

1233

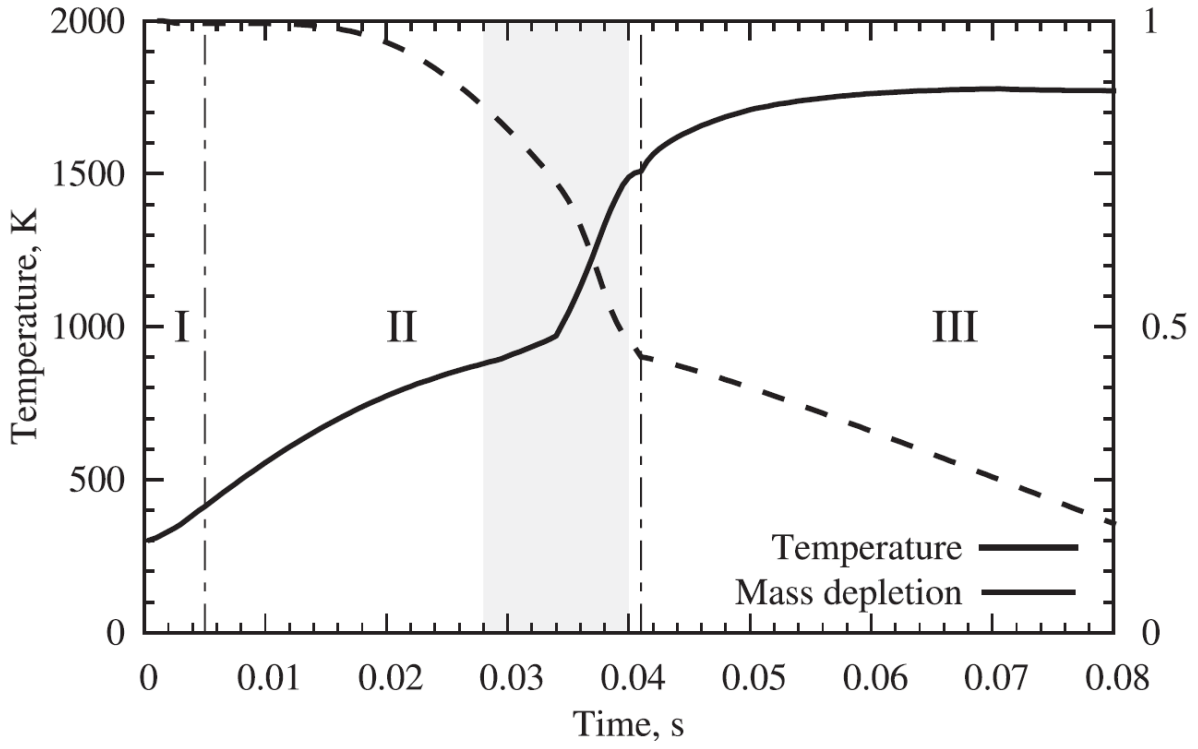

b)

Fig. 21 a) Time-averaged numerical OH radicals and experimental CH* as a function of coal particle residence time I – drying, II – devolatilization, III – char combustion, b) Particle temperature and non-dimensional mass depletion. Reprinted with permission from [211].

Goshayeshi and Sutherland [47] investigated the ignition delay of coal for different criteria of ignition onset definition. Based on the experimental results applied in their work, the CH* emission is considered as an indicator of ignition, with the ignition point defined as 50% of the maximum CH* signal. Judging their results presented in Fig. 22, it can be observed there is a substantial impact of different criteria of ignition onset definition on the ignition delay. The bars represent 25% - 75% of the maximum mass fraction in species profiles. Numerical application of CH mass fraction at the value of 50% of its maximum as a criterion provides the best agreement with experimental data.

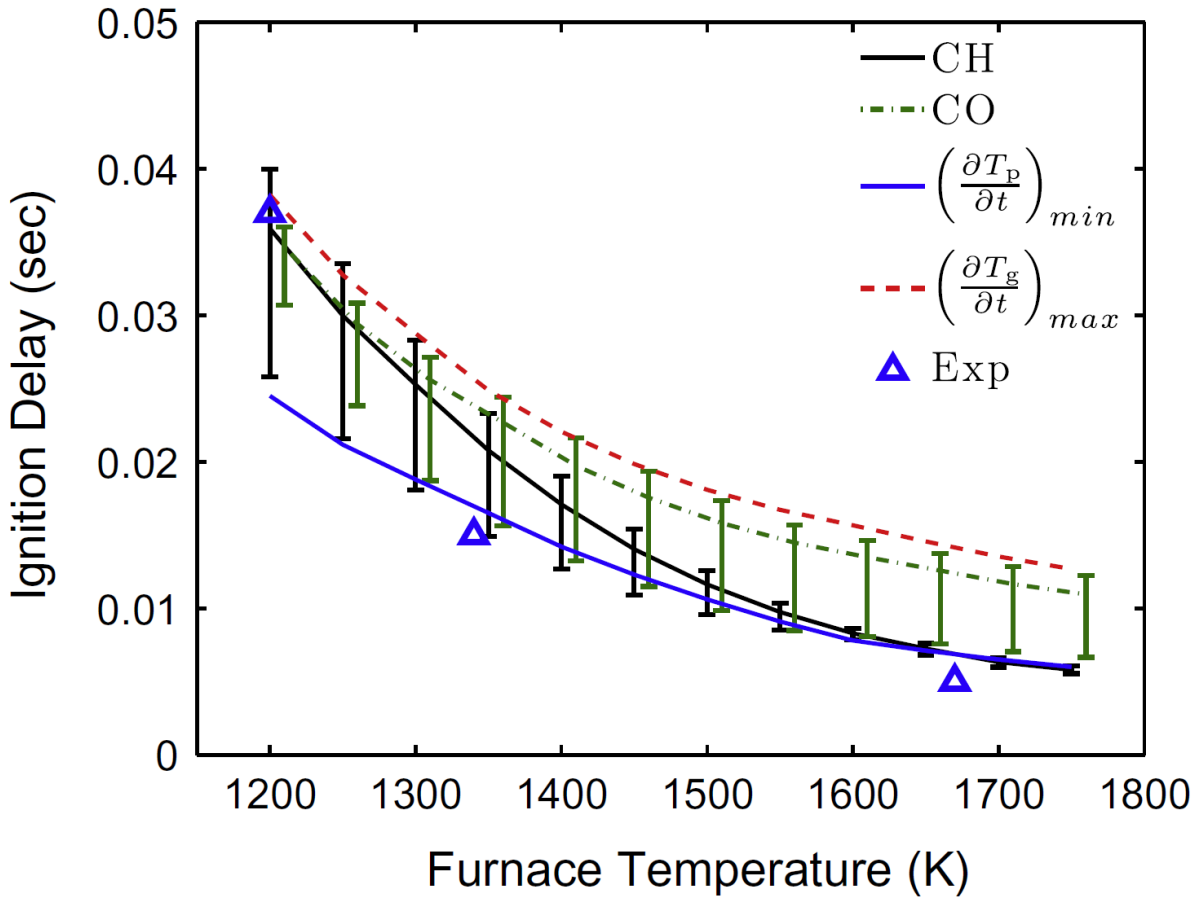

Fig. 22 Ignition delay of coal for different criteria. Species criteria relate to the time at which species mass fractions reach 50% of their maximum. Reprinted with permission from [47].

Goshayeshi and Sutherland [47] studied the impact of both coal devolatilization and gas-phase chemistry on the ignition delay, and indicated that ignition takes place during the release of volatile matter where both devolatilization and gas-phase reactions play a key role, while heterogeneous reactions are of minor importance – Fig. 23.

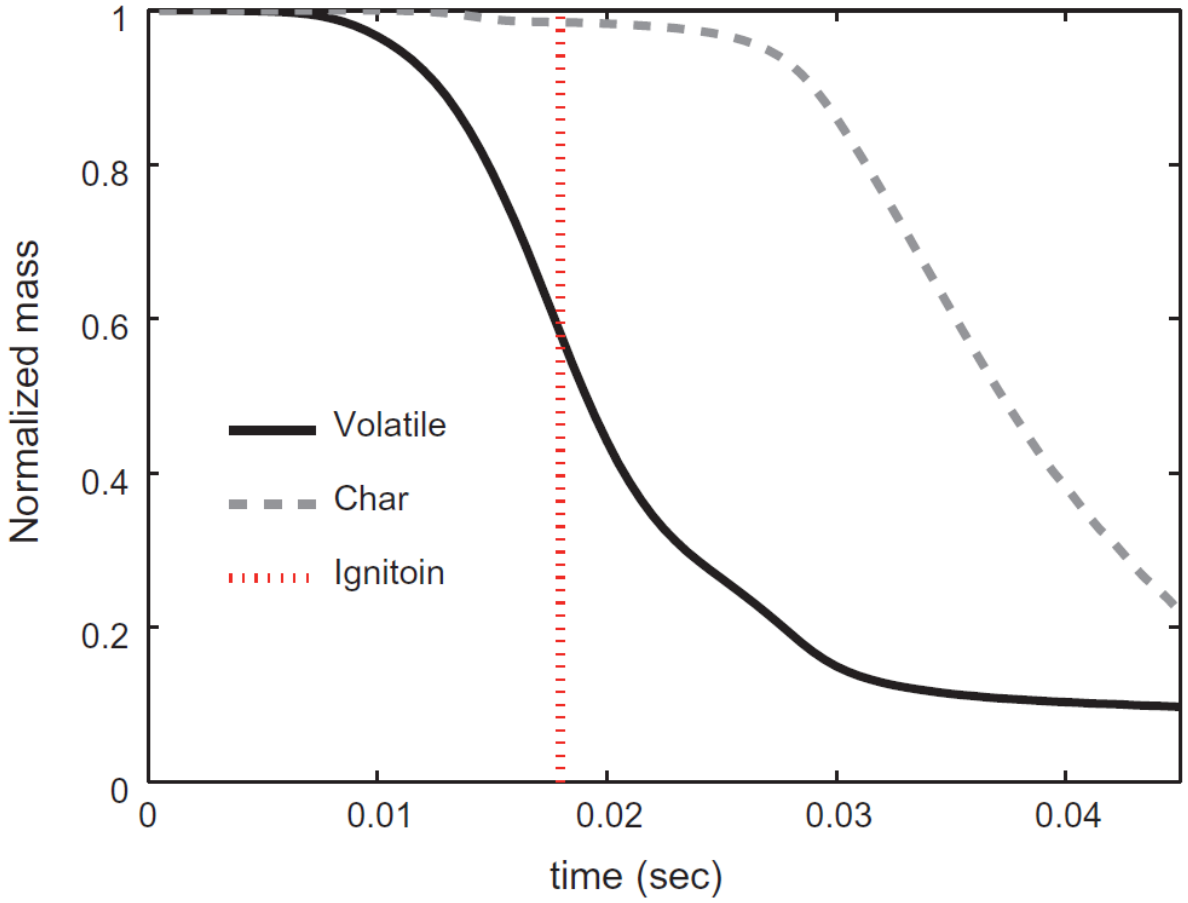

Fig. 23 Volatile and char content in coal particle with respect to time. Reprinted with permission from [47].

Goshayeshi and Sutherland [47] incorporated two widely applied devolatilization models, namely the competing two-step mechanism (C2SM) [132], commonly referred to as the Kobayashi model, and the complex chemical percolation devolatilization (CPD) [139,212–214] model. While the former model is the global approach that considers two parallel reactions governing devolatilization where one reaction dominates at low heating rates, whereas the second reaction dominates at high heating rates, the latter approach is a network model accounting for fuel structure characterization. The gas phase was modeled by the detailed chemical kinetics based on GRI-Mech 3.0 (GRI3.0) [147]. In the C2SM approach, the devolatilization decomposition reaction took the following form:

$$CH_xO_y \rightarrow yCO + \frac{x+z-1}{2}H_2 + \frac{1-y}{2}C_2H_2 \quad \text{(R6)}$$

where x and z coefficients were calculated on the basis of proximate and ultimate analyses. Kinetic parameters were taken from [215]. In this study, C_2H_2 represents heavy-tar species and its implementation was mainly motivated by its availability in GRI3.0. It was also found that choosing CH_4 instead of C_2H_2 resulted in no change in the ignition delay. Fig. 24 shows a substantial influence of devolatilization on the ignition delay. Knowing that in CFD models, volatiles composition and the kinetic parameters are the major input parameters defining devolatilization models, there are considered to be extremely important factors in ignition characteristics. It is also evident that the complex approach yields more accurate results than the global C2SM mechanism.

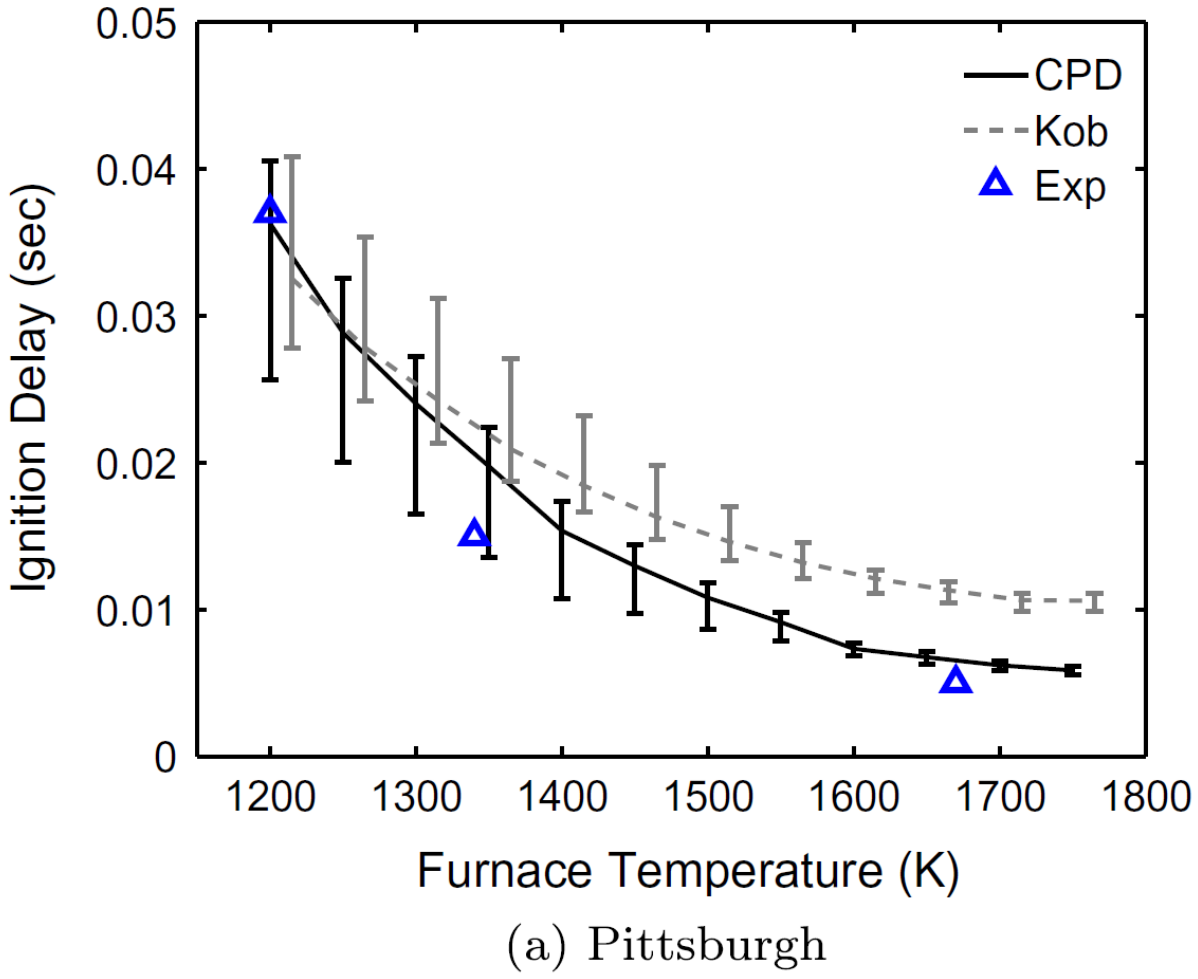

(a) Pittsburgh

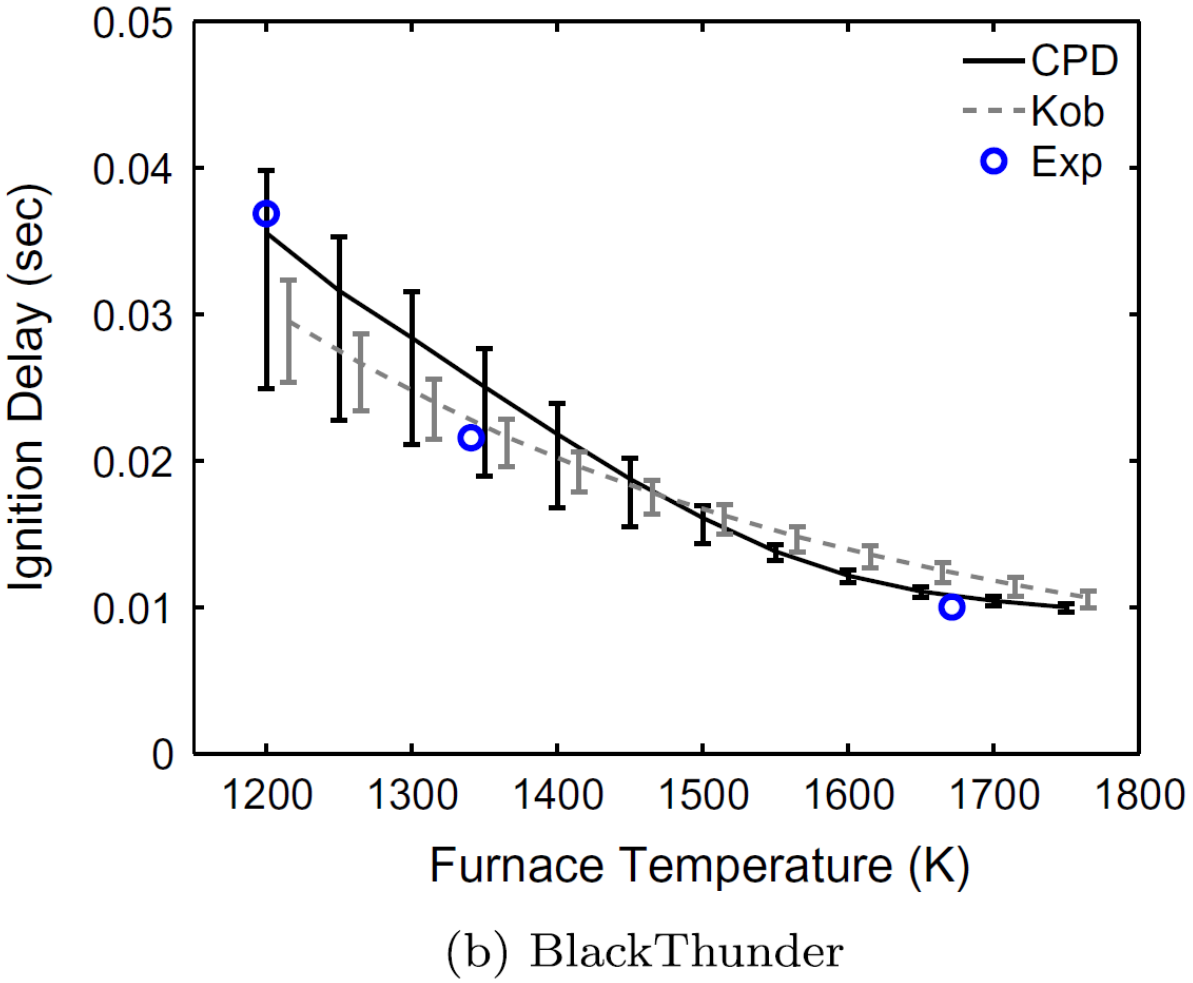

Fig. 24 Effect of devolatilization models on ignition delay. a) Pittsburg coal, b) Blackthunder coal. In both models, detailed gas-phase chemistry was applied. Reprinted with permission from [47].

Goshayeshi and Sutherland [47] studied also the impact of two gas-phase chemistry models in terms of the ignition onset – the GRI-Mech mechanism and the flame-sheet model which assumes infinitely fast chemistry. The results of the analysis are illustrated in Figure 25. One can observe that the impact of investigated gas-phase modeling approaches is substantial. It must be underlined that Fig. 25a considers CH radical species as a measure of ignition onset, whereas in the flame-sheet model, the CO profile at particle position and inflection points are considered. Consequently, these two sub-figures should not be directly compared as they have different criteria for

ignition onset. However, for the flame-sheet chemistry, the inflection points turned out to be in better agreement with experiments than CO mass fractions.

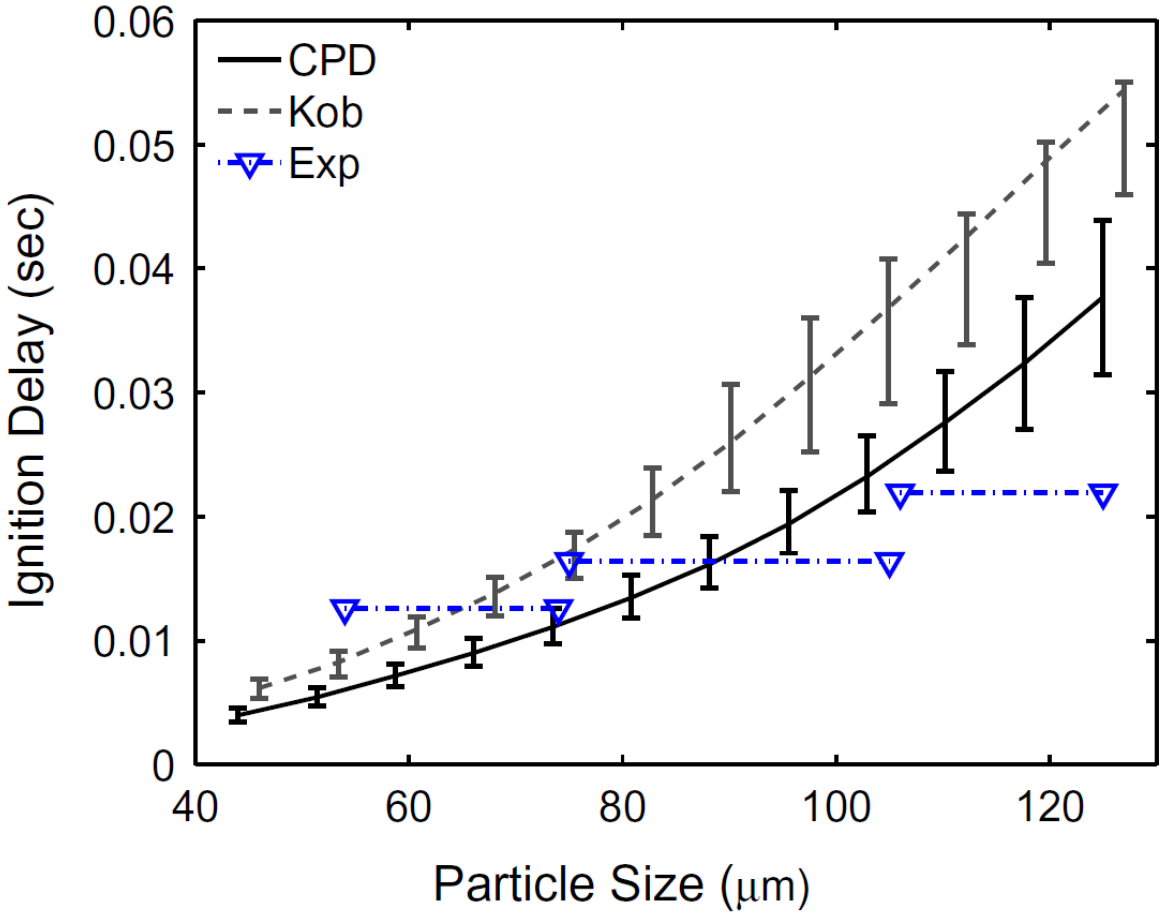

(a) Detailed kinetics

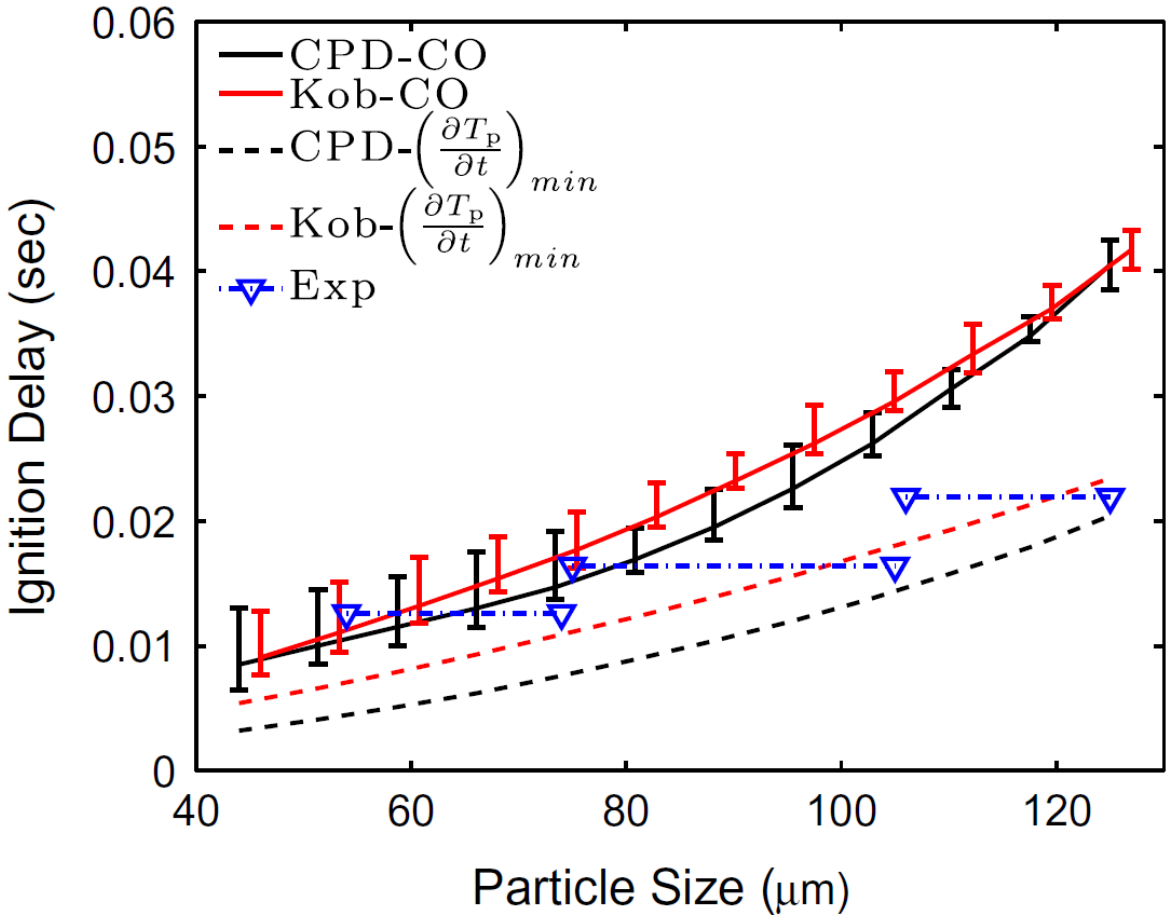

(b) Flame-sheet chemistry

Fig. 25 (a,b) Ignition delay with respect to particle size. 12vol% O_2 and N_2 at 1320K for two gas-phase modelling approaches. Reprinted with permission from [47].

Yuan et al. [216] investigated experimentally and numerically the transition of hetero-homogeneous ignition of dispersed coal particle streams. The particles of 65-74 μm are injected into a Hencken flat-flame burner. The authors have decided to include this particular coal study as it reports a substantial impact of devolatilization on the ignition mode and an analogous study could be carried out for biomass fuels. Fig. 26 depicts the emission signal intensity along the height above burner for three temperatures – 1200 K, 1500 K, 1800 K. One can observe that for the temperature of 1200 K, a monotonous increment before the peak is present, whereas for temperatures of 1500 K and 1800 K, there is a convexity before the peak. In the particle image, for

temperature of 1200 K, flames are separately distributed around individual particles, whereas for temperatures of 1500 K and 1800 K, a forming of coherent volatile flames can be observed. One may attribute these two different signal profiles to the ignition mechanism, either heterogeneous or hetero-homogeneous.

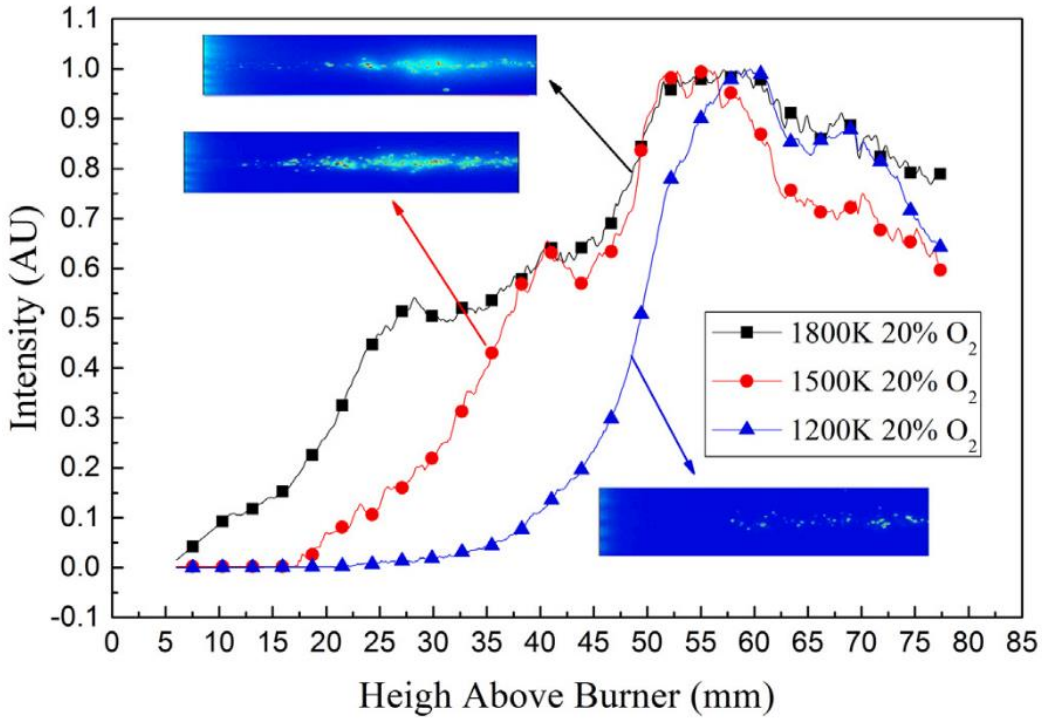

Fig. 26. Signal intensity along the burner height for three temperatures: 1200K, 1500K, 1800K. Reprinted with permission from [216].

Fig. 27a depicts the normalized particle temperature, and the released volatile volume with respect to residence time. Fig. 27b illustrates particle temperature controlled by different heat sources, whereas Fig. 27c shows the pyrolysis rate for three different temperatures. The convection term dominates the heating stage, especially, before ignition whereas the contribution of radiation and chemical reactions before the ignition is insignificant. Based on this assumption and assuming pyrolysis decomposition to be defined in an Arrhenius form [130], the characteristic heating time and pyrolysis times were defined. It was reported that at lower temperatures, the degree of devolatilization

was very low before the ignition indicating a heterogeneous mechanism. At higher temperatures, the devolatilization rate increased resulting in a shift to hetero-homogeneous ignition mode. The research further confirms a substantial impact of pyrolysis dynamics on the ignition mode and the usefulness of incorporating pyrolysis-related parameters in the determination of ignition mechanism.

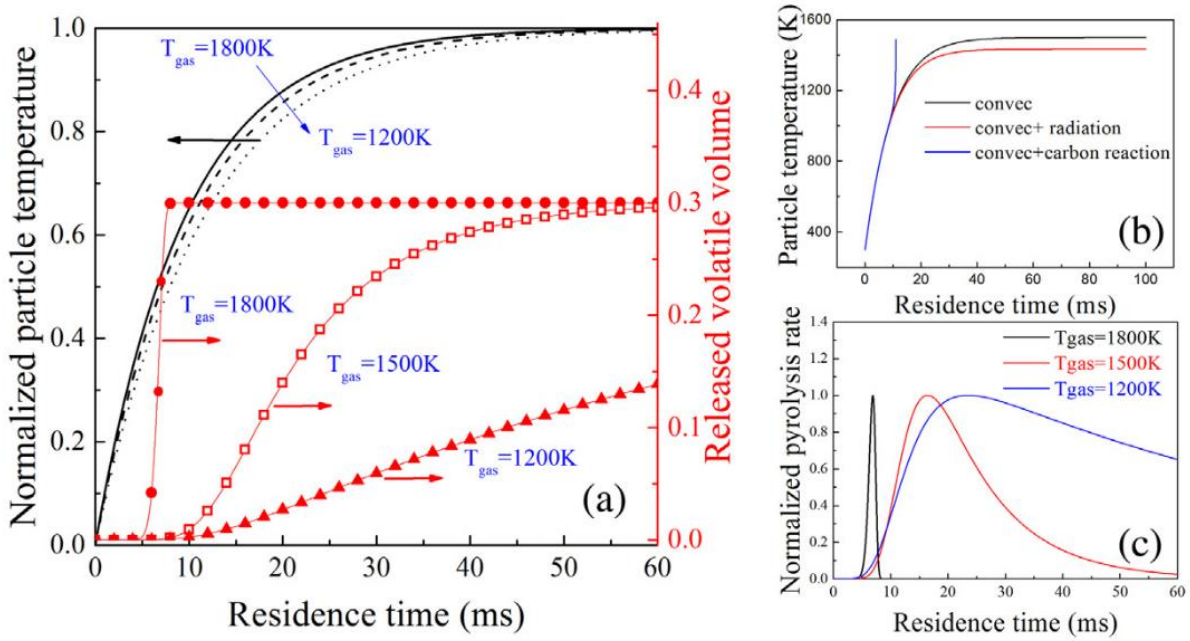

Fig. 27. (a) Normalized particle temperature and released volatile matter, (b) particle temperature controlled by different heat sources, (c) pyrolysis rate. Reprinted with permission from [216].

Jovanovic et al. [217] investigated the influence of homogeneous/heterogeneous ignition/combustion mechanisms on ignition point position during pulverized coal combustion. The default CFD code, like FLUENT [218] assumes that devolatilization and char combustion occur after one another. Thus, in the CFD code, char combustion takes place only after devolatilization is over. In reality, char combustion can occur simultaneously with devolatilization or even before. This combustion sequence becomes very important in the numerical determination of ignition mechanism. In [217],

1338 the criteria for the mechanism during which a particle will ignite are identified by
1339 comparing the reaction rates from Table 7.

1340 Table 7. Main criteria for ignition mechanisms

<table>
<tr><th colspan="3">Conditions for each of three mechanisms</th></tr>
<tr><td>Glowing surface char ignition</td><td>Homogeneous ignition</td><td>Sparking heterogeneous ignition</td></tr>
<tr><td>rate of devolatilization greater than the rate of heterogeneous oxidation of non-devolatilized coal
$r_{devol} > r_{het,coal}$</td><td>rate of devolatilization greater than the rate of heterogeneous oxidation of non-devolatilized coal
$r_{devol} > r_{het,coal}$</td><td rowspan="2">rate of heterogeneous oxidation of non-devolatilized coal greater than the rate of devolatilization
$r_{het,coal} > r_{devol}$</td></tr>
<tr><td>rate of heterogeneous oxidation of char greater than the rate of homogeneous oxidation of volatiles
$r_{het,char} > r_{hom,vol}$</td><td>rate of homogeneous oxidation of volatiles greater than the rate of heterogeneous oxidation of char
$r_{hom,vol} > r_{het,char}$</td></tr>
</table>

1341

1342 Conditions were examined for each tracked particle. For instance, if the second
1343 condition is satisfied, the char combustion reaction will be stopped, while
1344 devolatilization and homogeneous volatiles combustion will take place for the tracked
1345 particle. Inflection points of the particle temperature versus time and particle

temperature versus time length were considered as initial ignition signs. As a result of the applied combustion model, the ignition point position was better predicted than with the standard sequential FLUENT routine.

Xu et al. [219] focused on the competition between the homogeneous and heterogeneous ignition modes investigating the underlying mechanisms of ignition mode transition. They proposed a quantitative index $\Delta t = t_{homo} - t_{hetero}$ to reveal the contributions of these two ignition mechanisms to the whole ignition process. The inflection point criterion for heterogeneous ignition was used, whereas for homogeneous ignition, the assumption was made that the gas temperature of a shell is greater than the temperature of both its adjacent cells. The proposed quantitative index is a new criterion that allows identifying ignition mode by comparing characteristic heterogeneous/homogeneous ignition time.

Zhang et al. [220] proposed a method of ignition mode determination with a transient coal ignition model. The new ignition criteria were developed by comparing the ignition time scales magnitude, including homogeneous and heterogenous delay times and devolatilization start time and end time. Eventually, five ignition regimes were proposed: homogeneous gas-phase, homo-heterogeneous, hetero-homogeneous, heterogeneous ignition of coal particle, and heterogeneous ignition of char particle. Farmand et al. [221] reported that detailed devolatilization models with finite-rate chemistry could correctly capture the homogeneous ignition mode and particles group combustion.

A special attention should be paid to the synergistic effect of co-firing biomass with coal. In general, the synergistic effects on the ignition could be divided into two main categories: thermal characteristics and the released product characteristics. Abbas et al. [222] revealed that early ignition of sawdust volatiles resulted in a faster

devolatilization rate of coal particles. The reason lied in the liberated heat from sawdust combustion that impacted the coal particles through the intensification of both heat transfer and the kinetics of homogeneous and heterogeneous processes. Riaza et al. [95] observed a reduction in the ignition temperatures of both examined coals in all the atmospheres studied when biomass was co-fired. Faúndez et al. [223] revealed that in the case of blending fuels with different content of volatile matter, the ignition of the higher volatile component improves the ignition characteristics of the lower volatile component. However, for blends with comparable volatile content, such fuels compete for the available oxygen and, therefore, the improvement of ignition characteristics would be less remarkable. In the meantime, some studies reported no synergistic effects [224].

With respect to the single-particle modeling approach and CFD studies, it must be emphasized that the ignition behavior of single particles deviates from the stream or cloud ignition due to much more complex phenomena involved [225–227]. Heat and mass transfer exchange in the particle's surroundings become influenced by mutual interactions between particles. It will be therefore of key importance to determine whether the ignition will initiate around individual particles or in a gas mixture, away from particles.

Cassel and Liebman [228] combusted single particles of magnesium and magnesium-aluminum alloys. Depending on the concentration, the ignition temperature of clouds was lower than for single particles. This was explained by the cooperative effect of heat transfer from neighboring reacting particles. For coal studies, experiments have shown that the ignition temperatures could be reduced even by 300^{o}C owing to the cooperative effect associated with particle clouds [228–231]. As a result, the single-particle approach cannot predict the ignition characteristics from real-

life processes with extreme accuracy. For this purpose, a complex CFD numerical model that accounts for the interparticle phenomena would be much more desirable.

In [49,232], it was reported that particle interaction could weaken the devolatilization and delay to volatiles release rate.

The particle number density (PND) or particle concentration was considered a critical parameter to characterize particle group ignition modes. Liu et al. [44,233] studied a wide range of particle concentrations and observed faster ignition in the linear particle streak followed by increased ignition times for larger particle concentrations were higher feeding rates were set.

Tufano et al. [102,112] investigated coal particle heating up, devolatilization, ignition, and volatiles combustion by applying DNS in laminar and turbulent flows. For both single particles and array combustion [112], ignition occurred in the particle wake at very lean conditions where scalar dissipation was low. In [102], it was observed that the increased turbulent intensity delayed the ignition with local extinctions.

Muto et al. [234] simulated the ignition in pulverized coal combustion with a detailed chemical reaction mechanism. A 2-D DNS with a chemistry model consisting of 158 species and 1804 reactions were investigated in a mixing layer. The results indicated that the ignition occurred in the rich mixture fraction condition when the particle was preheated to 2000 K. It was also observed that the evolution of CH and OH radicals up to 10 ms was almost identical.

Recently, Li et al. [235] investigated experimentally single-particle and particle group combustion of coal in a laminar flow reactor using simultaneous volumetric OH-LIF imaging. Fig. 28 illustrates individual snapshots for different particle densities. For the low density case in Fig. 28a, nearly spherical flames can be noticed near individual particles with burnt gas regions forming an apparent joint flame indicating that the

ignition of single particles is not substantially affected at low particle densities. For higher densities, no spherical flames could be noticed indicating that ignition and volatile flame of individual particles interact substantially. The lack of OH signal in the particle group center implies that the mixture is beyond the flammability limit which result in a flame extinction. Judging by the three sub-figures, the increase in particle concentration expands the volatile flame structure and delays the ignition. This can be explained by the greater heat demand for particle groups in comparison with single particles. This results in a lower gas temperature and lower heating rate which delay the particle temperature rise, and consequently, devolatilization.

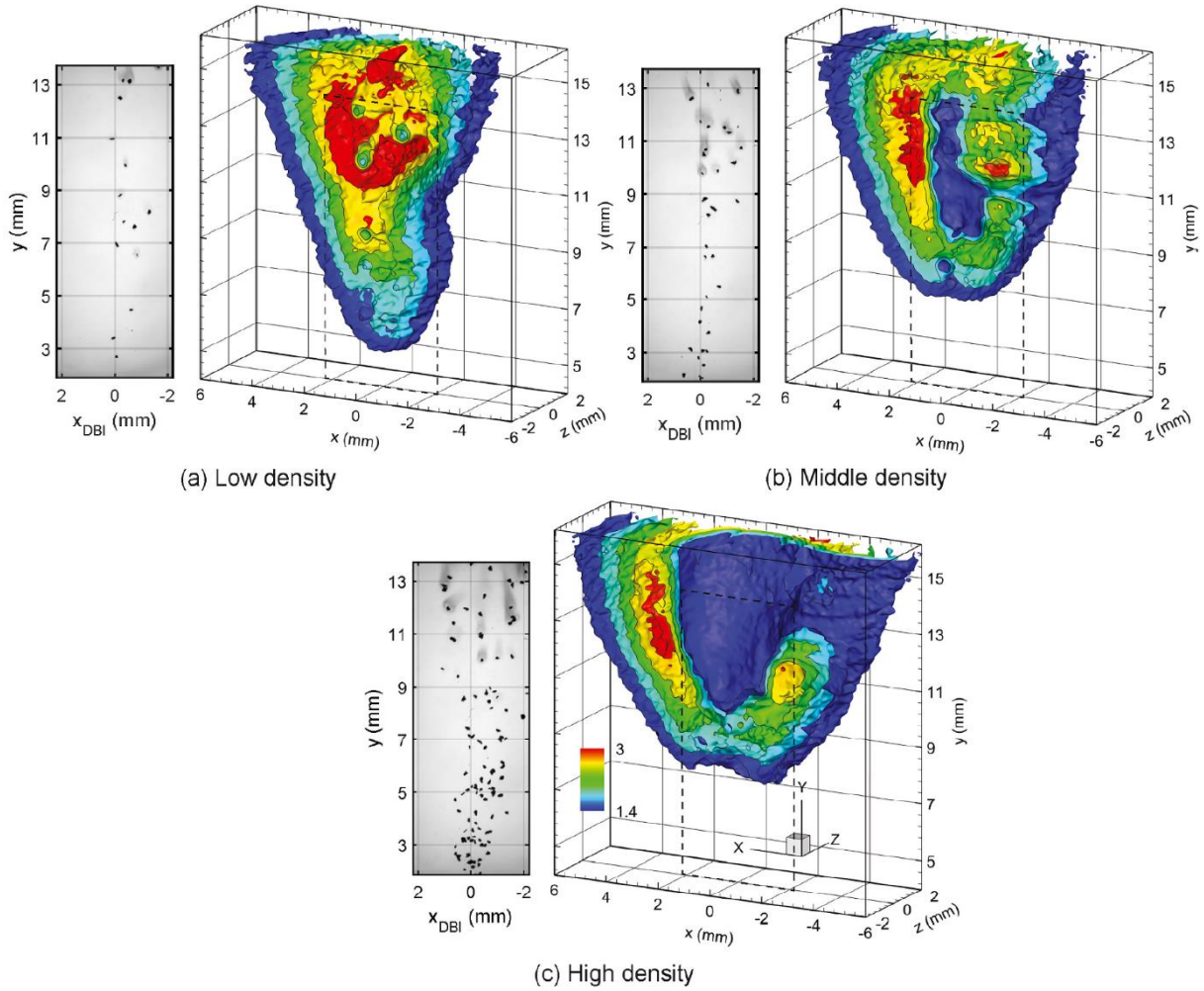

Fig. 28 Snapshots of volatile flame topology for three different particle concentrations. Grey figure from the left: diffuse backlight-illumination (DBI) images providing

information about particle number and location, pictures from the right: 3D volatile flame structure. Reprinted with permission from [235].

Section 5 summarized the state-of-art information from coal ignition-related research. The key findings that are recommendable for studies of biomass ignitions are highlighted below:

- Using CH and OH radicals as ignition indicators for ignition modeling yielded the most accurate ignition delay results against reported experimental data, and the predicted ignition delay using the two indicators occurred almost simultaneously. However, it must be emphasized that the experimental investigation considered mainly CH* chemiluminescence and laser-induced fluorescence of OH radicals (OH-LIF). In contrast to tracked unexcited OH species with the OH-LIF technique, CH* species from chemiluminescence are excited and it poses some level of uncertainty between the numerically determined ignition delay by CH radicals and experimentally determined ignition delay by CH* radicals. So far, current combustion models do not consider excited species.
- The commonly applied models like in CFD are based on the fundamental assumption that particle combustion is governed by the following sequence of processes: inert heating, drying, devolatilization, and char combustion. This implies that char oxidation always occurs after devolatilization which is untrue for the heterogeneous ignition mode where a non-devolatilized coal/biomass is being ignited. As a result, in the future, a modeling routine should be introduced to calculate the competitiveness of main combustion sub-mechanisms and to determine the potential sequence of these mechanisms based on the reactor operating conditions and fuel properties.

- The pyrolysis rate was found to hugely affect ignition characteristics. Pyrolysis time and the degree of pyrolysis were found to be useful modelling parameters in assessing the ignition characteristics.
- More ignition-related research should be carried out with particle streams/clusters as substantial differences could be observed in ignition characteristics between single particles and particle streams.

6. Ignition-related CFD biomass combustion modeling

Due to the same combustion steps for coal and biomass, the modeling framework for these combustion mechanisms remains generally the same for both fuels. However, in comparison with coal, biomass particles are bigger in size, lighter in density, and have a non-spherical shape. These properties will affect the particle motion and conversion in the reactor, which can have a direct impact on ignition. A common modeling practice was to consider biomass particles either as spherical or non-spherical. The non-spherical effects are accounted for by modifying the drag coefficient, or by consideration of rotation. The resultant motion will therefore consider both translation and rotation. For details please refer to [103]. The second issue is a direct consequence of non-sphericity. For instance, Lu et al. [20] observed that the thermal behavior for particle sizes above 200-300 μm of non-spherical shape was poorly predicted by the spherical-particle approximations. Therefore, the first combustion step – inert heating, should be modeled differently with respect to spherical coal particles.

The second combustion step – drying, gains significance for biomass fuels with

relatively large moisture content as it is generally greater than for coals. For instance, a high initial biomass moisture content can reduce the particle heating rate by a factor of 3 to 5 [16]. Knowing that the heating rate strongly impacts the ignition behavior, misprediction of it can lead to an erroneous time frame of the drying process, and consequently, as the combustion steps are usually modeled sequentially, the onset of devolatilization and subsequent combustion steps will also be evaluated incorrectly.

As regards char combustion, biomass char is generally more reactive than coal char. Coal chars also soften and tend to remain spherical, whereas biomass chars tend to keep their irregular shape. This can lead to a partially activated char with a high surface area which contributes to a higher oxygen flux into the particle and higher char consumption rate than spherical coal particles [103].

Fatehi et al. [17], the detailed devolatilization Ranzi's model [109–111] and GRI3.0 [147] mechanism were employed to study biomass ignition characteristics. The results concern the flame with respect to temperature and heat release, reference to gas and particle velocity, and fuel and oxidizer gradients - Figs 29, 30 and 31. Fig. 29 illustrates the experimental CH* emission intensity in the time ranges 30 ms – 110 ms, numerical results of heat release in the same time ranges, and numerical temperature results around the particle for the same time ranges. The investigation considers a pinewood particle with a diameter of 230 μm and an initial velocity of 1 m/s. One can observe that during 30-50 ms, the reaction takes place in a circular shape envelope. It coincides well with experimental images as a uniform CH* distribution can be noticed. The flame circular shape results from the low particle devolatilization rate at the time of 30-50ms, and the inconsiderable changes in velocity between the gas and particle. From 50 ms, the particle velocity starts to decrease due to the effect of gravity – Fig. 30. As a result, the heat release starts to play a dominant role beneath the particle – Fig. 29b where

the circular shape becomes no longer visible. The same behavior can be noticed from the experimental images. In Fig. 31, the β parameter is introduced as a product of CH_4 and O_2 mass fraction gradients ($\beta = \nabla \mathrm{CH}_4 \cdot \nabla O_2$). The blue color signifies that both CH_4 and O_2 have steep gradients toward one another, whereas red color signifies the alignment of gradients. Three key stages of time instances are illustrated. At 30 ms, the gas velocity is lower than the particle velocity (Fig. 30) and the gradient steepness is the biggest at the particle top (Fig. 31). The combustion products flow to the particle bottom. After 42 ms, there is no relative velocity between particles and gas. Therefore, there is a symmetric flame shape. After 70 ms, the particle velocity is lower than the gas velocity (Fig. 30). The oxygen flows toward the particle bottom. The flame is diluted at the particle top due to combustion products and the heat release is consequently lower. In Fig 30, one can also notice a sudden peak in gas velocity which can be attributed to the gas expansion. Such a peak can also be seen during char reaction stage, although this peak is much smoother. The difference in the peaks are related to the volatile flux which is much greater during devolatilization than during char conversion/char combustion. Based on the outcome, one can clearly state that numerical simulations can accurately and reliably reflect the process based on the experimental results.

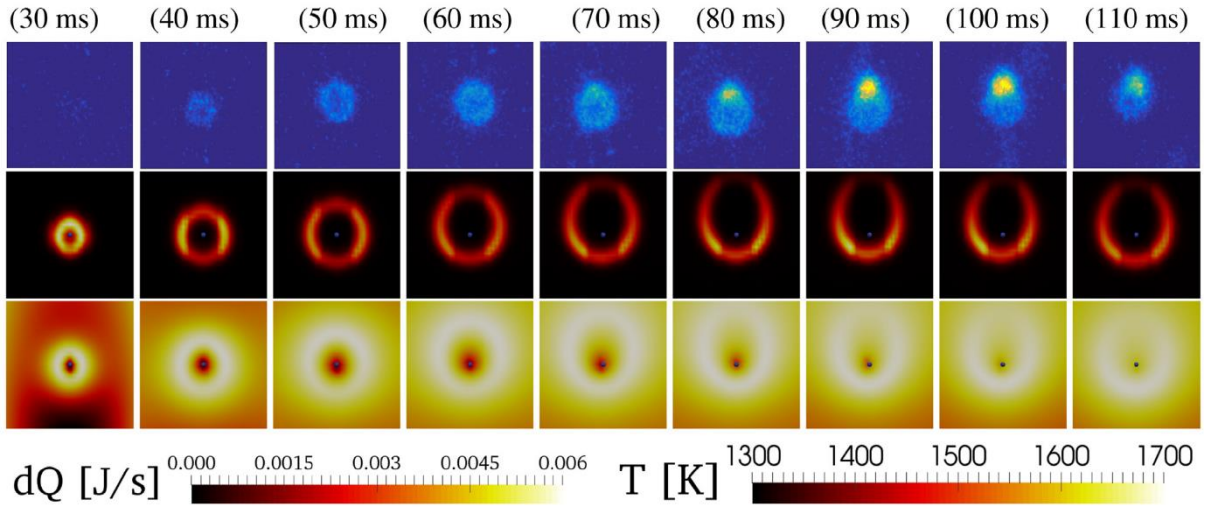

Fig. 29 Top first row: Experimental CH* emission intensity starting from 30 ms to 110 ms. Second row: CFD results of biomass heat release dQ (J/S) from volatiles combustion at the same time of the experimental ranges. Bottom last row: Numerical temperature results T(K) around the particle at the same time of the experimental ranges. Reprinted with permission from [17].

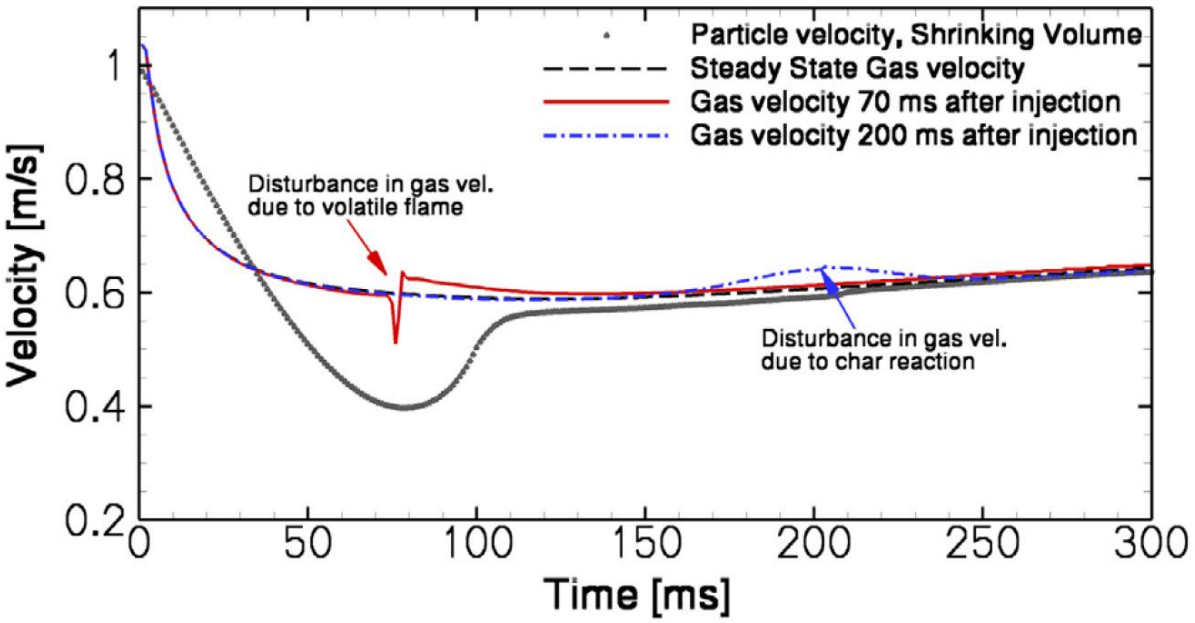

Fig. 30 Pinewood particles velocity and gas velocity. Reprinted with permission from [17].

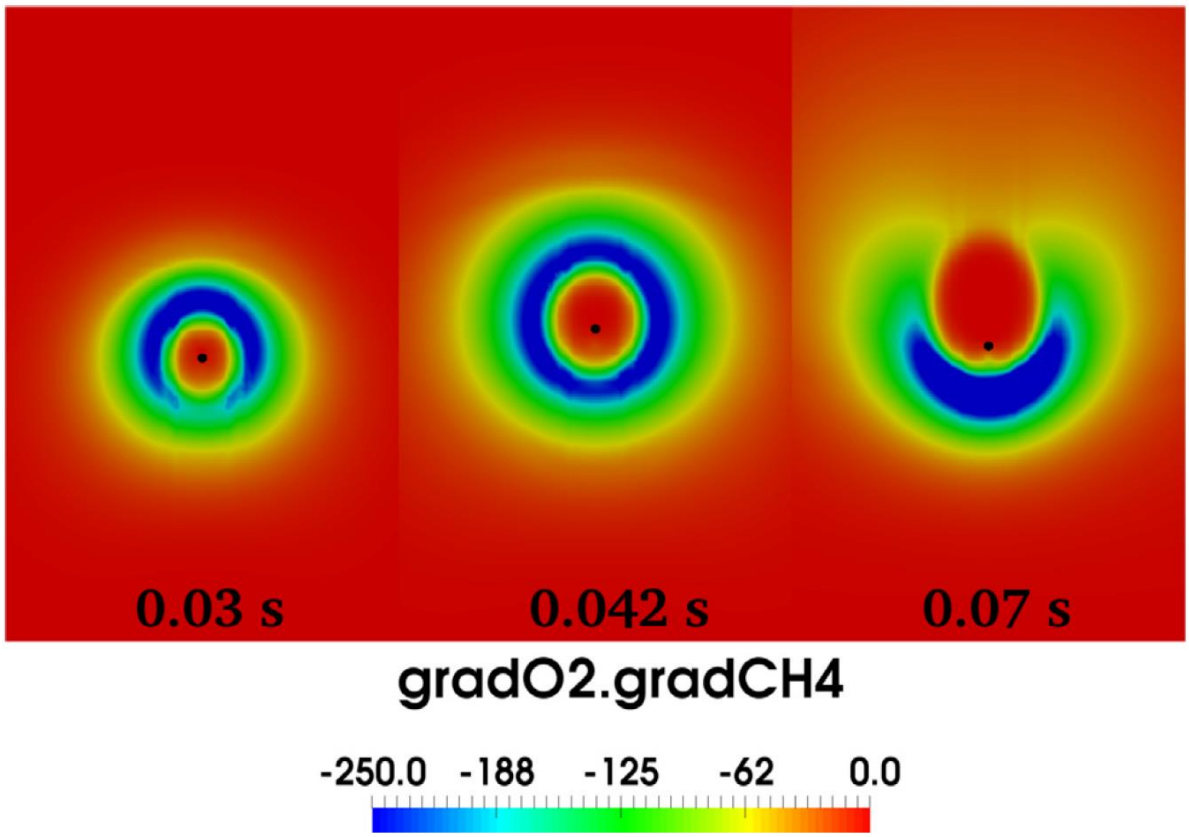

Fig. 31 Vector product of CH_4 and O_2 mass fraction gradients for three time instances. Reprinted with permission from [17].

Rieth et al. [106,107] presented first-of-its-kind carrier-phase DNS of biomass combustion in a turbulent mixing layer, applying a detailed CRECK-reduced mechanism and a pyrolysis Ranzi's mechanism [109–111] to calculate the pyrolysis rate and final products of primary pyrolysis. The simulations were performed with the in-house code. Fig. 32 depicts the temperature contours and OH mass fraction of biomass. One may observe a strong relation of the temperature increase and OH radical concentration increase with respect to time which is treated as the ignition onset. It would be generally advisable to continue the research of biomass ignition with complex DNS simulations, analyzing the evolution of different species such as CH, OH or CO/CO_2 ratio, and temperature, comparing the data with complex experimental

measurements in order to evaluate the most effective method of ignition onset determination.

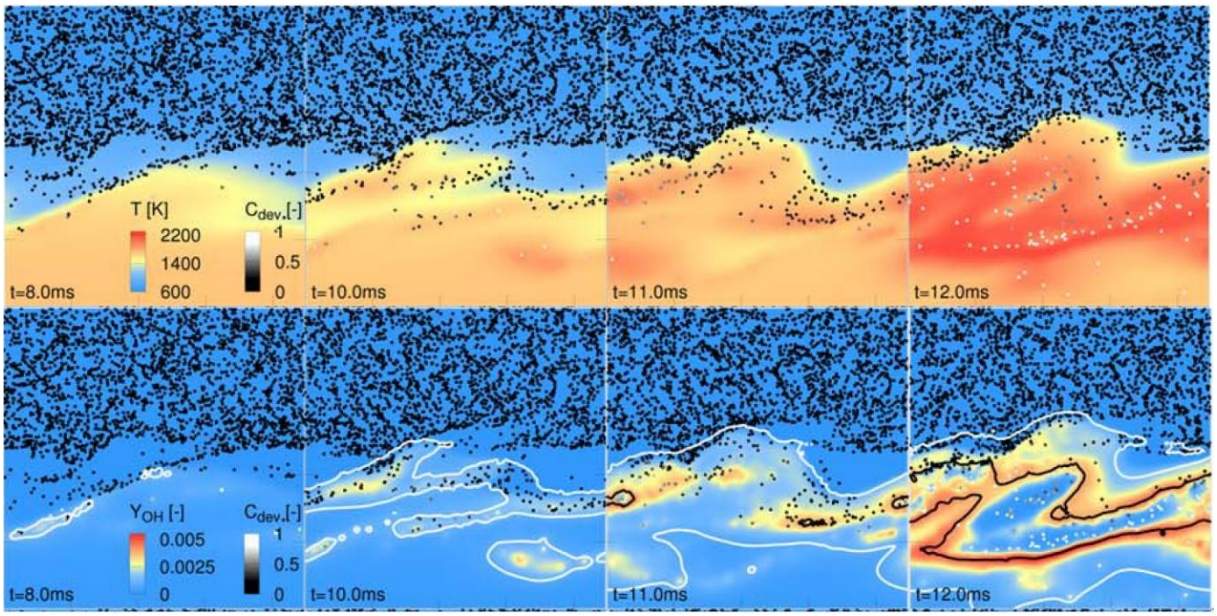

Fig. 32 Temperature and OH mass fraction for biomass. Reprinted with permission from [106,107].

Awasthi et al. [236] applied a DNS simulation and investigated, among others, the effect of gas-phase reactions on the pyrolysis time and combustion time of biomass. They investigated the combustion of CO, H_2, and the water-gas shift reaction. Judging by Fig. 33 one can observe that the effect of gas-phase reactions in terms of the pyrolysis time is greater for smaller particles. In contrast to pyrolysis, the effect of gas-phase reactions on the combustion time is the opposite.

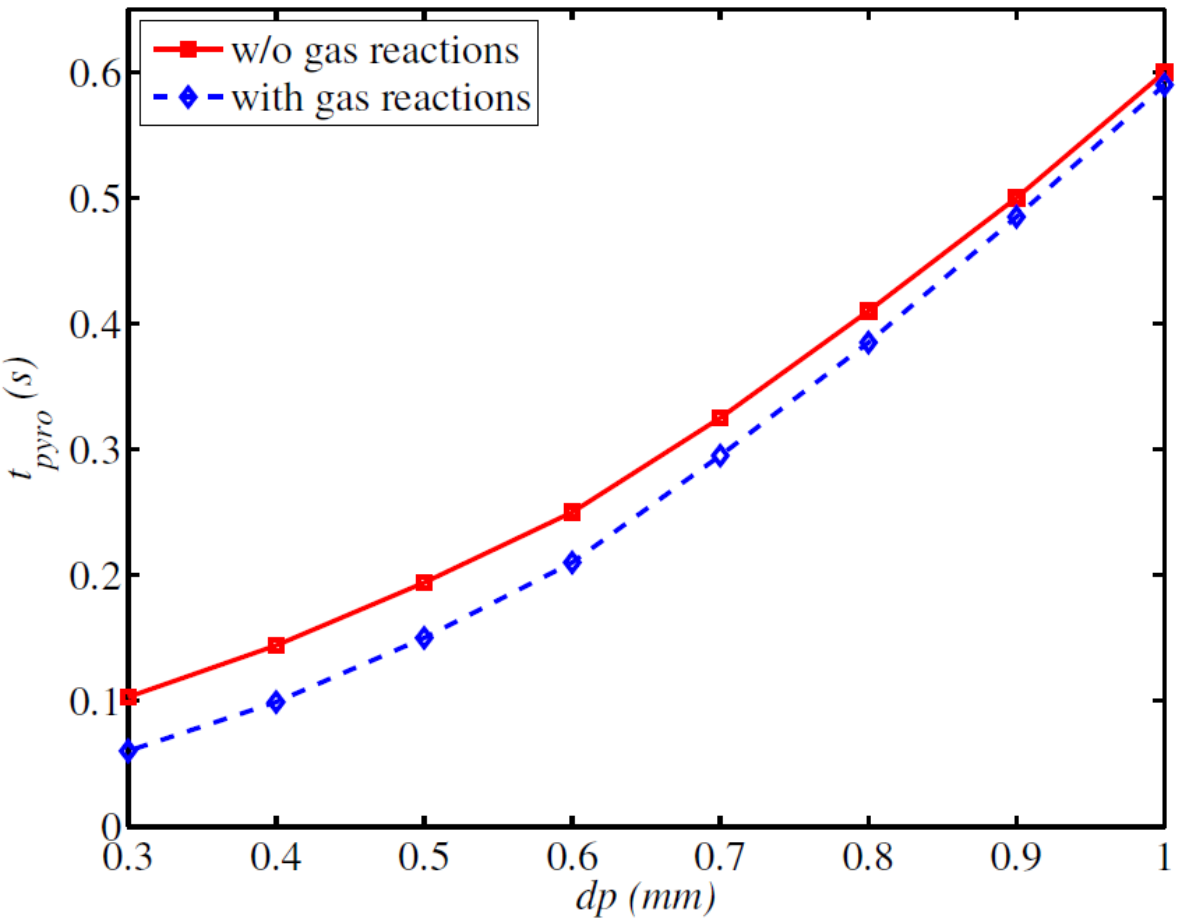
w/o gas reactions
with gas reactions
0.6
0.5
0.4
0.3
0.2
0.1
0
t_{pyro} (s)
0.3
0.4
0.5
0.6
0.7
0.8
0.9
1
dp (mm)

1558

1559 a)

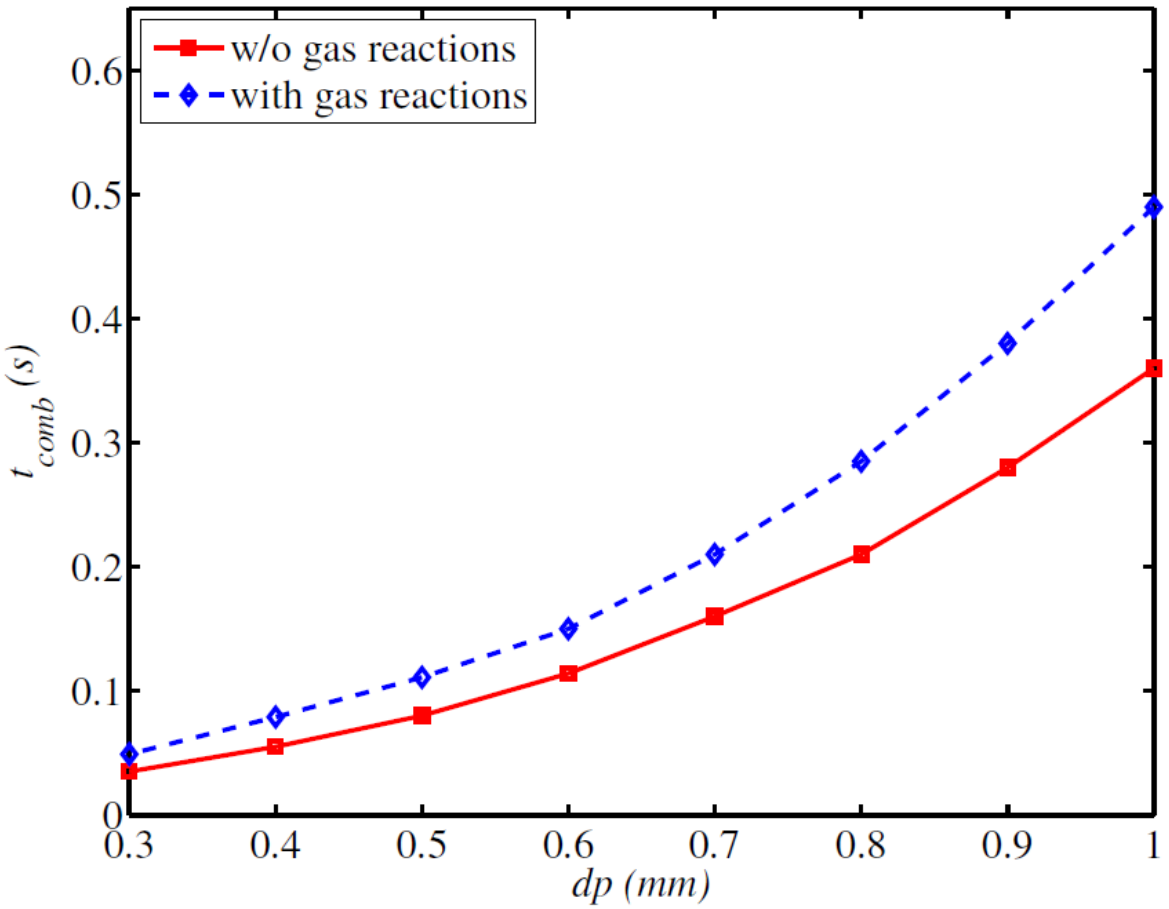

b)

Fig. 33 a) pyrolysis time vs particle diameter with and without gas reactions, b) combustion time vs particle diameter with and without gas reactions. Reprinted with permission from [236].

In general, the effect of homogeneous reactions on the conversion of biomass particles during pyrolysis is not well investigated. Majority of publications incorporate global reaction models consisting of 4-5 gas-phase reactions with literature-taken kinetic parameters. Such an assumption can provide only a general trend and does not allow an in-depth investigation of radical evolution and their impact on ignition onset.

7. Conclusions and summary remarks

This review has been focusing on the current state of knowledge on biomass ignition with respect to experimental techniques measuring the ignition onset, the effect of fuel properties and operating conditions on ignition characteristics, and the combustion models focusing on their capabilities of ignition prediction. The review considered several fields:

(1) Impact of particle size and shape, presence of alkali metals, different pre-treatment methods, such as torrefaction, pyrolysis and water leaching, combustion atmosphere, volatile matter content in the fuel, devolatilization dynamics, cellulose, hemicellulose, and lignin content in the fuel, temperature, different ignition onset definitions on ignition delay, and experimental determination of different ignition mechanism.

(2) Similarities and differences between coal ignition modeling and biomass ignition modeling.

(3) List of the most widely applied global and detailed models of the most important combustion steps that have an impact on ignition: inert heating, drying, devolatilization, gas-phase chemistry, char conversion, and capabilities of the models in terms of ignition prediction.

The following conclusions can be drawn from the review:

The quantities related to reactor operating conditions and fuel properties investigated in the first field **(1)** were found to exhibit a strong sensitivity to ignition mechanism and ignition delay prediction. With respect to the *reactor temperature*, ignition delay decreased with increasing reactor temperatures. For very high reactor temperatures, the heterogeneous ignition mechanism tended to occur more often. As for the

combustion atmosphere, the replacement of N_2 with CO_2 resulted in an increase in the ignition delay, ignition temperature, and volatile matter combustion time. In higher O_2 concentrations, a shift from homogeneous to heterogeneous ignition mode could be observed. In O_2/H_2O atmosphere, gasification reactions became more impactful which resulted in a reduction of the ignition delay as well as promotion of the homogeneous ignition mode.

The literature review has indicated that the ignition was mainly studied under laminar flow conditions for single particles. Some research reported that the increase in particle concentration expanded the volatile flame structure and was found to delay the ignition. Unfortunately, the effect of turbulence was yet not well investigated. The problem becomes crucial in large-scale reactors where high mass flow rates and highly turbulent flows are present.

As regards the *biomass fuel properties*, under very high temperatures, biomass size and shape affected the ignition delay more significantly than the biomass composition. The biomass particle shape and size also substantially affected the type of the ignition mechanism. Very small and elongated particles with hot spots tended to ignite heterogeneously, whereas larger and cylindrical particles ignited homogeneously. Particle's higher aspect ratio also resulted in a slightly shorter ignition delay but further research would be required in this respect. The biomass particle's critical size was found as an important parameter in determining the ignition mechanism. Pyrolysis non-uniformity and biomass shrinking can change the particle's critical size resulting in a shift from one ignition mechanism to the other. The ignition mechanism was also strongly correlated with the lignin content. Biomass particles with very high lignin content exhibited hetero-homogeneous ignition, whereas particles with high and moderate content showed a homogeneous type of ignition. The ignition

temperature was reported to depend strongly on the cellulose content regardless of whether the ignition mode is hetero-homogeneous or homogeneous. High-volatile-matter-content biomass fuels generally promoted homogeneous ignition with a shorter ignition delay, but for some biomass fuels, an optimum volatile matter content of 60-65% was specified when the lowest ignition temperatures occurred. Further research would be recommended in this field. Fiber orientation was also found to be an important parameter affecting the particle's potential acceleration in the reactor acting as a propulsion force that could affect the ignition. As regards the *presence of alkali metals*, the ignition delay was found to increase with the biomass demineralization process confirming a catalytic effect of potassium (K) and calcium (Ca). As for the *biomass pretreatment methods*, among torrefaction, slow pyrolysis, and fast pyrolysis, slow pyrolysis increased the ignition delay time of biomass fuels most substantially. The impact of torrefaction and fast pyrolysis was not definitive and depended on fuel composition.

As regards the second field **(2)** and the third field **(3)**, the reviewed 1-D models, CFD models and DNS simulations yielded very accurate ignition characteristics in biomass thermochemical conversion. However, it could be observed that most of the global drying, devolatilization, gas-phase and char conversion biomass models were the same as for coal modeling studies. The main difference regarded initial physico-chemical fuel properties, kinetic parameters, such as the pre-exponential factor and activation energy and the non-sphericity factor. These basic models, however, were found to yield worse ignition predictions than the detailed approaches which are devoted to specific fuels such as biomass or coal.

The main future goals in terms of ignition studies should consider above all a unified definition of ignition onset based on experimental techniques and DNS/LES

simulations. Moreover, there should be an integration of advanced devolatilization, gas-phase, and char conversion biomass models into CFD with LES-based or DNS-based simulations. Unfortunately, most of the reviewed studies analyzed simple RANS-based one-step or two-step models. Such an approach cannot provide highly accurate results. So far, only a few DNS studies are available, but these provide valuable information, such as unsteadiness, ignition, and instabilities. These information can be used, e.g., for the development of models in terms of the ignition prediction, turbulence-chemistry interaction or turbulence-radiation interaction. However, the DNS application is currently computationally expensive. Therefore, it would be advisable to develop a robust and fast ignition delay determination method for wider application. One also has to consider an accurate coupling of drying, devolatilization, turbulence-chemistry interaction, and char conversion models within CFD. So far, for the sake of simplification, the processes are assumed to occur sequentially. This assumption is no longer valid for thermally thick particles. Special attention should also be paid to the research considering biomass microstructure. Pore-scale simulations could provide key insights and better understanding of transport phenomena. It especially concerns larger biomass particles and higher heating rates where, because of an abrupt volatile matter release during pyrolysis, the dynamic morphological structure changes. The detailed knowledge of ignition behavior of different biomass fuels is important when one considers biomass combustion or co-firing biomass with coal. The key differences that may impact the reactor design and its performance have to be accurately established.

Acknowledgements

This work was supported by the Erasmus+ program.

Declaration of competing interests

The authors declare that they have no known competing financial interests or personal relationships that could have appeared to influence the work reported in this paper.

References

[1] Government subsidies for electricity generation and combined heat and power (CHP) from solid biomass 2022. https://trinomics.eu/project/government-subsidies-for-electricity-generation-and-combined-heat-and-power-chp-from-solid-biomass/.

[2] Álvarez L, Gharebaghi M, Jones JM, Pourkashanian M, Williams A, Riaza J, et al. Numerical investigation of NO emissions from an entrained flow reactor under oxy-coal conditions. Fuel Process Technol 2012;93:53–64. https://doi.org/10.1016/j.fuproc.2011.09.011.

[3] Rybak W, Moroń W, Ferens W. Dust ignition characteristics of different coal ranks, biomass and solid waste. Fuel 2019;237:606–18. https://doi.org/10.1016/j.fuel.2018.10.022.

[4] Tumuluru JS. Biomass Preprocessing and Pretreatments for Production of Biofuels: Mechanical, Chemical and Thermal Methods. 2018. https://doi.org/10.1201/9781315153735.

[5] Mamvura TA, Danha G. Biomass torrefaction as an emerging technology to aid in energy production. Heliyon 2020;6:e03531. https://doi.org/10.1016/j.heliyon.2020.e03531.

[6] Gürel K, Magalhães D, Kazanç F. The effect of torrefaction, slow, and fast pyrolysis on the single particle combustion of agricultural biomass and lignite coal at high heating rates. Fuel 2022;308. https://doi.org/10.1016/j.fuel.2021.122054.

[7] Demirbaş A. Biomass resource facilities and biomass conversion processing for fuels and chemicals. Energy Convers Manag 2001;42:1357–78. https://doi.org/10.1016/S0196-8904(00)00137-0.

[8] Zhang L, Xu C (Charles), Champagne P. Overview of recent advances in thermo-chemical conversion of biomass. Energy Convers Manag 2010;51:969–82. https://doi.org/10.1016/j.enconman.2009.11.038.

[9] Kuo PC, Wu W. Design and thermodynamic analysis of a hybrid power plant using torrefied biomass and coal blends. Energy Convers Manag 2016;111:15–26. https://doi.org/10.1016/j.enconman.2015.12.021.

[10] Garcia Torrent J, Fernandez Anez N, Medic Pejic L, Montenegro Mateos L. Assessment of self-ignition risks of solid biofuels by thermal analysis. Fuel 2015;143:484–91. https://doi.org/10.1016/j.fuel.2014.11.074.

[11] García Torrent J, Ramírez-Gómez Á, Fernandez-Anez N, Medic Pejic L, Tascón A. Influence of the composition of solid biomass in the flammability and susceptibility to spontaneous combustion. Fuel 2016;184:503–11. https://doi.org/10.1016/j.fuel.2016.07.045.

[12] Ramírez Á, García-Torrent J, Tascón A. Experimental determination of self-heating and self-ignition risks associated with the dusts of agricultural materials commonly stored in silos. J Hazard Mater 2010;175:920–7. https://doi.org/10.1016/j.jhazmat.2009.10.096.

[13] Li J, Paul MC, Czajka KM. Studies of Ignition Behavior of Biomass Particles in a Down-Fire Reactor for Improving Co-firing Performance. Energy and Fuels 2016;30:5870–7. https://doi.org/10.1021/acs.energyfuels.6b01065.

[14] Wang S, Zou C, Lou C, Yang H, Mei M, Jing H, et al. Effects of hemicellulose, cellulose and lignin on the ignition behaviors of biomass in a drop tube furnace. Bioresour Technol 2020;310:123456. https://doi.org/10.1016/j.biortech.2020.123456.

[15] Zhang D ke, Wall TF. An analysis of the ignition of coal dust clouds. Combust Flame 1993;92:475–80. https://doi.org/10.1016/0010-2180(93)90159-Z.

[16] Di Blasi C, Branca C, Sparano S, La Mantia B. Drying characteristics of wood cylinders for conditions pertinent to fixed-bed countercurrent gasification. Biomass and Bioenergy 2003;25:45–58. https://doi.org/10.1016/S0961-9534(02)00180-0.

[17] Fatehi H, Weng W, Costa M, Li Z, Rabaçal M, Aldén M, et al. Numerical simulation of ignition mode and ignition delay time of pulverized biomass particles. Combust Flame 2019;206:400–10. https://doi.org/10.1016/j.combustflame.2019.05.020.

[18] Flower M, Gibbins J. A radiant heating wire mesh single-particle biomass combustion apparatus. Fuel 2009;88:2418–27. https://doi.org/10.1016/j.fuel.2009.02.036.

[19] Baxter L. Biomass-coal co-combustion: Opportunity for affordable renewable energy. Fuel 2005;84:1295–302. https://doi.org/10.1016/j.fuel.2004.09.023.

[20] Lu H, Ip E, Scott J, Foster P, Vickers M, Baxter LL. Effects of particle shape

and size on devolatilization of biomass particle. Fuel 2010;89:1156–68. https://doi.org/10.1016/j.fuel.2008.10.023.

[21] Levendis YA, Joshi K, Khatami R, Sarofim AF. Combustion behavior in air of single particles from three different coal ranks and from sugarcane bagasse. Combust Flame 2011;158:452–65. https://doi.org/10.1016/j.combustflame.2010.09.007.

[22] Mason PE, Darvell LI, Jones JM, Pourkashanian M, Williams A. Single particle flame-combustion studies on solid biomass fuels. Fuel 2015;151:21–30. https://doi.org/10.1016/j.fuel.2014.11.088.

[23] Mock C, Lee H, Choi S, Manovic V. Combustion Behavior of Relatively Large Pulverized Biomass Particles at Rapid Heating Rates. Energy and Fuels 2016;30:10809–22. https://doi.org/10.1021/acs.energyfuels.6b01457.

[24] Grotkjær T, Dam-Johansen K, Jensen AD, Glarborg P. An experimental study of biomass ignition. Fuel 2003;82:825–33. https://doi.org/10.1016/S0016-2361(02)00369-1.

[25] Miccio F, Russo S, Silvestri N. Assessment of the devolatilization behavior of fuel pellets in fluidized bed. Fuel Process Technol 2013;115:122–9. https://doi.org/10.1016/j.fuproc.2013.04.016.

[26] Sharifzadeh M, Sadeqzadeh M, Guo M, Borhani TN, Murthy Konda NVSN, Garcia MC, et al. The multi-scale challenges of biomass fast pyrolysis and bio-oil upgrading: Review of the state of art and future research directions. Prog Energy Combust Sci 2019;71:1–80. https://doi.org/10.1016/j.pecs.2018.10.006.

[27] Haberle I, Skreiberg Ø, Łazar J, Haugen NEL. Numerical models for

thermochemical degradation of thermally thick woody biomass, and their application in domestic wood heating appliances and grate furnaces. Prog Energy Combust Sci 2017;63:204–52. https://doi.org/10.1016/j.pecs.2017.07.004.

[28] Richter A, Vascellari M, Nikrityuk PA, Hasse C. Detailed analysis of reacting particles in an entrained-flow gasifier. Fuel Process Technol 2016;144:95–108. https://doi.org/10.1016/j.fuproc.2015.12.014.

[29] Meesri C, Moghtaderi B. Experimental and numerical analysis of sawdust-char combustion reactivity in a drop tube reactor. Combust Sci Technol 2003;175:793–823. https://doi.org/10.1080/00102200302392.

[30] Di Blasi C. Modeling chemical and physical processes of wood and biomass pyrolysis. Prog Energy Combust Sci 2008;34:47–90. https://doi.org/10.1016/j.pecs.2006.12.001.

[31] Fatehi H, Weng W, Li Z, Bai XS, Aldén M. Recent development in numerical simulations and experimental studies of biomass thermochemical conversion. Energy and Fuels 2021;35:6940–63. https://doi.org/10.1021/acs.energyfuels.0c04139.

[32] Zhou L. Chapter 3. Fundamentals of Combustion Theory. 2018. https://doi.org/10.1016/b978-0-12-813465-8.00003-x.

[33] Qi S, Wang Z, Costa M, He Y, Cen K. Ignition and combustion of single pulverized biomass and coal particles in N2/O2 and CO2/O2 environments. Fuel 2021;283:118956. https://doi.org/10.1016/j.fuel.2020.118956.

[34] Weng W, Costa M, Aldén M, Li Z. Single particle ignition and combustion of

pulverized pine wood, wheat straw, rice husk and grape pomace. Proc Combust Inst 2019;37:2663–71. https://doi.org/10.1016/j.proci.2018.05.095.

[35] Weng W, Costa M, Li Z, Aldén M. Temporally and spectrally resolved images of single burning pulverized wheat straw particles. Fuel 2018;224:434–41. https://doi.org/10.1016/j.fuel.2018.03.101.

[36] Khatami R, Stivers C, Joshi K, Levendis YA, Sarofim AF. Combustion behavior of single particles from three different coal ranks and from sugar cane bagasse in O 2/N 2 and O 2/CO 2 atmospheres. Combust Flame 2012;159:1253–71. https://doi.org/10.1016/j.combustflame.2011.09.009.

[37] Khatami R, Stivers C, Levendis YA. Ignition characteristics of single coal particles from three different ranks in O 2/N 2 and O 2/CO 2 atmospheres. Combust Flame 2012;159:3554–68. https://doi.org/10.1016/j.combustflame.2012.06.019.

[38] Riaza J, Khatami R, Levendis YA, Álvarez L, Gil M V., Pevida C, et al. Combustion of single biomass particles in air and in oxy-fuel conditions. Biomass and Bioenergy 2014;64:162–74. https://doi.org/10.1016/j.biombioe.2014.03.018.

[39] Sarroza AC, Bennet TD, Eastwick C, Liu H. Characterising pulverised fuel ignition in a visual drop tube furnace by use of a high-speed imaging technique. Fuel Process Technol 2017;157:1–11. https://doi.org/10.1016/j.fuproc.2016.11.002.

[40] Simões G, Magalhães D, Rabaçal M, Costa M. Effect of gas temperature and oxygen concentration on single particle ignition behavior of biomass fuels. Proc Combust Inst 2017;36:2235–42. https://doi.org/10.1016/j.proci.2016.06.102.

1811 [41] Köser J, Becker LG, Vorobiev N, Schiemann M, Scherer V, Böhm B, et al.
1812 Characterization of single coal particle combustion within oxygen-enriched
1813 environments using high-speed OH-PLIF. Appl Phys B Lasers Opt
1814 2015;121:459–64. https://doi.org/10.1007/s00340-015-6253-3.

1815 [42] Köser J, Becker LG, Goßmann AK, Böhm B, Dreizler A. Investigation of ignition
1816 and volatile combustion of single coal particles within oxygen-enriched
1817 atmospheres using high-speed OH-PLIF. Proc Combust Inst 2017;36:2103–11.
1818 https://doi.org/10.1016/j.proci.2016.07.083.

1819 [43] Molina A, Shaddix CR. Ignition and devolatilization of pulverized bituminous
1820 coal particles during oxygen/carbon dioxide coal combustion. Proc Combust
1821 Inst 2007;31 II:1905–12. https://doi.org/10.1016/j.proci.2006.08.102.

1822 [44] Liu Y, Geier M, Molina A, Shaddix CR. Pulverized coal stream ignition delay
1823 under conventional and oxy-fuel combustion conditions. Int J Greenh Gas
1824 Control 2011;5:S36–46. https://doi.org/10.1016/j.ijggc.2011.05.028.

1825 [45] Karnani S, Dunn-Rankin D. Visualizing CH* chemiluminescence in sooting
1826 flames. Combust Flame 2013;160:2275–8.
1827 https://doi.org/10.1016/j.combustflame.2013.05.002.

1828 [46] Yuan Y, Li S, Zhao F, Yao Q, Long MB. Characterization on hetero-
1829 homogeneous ignition of pulverized coal particle streams using
1830 CH∗chemiluminescence and 3 color pyrometry. Fuel 2016;184:1000–6.
1831 https://doi.org/10.1016/j.fuel.2015.11.032.

1832 [47] Goshayeshi B, Sutherland JC. A comparison of various models in predicting
1833 ignition delay in single-particle coal combustion. Combust Flame
1834 2014;161:1900–10. https://doi.org/10.1016/j.combustflame.2014.01.010.

[48] Köser J, Li T, Vorobiev N, Dreizler A, Schiemann M, Böhm B. Multi-parameter diagnostics for high-resolution in-situ measurements of single coal particle combustion. Proc Combust Inst 2019;37:2893–900. https://doi.org/10.1016/j.proci.2018.05.116.

[49] Li T, Farmand P, Geschwindner C, Greifenstein M, Köser J, Schumann C, et al. Homogeneous ignition and volatile combustion of single solid fuel particles in air and oxy-fuel conditions. Fuel 2021;291. https://doi.org/10.1016/j.fuel.2020.120101.

[50] Shaddix CR, Molina A. Particle imaging of ignition and devolatilization of pulverized coal during oxy-fuel combustion. Proc Combust Inst 2009;32 II:2091–8. https://doi.org/10.1016/j.proci.2008.06.157.

[51] Magalhães D, Kazanç F, Ferreira A, Rabaçal M, Costa M. Ignition behavior of Turkish biomass and lignite fuels at low and high heating rates. Fuel 2017;207:154–64. https://doi.org/10.1016/j.fuel.2017.06.069.

[52] Chen Y, Mori S, Pan WP. Studying the mechanisms of ignition of coal particles by tg-dta. Thermochim Acta 1996;275:149–58. https://doi.org/10.1016/0040-6031(95)02727-0.

[53] Magalhães D, Panahi A, Kazanç F, Levendis YA. Comparison of single particle combustion behaviours of raw and torrefied biomass with Turkish lignites. Fuel 2019;241:1085–94. https://doi.org/10.1016/j.fuel.2018.12.124.

[54] Momeni M, Yin C, Kær SK, Hansen TB, Jensen PA, Glarborg P. Experimental study on effects of particle shape and operating conditions on combustion characteristics of single biomass particles. Energy and Fuels 2013;27:507–14. https://doi.org/10.1021/ef301343q.

1859 [55] Jones JM, Saddawi A, Dooley B, Mitchell EJS, Werner J, Waldron DJ, et al.
1860 Low temperature ignition of biomass. Fuel Process Technol 2015;134:372–7.
1861 https://doi.org/10.1016/j.fuproc.2015.02.019.

1862 [56] Holmgren P, Wagner DR, Strandberg A, Molinder R, Wiinikka H, Umeki K, et
1863 al. Size, shape, and density changes of biomass particles during rapid
1864 devolatilization. Fuel 2017;206:342–51.
1865 https://doi.org/10.1016/j.fuel.2017.06.009.

1866 [57] Ku X, Li T, Løvås T. Effects of Particle Shrinkage and Devolatilization Models
1867 on High-Temperature Biomass Pyrolysis and Gasification. Energy and Fuels
1868 2015;29:5127–35. https://doi.org/10.1021/acs.energyfuels.5b00953.

1869 [58] Elfasakhany A, Tao L, Espenas B, Larfeldt J, Bai XS. Pulverised wood
1870 combustion in a vertical furnace: Experimental and computational analyses.
1871 Appl Energy 2013;112:454–64. https://doi.org/10.1016/j.apenergy.2013.04.051.

1872 [59] Ciesielski PN, Pecha MB, Lattanzi AM, Bharadwaj VS, Crowley MF, Bu L, et al.
1873 Advances in Multiscale Modeling of Lignocellulosic Biomass. ACS Sustain
1874 Chem Eng 2020;8:3512–31. https://doi.org/10.1021/acssuschemeng.9b07415.

1875 [60] Ciesielski PN, Crowley MF, Nimlos MR, Sanders AW, Wiggins GM, Robichaud
1876 D, et al. Biomass particle models with realistic morphology and resolved
1877 microstructure for simulations of intraparticle transport phenomena. Energy and
1878 Fuels 2015;29:242–54. https://doi.org/10.1021/ef502204v.

1879 [61] Pecha MB, Ramirez E, Wiggins GM, Carpenter D, Kappes B, Daw S, et al.
1880 Integrated Particle- and Reactor-Scale Simulation of Pine Pyrolysis in a
1881 Fluidized Bed. Energy and Fuels 2018;32:10683–94.
1882 https://doi.org/10.1021/acs.energyfuels.8b02309.

[62] Wang C, Bi H, Jiang X, Jiang C, Lin Q. Experimental study on ignition and combustion of coal-rice husk blends pellets in air and oxy-fuel conditions. J Energy Inst 2020;93:1544–58. https://doi.org/10.1016/j.joei.2020.01.017.

[63] Mostafa ME, Khedr YM, Ling P, Chi H, Hu S, Wang Y, et al. Experimental and numerical modelling of solid and hollow biomass pellets high-temperature rapid oxy-steam combustion: The effect of integrated CO2/H2O concentration. Fuel 2021;303. https://doi.org/10.1016/j.fuel.2021.121249.

[64] Yan Y, Meng Y, Tang L, Kostas ET, Lester E, Wu T, et al. Ignition and Kinetic Studies: The Influence of Lignin on Biomass Combustion. Energy and Fuels 2019;33:6463–72. https://doi.org/10.1021/acs.energyfuels.9b01089.

[65] Tomohiro T, Shigeru Y. Research on the minimum temperature for ignition of agricultural dusts. Int Chem Eng 1984;24:556–66.

[66] Sharma A, Pareek V, Zhang D. Biomass pyrolysis - A review of modelling, process parameters and catalytic studies. Renew Sustain Energy Rev 2015;50:1081–96. https://doi.org/10.1016/j.rser.2015.04.193.

[67] Chen WH, Wang CW, Ong HC, Show PL, Hsieh TH. Torrefaction, pyrolysis and two-stage thermodegradation of hemicellulose, cellulose and lignin. Fuel 2019;258:116168. https://doi.org/10.1016/j.fuel.2019.116168.

[68] Farrokh NT, Suopajärvi H, Sulasalmi P, Fabritius T. A thermogravimetric analysis of lignin char combustion. Energy Procedia 2019;158:1241–8. https://doi.org/10.1016/j.egypro.2019.01.413.

[69] Li J, Bai X, Fang Y, Chen Y, Wang X, Chen H, et al. Comprehensive mechanism of initial stage for lignin pyrolysis. Combust Flame 2020;215:1–9.

https://doi.org/10.1016/j.combustflame.2020.01.016.

[70] Qiao Y, Wang B, Ji Y, Xu F, Zong P, Zhang J, et al. Thermal decomposition of castor oil, corn starch, soy protein, lignin, xylan, and cellulose during fast pyrolysis. Bioresour Technol 2019;278:287–95. https://doi.org/10.1016/j.biortech.2019.01.102.

[71] Yang H, Liu M, Chen Y, Xin S, Zhang X, Wang X, et al. Vapor–solid interaction among cellulose, hemicellulose and lignin. Fuel 2020;263:116681. https://doi.org/10.1016/j.fuel.2019.116681.

[72] Yang H, Yan R, Chen H, Lee DH, Zheng C. Characteristics of hemicellulose, cellulose and lignin pyrolysis. Fuel 2007;86:1781–8. https://doi.org/10.1016/j.fuel.2006.12.013.

[73] Yeo JY, Chin BLF, Tan JK, Loh YS. Comparative studies on the pyrolysis of cellulose, hemicellulose, and lignin based on combined kinetics. J Energy Inst 2019;92:27–37. https://doi.org/https://doi.org/10.1016/j.joei.2017.12.003.

[74] Chen D, Cen K, Zhuang X, Gan Z, Zhou J, Zhang Y, et al. Insight into biomass pyrolysis mechanism based on cellulose, hemicellulose, and lignin: Evolution of volatiles and kinetics, elucidation of reaction pathways, and characterization of gas, biochar and bio-oil. Combust Flame 2022;242. https://doi.org/10.1016/j.combustflame.2022.112142.

[75] Burhenne L, Messmer J, Aicher T, Laborie MP. The effect of the biomass components lignin, cellulose and hemicellulose on TGA and fixed bed pyrolysis. J Anal Appl Pyrolysis 2013;101:177–84. https://doi.org/10.1016/j.jaap.2013.01.012.

[76] Zhang Z, Zhu M, Zhang D. A Thermogravimetric study of the characteristics of pyrolysis of cellulose isolated from selected biomass. Appl Energy 2018;220:87–93. https://doi.org/10.1016/j.apenergy.2018.03.057.

[77] Pang CH, Lester E, Wu T. Influence of lignocellulose and plant cell walls on biomass char morphology and combustion reactivity. Biomass and Bioenergy 2018;119:480–91. https://doi.org/10.1016/j.biombioe.2018.10.011.

[78] Ma Z, Yang Y, Wu Y, Xu J, Peng H, Liu X, et al. In-depth comparison of the physicochemical characteristics of bio-char derived from biomass pseudo components: Hemicellulose, cellulose, and lignin. J Anal Appl Pyrolysis 2019;140:195–204. https://doi.org/10.1016/j.jaap.2019.03.015.

[79] Shan L, Kong M, Bennet TD, Sarroza AC, Eastwick C, Sun D, et al. Studies on combustion behaviours of single biomass particles using a visualization method. Biomass and Bioenergy 2018;109:54–60. https://doi.org/10.1016/j.biombioe.2017.12.008.

[80] Mlonka-Mędrala A, Magdziarz A, Gajek M, Nowińska K, Nowak W. Alkali metals association in biomass and their impact on ash melting behaviour. Fuel 2020;261:116421. https://doi.org/10.1016/j.fuel.2019.116421.

[81] Kassman H, Pettersson J, Steenari BM, Åmand LE. Two strategies to reduce gaseous KCl and chlorine in deposits during biomass combustion - Injection of ammonium sulphate and co-combustion with peat. Fuel Process Technol 2013;105:170–80. https://doi.org/10.1016/j.fuproc.2011.06.025.

[82] Fahmi R, Bridgwater A V., Darvell LI, Jones JM, Yates N, Thain S, et al. The effect of alkali metals on combustion and pyrolysis of Lolium and Festuca grasses, switchgrass and willow. Fuel 2007;86:1560–9.

https://doi.org/10.1016/j.fuel.2006.11.030.

[83] Jones JM, Darvell LI, Bridgeman TG, Pourkashanian M, Williams A. An investigation of the thermal and catalytic behaviour of potassium in biomass combustion. Proc Combust Inst 2007;31 II:1955–63. https://doi.org/10.1016/j.proci.2006.07.093.

[84] Carvalho A, Rabaçal M, Costa M, Alzueta MU, Abián M. Effects of potassium and calcium on the early stages of combustion of single biomass particles. Fuel 2017;209:787–94. https://doi.org/10.1016/j.fuel.2017.08.045.

[85] Cao W, Martí-Rosselló T, Li J, Lue L. Prediction of potassium compounds released from biomass during combustion. Appl Energy 2019;250:1696–705. https://doi.org/10.1016/j.apenergy.2019.05.106.

[86] Cao W, Li J, Zhang X. Evaluation of the effects and interactions of initial chlorine and sulphur contents on the release of potassium compounds during biomass combustion. J Energy Inst 2022;101:178–86. https://doi.org/10.1016/j.joei.2022.01.014.

[87] Pettersson A, Åmand LE, Steenari BM. Chemical fractionation for the characterisation of fly ashes from co-combustion of biofuels using different methods for alkali reduction. Fuel 2009;88:1758–72. https://doi.org/10.1016/j.fuel.2009.03.038.

[88] Pettersson A, Zevenhoven M, Steenari BM, Åmand LE. Application of chemical fractionation methods for characterisation of biofuels, waste derived fuels and CFB co-combustion fly ashes. Fuel 2008;87:3183–93. https://doi.org/10.1016/j.fuel.2008.05.030.

[89] Zevenhoven M, Yrjas P, Backman R, Skrifvars BJ, Hupa M. The åbo akademi database -fuel characterization. Proc 18th Int Conf Fluid Bed Combust 2005 2005:667–78. https://doi.org/10.1115/fbc2005-78093.

[90] Cen S, Xiaolin W, Teng L, Li Z, Qinzheng T, Sen L. Potassium release during pulverized biomass combustion in a tubular burner investigated by TDLAS. Fuel 2022;317:123570. https://doi.org/10.1016/j.fuel.2022.123570.

[91] Qu Z, Fatehi H, Schmidt FM. Potassium release from biomass particles during combustion—real-time in situ tdlas detection and numerical simulation. Appl Sci 2021;11. https://doi.org/10.3390/app11198887.

[92] Fatehi H, He Y, Wang Z, Li ZS, Bai XS, Aldén M, et al. LIBS measurements and numerical studies of potassium release during biomass gasification. Proc Combust Inst 2015;35:2389–96. https://doi.org/10.1016/j.proci.2014.06.115.

[93] Fatehi H, Li ZS, Bai XS, Aldén M. Modeling of alkali metal release during biomass pyrolysis. Proc Combust Inst 2017;36:2243–51. https://doi.org/10.1016/j.proci.2016.06.079.

[94] Fatehi H, Costa M, Bai XS. Numerical study on K/S/Cl release during devolatilization of pulverized biomass at high temperature. Proc Combust Inst 2021;38:3909–17. https://doi.org/10.1016/j.proci.2020.06.079.

[95] Riaza J, Álvarez L, Gil M V., Pevida C, Pis JJ, Rubiera F. Ignition and NO emissions of coal and biomass blends under different oxy-fuel atmospheres. Energy Procedia 2013;37:1405–12. https://doi.org/10.1016/j.egypro.2013.06.016.

[96] Riaza J, Gil M V., Álvarez L, Pevida C, Pis JJ, Rubiera F. Oxy-fuel combustion

1999 of coal and biomass blends. Energy 2012;41:429–35.
2000 https://doi.org/10.1016/j.energy.2012.02.057.

2001 [97] Shan F, Lin Q, Zhou K, Wu Y, Fu W, Zhang P, et al. An experimental study of
2002 ignition and combustion of single biomass pellets in air and oxy-fuel. Fuel
2003 2017;188:277–84. https://doi.org/10.1016/j.fuel.2016.09.069.

2004 [98] Zhou H, Li Y, Li N, Cen K. Experimental investigation of ignition and
2005 combustion characteristics of single coal and biomass particles in O 2 /N 2 and
2006 O 2 /H 2 O. J Energy Inst 2019;92:502–11.
2007 https://doi.org/10.1016/j.joei.2018.04.008.

2008 [99] Borrego AG, Garavaglia L, Kalkreuth WD. Characteristics of high heating rate
2009 biomass chars prepared under N2 and CO2 atmospheres. Int J Coal Geol
2010 2009;77:409–15. https://doi.org/10.1016/j.coal.2008.06.004.

2011 [100] Botelho T, Costa M, Wilk M, Magdziarz A. Evaluation of the combustion
2012 characteristics of raw and torrefied grape pomace in a thermogravimetric
2013 analyzer and in a drop tube furnace. Fuel 2018;212:95–100.
2014 https://doi.org/10.1016/j.fuel.2017.09.118.

2015 [101] Wang X, Adeosun A, Hu Z, Xiao Z, Khatri D, Li T, et al. Effect of feedstock
2016 water leaching on ignition and PM1.0 emission during biomass combustion in a
2017 flat-flame burner reactor. Proc Combust Inst 2019;37:2705–13.
2018 https://doi.org/10.1016/j.proci.2018.05.096.

2019 [102] Tufano GL, Stein OT, Wang B, Kronenburg A, Rieth M, Kempf AM. Coal
2020 particle volatile combustion and flame interaction. Part II: Effects of particle
2021 Reynolds number and turbulence. Fuel 2018;234:723–31.
2022 https://doi.org/10.1016/j.fuel.2018.07.054.

[103] Tabet F, Gökalp I. Review on CFD based models for co-firing coal and biomass. Renew Sustain Energy Rev 2015;51:1101–14. https://doi.org/10.1016/j.rser.2015.07.045.

[104] Mularski J, Pawlak-Kruczek H, Modlinski N. A review of recent studies of the CFD modelling of coal gasification in entrained flow gasifiers, covering devolatilization, gas-phase reactions, surface reactions, models and kinetics. Fuel 2020;271:1–36. https://doi.org/10.1016/j.fuel.2020.117620.

[105] Hasse C, Debiagi P, Wen X, Hildebrandt K, Vascellari M, Faravelli T. Advanced modeling approaches for CFD simulations of coal combustion and gasification. Prog Energy Combust Sci 2021;86:100938. https://doi.org/10.1016/j.pecs.2021.100938.

[106] Rieth M, Kempf AM, Kronenburg A, Stein OT. Carrier-phase DNS of pulverized coal particle ignition and volatile burning in a turbulent mixing layer. Fuel 2018;212:364–74. https://doi.org/10.1016/j.fuel.2017.09.096.

[107] Rieth M, Rabaçal M, Kempf AM, Kronenburg A, Stein OT. Carrier-Phase DNS of biomass particle ignition and volatile burning in a turbulent mixing layer. Chem Eng Trans 2018;65:37–42. https://doi.org/10.3303/CET1865007.

[108] Niksa S. Predicting the macroscopic combustion characteristics of diverse forms of biomass in p. p. firing. Fuel 2021;283:118911. https://doi.org/10.1016/j.fuel.2020.118911.

[109] Ranzi E, Cuoci A, Faravelli T, Frassoldati A, Migliavacca G, Pierucci S, et al. Chemical kinetics of biomass pyrolysis. Energy and Fuels 2008;22:4292–300. https://doi.org/10.1021/ef800551t.

2046 [110] Corbetta M, Frassoldati A, Bennadji H, Smith K, Serapiglia MJ, Gauthier G, et
2047 al. Pyrolysis of centimeter-scale woody biomass particles: Kinetic modeling and
2048 experimental validation. Energy and Fuels 2014;28:3884–98.
2049 https://doi.org/10.1021/ef500525v.

2050 [111] Debiagi PEA, Pecchi C, Gentile G, Frassoldati A, Cuoci A, Faravelli T, et al.
2051 Extractives Extend the Applicability of Multistep Kinetic Scheme of Biomass
2052 Pyrolysis. Energy and Fuels 2015;29:6544–55.
2053 https://doi.org/10.1021/acs.energyfuels.5b01753.

2054 [112] Tufano GL, Stein OT, Wang B, Kronenburg A, Rieth M, Kempf AM. Coal
2055 particle volatile combustion and flame interaction. Part I: Characterization of
2056 transient and group effects. Fuel 2018;229:262–9.
2057 https://doi.org/10.1016/j.fuel.2018.02.105.

2058 [113] Niksa S, Liu GS, Hurt RH. Coal conversion submodels for design applications
2059 at elevated pressures. Part I. Devolatilization and char oxidation. Prog Energy
2060 Combust Sci 2003;29:425–77. https://doi.org/10.1016/S0360-1285(03)00033-
2061 9.

2062 [114] Niksa S. bio-FLASHCHAIN® theory for rapid devolatilization of biomass 1.
2063 Lignin devolatilization. Fuel 2020;263:116649.
2064 https://doi.org/10.1016/j.fuel.2019.116649.

2065 [115] Niksa S. bio-FLASHCHAIN® theory for rapid devolatilization of biomass 2.
2066 Predicting total yields for torrefied woods. Fuel 2020;263:116645.
2067 https://doi.org/10.1016/j.fuel.2019.116645.

2068 [116] Niksa S. bio-FLASHCHAIN® theory for rapid devolatilization of biomass 3.
2069 Predicting total yields for torrefied grasses and agricultural residues. Fuel

2020;263:116646. https://doi.org/10.1016/j.fuel.2019.116646.

[117] Niksa S. Predicting the rapid devolatilization of diverse forms of biomass with bio-FLASHCHAIN. Proc Combust Inst 2000;28:2727–33. https://doi.org/10.1016/S0082-0784(00)80693-1.

[118] Gubba SR, Ma L, Pourkashanian M, Williams A. Influence of particle shape and internal thermal gradients of biomass particles on pulverised coal/biomass co-fired flames. Fuel Process Technol 2011;92:2185–95. https://doi.org/10.1016/j.fuproc.2011.07.003.

[119] Yuen RKK, Yeoh GH, de Vahl Davis G, Leonardi E. Modelling the pyrolysis of wet wood - I. Three-dimensional formulation and analysis. Int J Heat Mass Transf 2007;50:4371–86. https://doi.org/10.1016/j.ijheatmasstransfer.2007.01.008.

[120] Yang YB, Sharifi VN, Swithenbank J, Ma L, Darvell LI, Jones JM, et al. Combustion of a single particle of biomass. Energy and Fuels 2008;22:306–16. https://doi.org/10.1021/ef700305r.

[121] Hasan MM, Hu X, Gunawan R, Li CZ. Pyrolysis of large mallee wood particles: Temperature gradients within a pyrolysing particle and effects of moisture content. Fuel Process Technol 2017;158:163–71. https://doi.org/10.1016/j.fuproc.2016.12.018.

[122] Bruch C, Peters B, Nussbaumer T. Modelling wood combustion under fixed bed conditions. Fuel 2003;82:729–38. https://doi.org/10.1016/S0016-2361(02)00296-X.

[123] Lu H, Robert W, Peirce G, Ripa B, Baxter LL. Comprehensive study of biomass

2093 particle combustion. Energy and Fuels 2008;22:2826–39.
2094 https://doi.org/10.1021/ef800006z.

2095 [124] Alves SS, Figueiredo JL. A model for pyrolysis of wet wood. Chem Eng Sci
2096 1989;44:2861–9. https://doi.org/10.1016/0009-2509(89)85096-1.

2097 [125] Fatehi H, Bai XS. A comprehensive mathematical model for biomass
2098 combustion. Combust Sci Technol 2014;186:574–93.
2099 https://doi.org/10.1080/00102202.2014.883255.

2100 [126] Rabacal M, Costa M, Vascellari M, Hasse C. Kinetic modelling of sawdust and
2101 beech wood pyrolysis in drop tube reactors using advanced predictive models.
2102 Chem Eng Trans 2014;37:79–84. https://doi.org/10.3303/CET1437014.

2103 [127] Fletcher TH, Pond HR, Webster J, Wooters J, Baxter LL. Prediction of tar and
2104 light gas during pyrolysis of black liquor and biomass. Energy and Fuels
2105 2012;26:3381–7. https://doi.org/10.1021/ef300574n.

2106 [128] Giudicianni P, Cardone G, Sorrentino G, Ragucci R. Hemicellulose, cellulose
2107 and lignin interactions on Arundo donax steam assisted pyrolysis. J Anal Appl
2108 Pyrolysis 2014;110:138–46. https://doi.org/10.1016/j.jaap.2014.08.014.

2109 [129] Ferreiro AI, Giudicianni P, Grottola CM, Rabaçal M, Costa M, Ragucci R.
2110 Unresolved Issues on the Kinetic Modeling of Pyrolysis of Woody and
2111 Nonwoody Biomass Fuels. Energy and Fuels 2017;31:4035–44.
2112 https://doi.org/10.1021/acs.energyfuels.6b03445.

2113 [130] Badzioch S, Hawksley P. Kinetics of thermal decomposition of pulverized coal
2114 particles. Ind Eng Chem Process Des Dev 1970;9:521–30.
2115 https://doi.org/10.1021/i260036a005.

2116 [131] Anthony DB, Howard JB, Hottel HC, Meissner HP. Rapid devolatilization of
2117 pulverized coal. Symp Combust 1975;15:1303–17.
2118 https://doi.org/10.1016/S0082-0784(75)80392-4.

2119 [132] Kobayashi H, Howard JB, Sarofim AF. Coal devolatilization at high
2120 temperatures. Symp Combust 1977;16:411–25. https://doi.org/10.1016/S0082-
2121 0784(77)80341-X.

2122 [133] Solomon PR, Colket MB. Coal devolatilization. Symp Combust 1979;17:131–
2123 43. https://doi.org/10.1016/S0082-0784(79)80016-8.

2124 [134] Perkins G. Underground coal gasification – Part II: Fundamental phenomena
2125 and modeling. Prog Energy Combust Sci 2018;67:234–74.
2126 https://doi.org/10.1016/j.pecs.2018.03.002.

2127 [135] Cai J, Wu W, Liu R. An overview of distributed activation energy model and its
2128 application in the pyrolysis of lignocellulosic biomass. Renew Sustain Energy
2129 Rev 2014;36:236–46. https://doi.org/10.1016/j.rser.2014.04.052.

2130 [136] Ferreiro AI, Rabaçal M, Costa M. A combined genetic algorithm and least
2131 squares fitting procedure for the estimation of the kinetic parameters of the
2132 pyrolysis of agricultural residues. Energy Convers Manag 2016;125:290–300.
2133 https://doi.org/10.1016/j.enconman.2016.04.104.

2134 [137] Chen Y, Charpenay S, Jensen A, Wójtowicz MA, Serio MA. Modeling of
2135 biomass pyrolysis kinetics. Symp Combust 1998;27:1327–34.
2136 https://doi.org/10.1016/S0082-0784(98)80537-7.

2137 [138] Solomon PR, Hamblen DG, Carangelo RM, Serio MA, Deshpande G V.
2138 General Model of Coal Devolatilization. ACS Div Fuel Chem Prepr 1987;32:83–

98. https://doi.org/10.1021/ef00010a006.

[139] Fletcher TH. Review of 30 Years of Research Using the Chemical Percolation Devolatilization Model. Energy & Fuels 2019;33:12123–53. https://doi.org/10.1021/acs.energyfuels.9b02826.

[140] Anca-Couce A, Scharler R. Modelling heat of reaction in biomass pyrolysis with detailed reaction schemes. Fuel 2017;206:572–9. https://doi.org/10.1016/j.fuel.2017.06.011.

[141] Anca-Couce A, Mehrabian R, Scharler R, Obernberger I. Kinetic scheme of biomass pyrolysis considering secondary charring reactions. Energy Convers Manag 2014;87:687–96. https://doi.org/10.1016/j.enconman.2014.07.061.

[142] Anca-Couce A, Mehrabian R, Scharler R, Obernberger I. Kinetic scheme to predict product composition of biomass torrefaction. Chem Eng Trans 2014;37:43–8. https://doi.org/10.3303/CET1437008.

[143] Anca-Couce A, Obernberger I. Application of a detailed biomass pyrolysis kinetic scheme to hardwood and softwood torrefaction. Fuel 2016;167:158–67. https://doi.org/10.1016/j.fuel.2015.11.062.

[144] Sheng C, Azevedo JLT. Modeling biomass devolatilization using the chemical percolation devolatilization model for the main components. Proc Combust Inst 2002;29:407–14. https://doi.org/10.1016/s1540-7489(02)80054-2.

[145] Niksa S. Bio-FLASHCHAIN® theory for rapid devolatilization of biomass. 4. V.2.0 decomposition mechanism for mineral-free cellulose. Fuel 2021;306:121726. https://doi.org/10.1016/j.fuel.2021.121726.

[146] Anca-Couce A. Reaction mechanisms and multi-scale modelling of

lignocellulosic biomass pyrolysis. Prog Energy Combust Sci 2016;53:41–79. https://doi.org/10.1016/j.pecs.2015.10.002.

[147] Smith G, Golden D, Frenklach M, Moriarty N, Eiteneer B, Goldenberg M, et al. GRI-Mech 3.0 2000. http://combustion.berkeley.edu/gri-mech/version30/text30.html (accessed October 14, 2018).

[148] Kazakov A, Frenklach M. Reduced reaction rates based on GRI-Mech 1.2 n.d. http://combustion.berkeley.edu/drm/ (accessed December 8, 2021).

[149] Ranzi E, Cavallotti C, Cuoci A, Frassoldati A, Pelucchi M, Faravelli T. New reaction classes in the kinetic modeling of low temperature oxidation of n-alkanes. Combust Flame 2015;162:1679–91. https://doi.org/10.1016/j.combustflame.2014.11.030.

[150] Ranzi E, Frassoldati A, Grana R, Cuoci A, Faravelli T, Kelley AP, et al. Hierarchical and comparative kinetic modeling of laminar flame speeds of hydrocarbon and oxygenated fuels. Prog Energy Combust Sci 2012;38:468–501. https://doi.org/10.1016/j.pecs.2012.03.004.

[151] Frassoldati A, Cuoci A, Faravelli T, Niemann U, Ranzi E, Seiser R, et al. An experimental and kinetic modeling study of n-propanol and iso-propanol combustion. Combust Flame 2010;157:2–16. https://doi.org/10.1016/j.combustflame.2009.09.002.

[152] Sommariva S, Maffei T, Migliavacca G, Faravelli T, Ranzi E. A predictive multi-step kinetic model of coal devolatilization. Fuel 2010;89:318–28. https://doi.org/10.1016/j.fuel.2009.07.023.

[153] Ranzi E, Frassoldati A, Stagni A, Pelucchi M, Cuoci A, Faravelli T. Reduced

kinetic schemes of complex reaction systems: Fossil and biomass-derived transportation fuels. vol. 46. 2014. https://doi.org/10.1002/kin.20867.

[154] Stagni A, Cuoci A, Frassoldati A, Faravelli T, Ranzi E. Lumping and reduction of detailed kinetic schemes: An effective coupling. Ind Eng Chem Res 2014;53:9004–16. https://doi.org/10.1021/ie403272f.

[155] Westbrook CK, Dryer FL. Chemical kinetic modeling of hydrocarbon combustion. Prog Energy Combust Sci 1984;10:1–57. https://doi.org/10.1016/0360-1285(84)90118-7.

[156] Dryer FL, Westbrook CK. Simplified Reaction Mechanisms for the Oxidation of Hydrocarbon Fuels in Flames. Combust Sci Technol 1981;27:31–43. https://doi.org/10.1080/00102208108946970.

[157] Jones WP, Lindstedt RP. Global reaction schemes for hydrocarbon combustion. Combust Flame 1988;73:233–49. https://doi.org/10.1016/0010-2180(88)90021-1.

[158] Lysenko DA, Ertesvåg IS, Rian KE. Numerical simulation of non-premixed turbulent combustion using the eddy dissipation concept and comparing with the steady laminar flamelet model. Flow, Turbul Combust 2014;93:577–605. https://doi.org/10.1007/s10494-014-9551-7.

[159] Cheng P. Two-dimensional radiating gas flow by a moment method. AIAA J 1964;2:1662–4. https://doi.org/10.2514/3.2645.

[160] Frassoldati A, Faravelli T, Ranzi E. The ignition, combustion and flame structure of carbon monoxide/hydrogen mixtures. Note 1: Detailed kinetic modeling of syngas combustion also in presence of nitrogen compounds. Int J

Hydrogen Energy 2007;32:3471–85. https://doi.org/10.1016/j.ijhydene.2007.01.011.

[161] Hewson JC, Kerstein AR. Stochastic simulation of transport and chemical kinetics in turbulent CO/H2/N2 flames. Combust Theory Model 2001;5:669–97. https://doi.org/10.1088/1364-7830/5/4/309.

[162] Cuoci A, Frassoldati A, Buzzi Ferraris G, Faravelli T, Ranzi E. The ignition, combustion and flame structure of carbon monoxide/hydrogen mixtures. Note 2: Fluid dynamics and kinetic aspects of syngas combustion. Int J Hydrogen Energy 2007;32:3486–500. https://doi.org/10.1016/j.ijhydene.2007.02.026.

[163] Caram HS, Amundson NR. Diffusion and Reaction in a Stagnant Boundary Layer about a Carbon Particle. Ind Eng Chem Fundam 1977;16:171–81. https://doi.org/10.1021/i160062a001.

[164] Riaza J, Gibbins J, Chalmers H. Ignition and combustion of single particles of coal and biomass. Fuel 2017;202:650–5. https://doi.org/10.1016/j.fuel.2017.04.011.

[165] Riaza J, Mason PE, Jones JM, Williams A, Gibbins J, Chalmers H. Shape and size transformations of biomass particles during combustion. Fuel 2020;261:116334. https://doi.org/10.1016/j.fuel.2019.116334.

[166] Di Blasi C. Combustion and gasification rates of lignocellulosic chars. Prog Energy Combust Sci 2009;35:121–40. https://doi.org/10.1016/j.pecs.2008.08.001.

[167] Field MA. Rate of combustion of size-graded fractions of char from a low-rank coal between 1 200°K and 2 000°K. Combust Flame 1969;13:237–52.

https://doi.org/10.1016/0010-2180(69)90002-9.

[168] BAUM MM, STREET PJ. Predicting the Combustion Behaviour of Coal Particles. Combust Sci Technol 1971;3:231–43. https://doi.org/10.1080/00102207108952290.

[169] Smith IW. The combustion rates of coal chars: A review. Symp Combust 1982;19:1045–65. https://doi.org/10.1016/S0082-0784(82)80281-6.

[170] Haynes BS. A turnover model for carbon reactivity. I. Development. Combust Flame 2001;126:1421–32. https://doi.org/10.1016/S0010-2180(01)00263-2.

[171] Shaw DW, Zhu X, Misra MK, Essenhigh RH. Determination of global kinetics of coal volatiles combustion. Symp Combust 1991;23:1155–62. https://doi.org/10.1016/S0082-0784(06)80375-9.

[172] Hurt R, Sun J-K, Lunden M. A Kinetic Model of Carbon Burnout in Pulverized Coal Combustion. Combust Flame 1998;113:181–97. https://doi.org/10.1016/S0010-2180(97)00240-X.

[173] Hurt R H, Lunden M M, Brehob E G, Maloney D J. Statistical kinetics for pulverized coal combustion. Symp Combust 1996;26:3169–77. https://doi.org/10.1016/S0082-0784(96)80162-7.

[174] Hurt RH, Calo JM. Semi-global intrinsic kinetics for char combustion modeling††Entry 2 has also been referred to as “Langmuir kinetics.” The present paper adopts common chemical engineering usage, in which the designation “Langmuir” is applied to the equilibrium adsorption. Combust Flame 2001;125:1138–49. https://doi.org/10.1016/S0010-2180(01)00234-6.

[175] Lang T, Hurt RH. Char Combustion Reactivities for a Suite of Diverse Solid

Fuels and Char-Forming Organic Model Compounds. Proc Combust Inst 2002;29:423–31. https://doi.org/10.1016/S1540-7489(02)80056-6.

[176] Niksa S, Liu GS. Coal conversion submodels for design applications at elevated pressures. Part II. Char gasification. Prog Energy Combust Sci 2004;30:679–717. https://doi.org/10.1016/j.pecs.2004.08.001.

[177] Niksa S. Predicting biomass gasification histories with CBK/G. Part 1. Kinetic parameter assignments. Fuel 2021;285:119232. https://doi.org/10.1016/j.fuel.2020.119232.

[178] Niksa S. Interpreting biomass gasification histories with CBK/G. Part 2. Extrapolations to entrained-flow gasification conditions. Fuel 2021;285:118993. https://doi.org/10.1016/j.fuel.2020.118993.

[179] Hurt RH, Mitchell RE. UNIFIED HIGH-TEMPERATURE CHAR COMBUSTION KINETICS FOR A SUITE OF COALS OF VARIOUS RANK. Symp Combust Combust Inst 1992:1243–50. https://doi.org/10.1016/S0082-0784(06)80146-3.

[180] Hurt RH, Mitchell RE. ON THE COMBUSTION KINETICS OF HETEROGENEOUS CHAR PARTICLE POPULATIONS. Symp Combust 1992:1233–41. https://doi.org/10.1016/S0082-0784(06)80145-1.

[181] Campbell PA. Investigation into the roles of surface oxide complexes and their distributions in the carbon-oxygen heterogeneous reaction mechanism. Stanford University, 2006.

[182] Campbell PA, Mitchell RE. The impact of the distributions of surface oxides and their migration on characterization of the heterogeneous carbon-oxygen reaction. Combust Flame 2008;154:47–66.

https://doi.org/10.1016/j.combustflame.2007.11.002.

[183] Ma L, Mitchell R. Modeling char oxidation behavior under Zone II burning conditions at elevated pressures. Combust Flame 2009;156:37–50. https://doi.org/10.1016/j.combustflame.2008.06.015.

[184] Tilghman MB, Mitchell RE. Coal and biomass char reactivities in gasification and combustion environments. Combust Flame 2015;162:3220–35. https://doi.org/10.1016/j.combustflame.2015.05.009.

[185] Tilghman MB, Haugen NEL, Mitchell RE. Comprehensive Char Particle Gasification Model Adequate for Entrained-Flow and Fluidized-Bed Gasifiers. Energy and Fuels 2017;31:2164–74. https://doi.org/10.1021/acs.energyfuels.6b02148.

[186] Debiagi P, Gentile G, Cuoci A, Frassoldati A, Ranzi E, Faravelli T. A predictive model of biochar formation and characterization. J Anal Appl Pyrolysis 2018;134:326–35. https://doi.org/10.1016/j.jaap.2018.06.022.

[187] Debiagi PEA, Gentile G, Cuoci A, Frassoldati A, Ranzi E, Faravelli T. Yield, composition and active surface area of char from biomass pyrolysis. Chem Eng Trans 2018;65:97–102. https://doi.org/10.3303/CET1865017.

[188] Ranzi E, Debiagi PEA, Frassoldati A. Mathematical Modeling of Fast Biomass Pyrolysis and Bio-Oil Formation. Note II: Secondary Gas-Phase Reactions and Bio-Oil Formation. ACS Sustain Chem Eng 2017;5:2882–96. https://doi.org/10.1021/acssuschemeng.6b03098.

[189] Ranzi E, Debiagi PEA, Frassoldati A. Mathematical Modeling of Fast Biomass Pyrolysis and Bio-Oil Formation. Note I: Kinetic Mechanism of Biomass

Pyrolysis. ACS Sustain Chem Eng 2017;5:2867–81. https://doi.org/10.1021/acssuschemeng.6b03096.

[190] Ranzi E, Corbetta M, Manenti F, Pierucci S. Kinetic modeling of the thermal degradation and combustion of biomass. Chem Eng Sci 2014;110:2–12. https://doi.org/10.1016/j.ces.2013.08.014.

[191] Debiagi PEA, Trinchera M, Frassoldati A, Faravelli T, Vinu R, Ranzi E. Algae characterization and multistep pyrolysis mechanism. J Anal Appl Pyrolysis 2017;128:423–36. https://doi.org/10.1016/j.jaap.2017.08.007.

[192] Yin C, Kær SK, Rosendahl L, Hvid SL. Co-firing straw with coal in a swirl-stabilized dual-feed burner: Modelling and experimental validation. Bioresour Technol 2010;101:4169–78. https://doi.org/10.1016/j.biortech.2010.01.018.

[193] Backreedy RI, Fletcher LM, Jones JM, Ma L, Pourkashanian M, Williams A. Co-firing pulverised coal and biomass: A modeling approach. Proc Combust Inst 2005;30 II:2955–64. https://doi.org/10.1016/j.proci.2004.08.085.

[194] Bhuiyan AA, Naser J. CFD modelling of co-firing of biomass with coal under oxy-fuel combustion in a large scale power plant. Fuel 2015;159:150–68. https://doi.org/10.1016/j.fuel.2015.06.058.

[195] Black S, Szuhánszki J, Pranzitelli A, Ma L, Stanger PJ, Ingham DB, et al. Effects of firing coal and biomass under oxy-fuel conditions in a power plant boiler using CFD modelling. Fuel 2013;113:780–6. https://doi.org/10.1016/j.fuel.2013.03.075.

[196] Fang Q, Musa AAB, Wei Y, Luo Z, Zhou H. Numerical simulation of multifuel combustion in a 200 MW tangentially fired utility boiler. Energy and Fuels

2012;26:313–23. https://doi.org/10.1021/ef201149p.

[197] Ghenai C, Janajreh I. CFD analysis of the effects of co-firing biomass with coal. Energy Convers Manag 2010;51:1694–701. https://doi.org/10.1016/j.enconman.2009.11.045.

[198] Ma L, Jones JM, Pourkashanian M, Williams A. Modelling the combustion of pulverized biomass in an industrial combustion test furnace. Fuel 2007;86:1959–65. https://doi.org/10.1016/j.fuel.2006.12.019.

[199] Mandø M, Rosendahl L, Yin C, Sørensen H. Pulverized straw combustion in a low-NOx multifuel burner: Modeling the transition from coal to straw. Fuel 2010;89:3051–62. https://doi.org/10.1016/j.fuel.2010.05.016.

[200] Pallarés J, Gil A, Cortés C, Herce C. Numerical study of co-firing coal and Cynara cardunculus in a 350 MWe utility boiler. Fuel Process Technol 2009;90:1207–13. https://doi.org/10.1016/j.fuproc.2009.05.025.

[201] Li J, Paul MC, Younger PL, Watson I, Hossain M, Welch S. Prediction of high-temperature rapid combustion behaviour of woody biomass particles. Fuel 2016;165:205–14. https://doi.org/10.1016/j.fuel.2015.10.061.

[202] Li J, Paul MC, Younger PL, Watson I, Hossain M, Welch S. Characterization of biomass combustion at high temperatures based on an upgraded single particle model. Appl Energy 2015;156:749–55. https://doi.org/10.1016/j.apenergy.2015.04.027.

[203] Martí-Rosselló T, Li J, Lue L, Karlström O, Brink A. Comprehensive Assessment of Particle-Scale Modeling for Biomass Pyrolysis: One-Dimensional versus Three-Dimensional Models. Energy and Fuels

2021;35:9937–49. https://doi.org/10.1021/acs.energyfuels.1c00283.

[204] Saastamoinen J, Aho M, Moilanen A, Sørensen LH, Clausen S, Berg M. Burnout of pulverized biomass particles in large scale boiler - Single particle model approach. Biomass and Bioenergy 2010;34:728–36. https://doi.org/10.1016/j.biombioe.2010.01.015.

[205] Haseli Y, van Oijen JA, de Goey LPH. A detailed one-dimensional model of combustion of a woody biomass particle. Bioresour Technol 2011;102:9772–82. https://doi.org/10.1016/j.biortech.2011.07.075.

[206] Porteiro J, Míguez JL, Granada E, Moran JC. Mathematical modelling of the combustion of a single wood particle. Fuel Process Technol 2006;87:169–75. https://doi.org/10.1016/j.fuproc.2005.08.012.

[207] Porteiro J, Granada E, Collazo J, Patiño D, Morán JC. A model for the combustion of large particles of densified wood. Energy and Fuels 2007;21:3151–9. https://doi.org/10.1021/ef0701891.

[208] Wurzenberger JC, Wallner S, Raupenstrauch H, Khinast JG. Thermal conversion of biomass: Comprehensive reactor and particle modeling. AIChE J 2002;48:2398–411. https://doi.org/10.1002/aic.690481029.

[209] Cao W, Li J, Lue L. Study on the ignition behavior and kinetics of combustion of biomass. Energy Procedia 2017;142:136–41. https://doi.org/10.1016/j.egypro.2017.12.022.

[210] Cao W, Li J, Martí-Rosselló T, Zhang X. Experimental study on the ignition characteristics of cellulose, hemicellulose, lignin and their mixtures. J Energy Inst 2019;92:1303–12. https://doi.org/https://doi.org/10.1016/j.joei.2018.10.004.

[211] Vascellari M, Xu H, Hasse C. Flamelet modeling of coal particle ignition. Proc Combust Inst 2013;34:2445–52. https://doi.org/10.1016/j.proci.2012.06.152.

[212] Grant DM, Pugmire RJ, Fletcher TH, Kerstein AR. Chemical Model of Coal Devolatilization Using Percolation Lattice Statistics. Energy and Fuels 1989;3:175–86. https://doi.org/10.1021/ef00014a011.

[213] Fletcher TH, Kerstein AR, Pugmire RJ, Grant DM. Chemical percolation model for devolatilization. 2. Temperature and heating rate effects on product yields. Energy & Fuels 1990;4:54–60. https://doi.org/10.1021/ef00019a010.

[214] Scott SA, Dennis JS, Davidson JF, Hayhurst AN. An algorithm for determining the kinetics of devolatilisation of complex solid fuels from thermogravimetric experiments. Chem Eng Sci 2006;61:2339–48. https://doi.org/10.1016/j.ces.2005.11.002.

[215] Ubhayakar SK, Stickler DB, Von Rosenberg CW, Gannon RE. Rapid devolatilization of pulverized coal in hot combustion gases. Symp Combust 1977;16:427–36. https://doi.org/10.1016/S0082-0784(77)80342-1.

[216] Yuan Y, Li S, Li G, Wu N, Yao Q. The transition of heterogeneous-homogeneous ignitions of dispersed coal particle streams. Combust Flame 2014;161:2458–68. https://doi.org/10.1016/j.combustflame.2014.03.008.

[217] Jovanovic R, Milewska A, Swiatkowski B, Goanta A, Spliethoff H. Numerical investigation of influence of homogeneous/heterogeneous ignition/combustion mechanisms on ignition point position during pulverized coal combustion in oxygen enriched and recycled flue gases atmosphere. Int J Heat Mass Transf 2011;54:921–31. https://doi.org/10.1016/j.ijheatmasstransfer.2010.10.011.

[218] ANSYS FLUENT 12.0 Theory Guide - Contents n.d. http://www.afs.enea.it/project/neptunius/docs/fluent/html/th/node1.htm (accessed May 12, 2018).

[219] Xu Y, Li S, Gao Q, Yao Q, Liu J. Characterization on Ignition and Volatile Combustion of Dispersed Coal Particle Streams: In Situ Diagnostics and Transient Modeling. Energy & Fuels 2018;32:9850–8. https://doi.org/10.1021/acs.energyfuels.8b01322.

[220] Zhang T, Hu Z, Zhou Y. The determination method of the ignition modes of single coal particle with a transient coal ignition and combustion model. Combust Flame 2022;241. https://doi.org/10.1016/j.combustflame.2022.112092.

[221] Farmand P, Nicolai H, Schumann C, Attili A, Berger L, Li T, et al. Numerical investigation and assessment of flamelet-based models for the prediction of pulverized solid fuel homogeneous ignition and combustion. Combust Flame 2022;235. https://doi.org/10.1016/j.combustflame.2021.111693.

[222] Abbas T, Costen P, Kandamby NH, Lockwood FC, Ou JJ. The influence of burner injection mode on pulverized coal and biomass co-fired flames. Combust Flame 1994;99:617–25. https://doi.org/10.1016/0010-2180(94)90055-8.

[223] Faúndez J, Arias B, Rubiera F, Arenillas A, García X, Gordon AL, et al. Ignition characteristics of coal blends in an entrained flow furnace. Fuel 2007;86:2076–80. https://doi.org/10.1016/j.fuel.2007.03.024.

[224] Gil M V., Riaza J, Álvarez L, Pevida C, Pis JJ, Rubiera F. Kinetic models for the oxy-fuel combustion of coal and coal/biomass blend chars obtained in N2 and

CO2 atmospheres. Energy 2012;48:510–8. https://doi.org/10.1016/j.energy.2012.10.033.

[225] Annamalai K, Ryan W. Interactive processes in gasification and combustion. Part I: Liquid drop arrays and clouds. Prog Energy Combust Sci 1992;18:221–95. https://doi.org/10.1016/0360-1285(92)90012-P.

[226] Annamalai K, Ryan W. Interactive processes in gasification and combustion-II. Isolated carbon, coal and porous char particles. Prog Energy Combust Sci 1993;19:383–446. https://doi.org/10.1016/0360-1285(93)90010-C.

[227] Annamalai K, Ryan W. Interactive processes in gasification and combustion - Part III : Coal/char particle arrays, streams and clouds. Prog Energy Combust Sci 1994;20:487–618. https://doi.org/10.1016/0360-1285(94)90002-7.

[228] Cassel HM, Liebman I. The cooperative mechanism in the ignition of dust dispersions. Combust Flame 1959;3:467–75. https://doi.org/10.1016/0010-2180(59)90052-5.

[229] Essenhigh RH, Misra MK, Shaw DW. Ignition of Coal Particles: A Review. Combust Flame 1989;77:3–30. https://doi.org/10.1016/0010-2180(89)90101-6.

[230] Hertzberg M. Autoignition temperatures for coal particles dispersed in air. Fuel 1991;70:1115–23. https://doi.org/10.1016/0016-2361(91)90231-X.

[231] Wall TF, Gururajan VS, Lucas J, Gupta RP, Dong-ke Z, Ryde N. THE IGNITION, BURNING RATE AND REACTIVITY OF PETROLEUM COKE. Symp Combust 1991:1177–84. https://doi.org/10.1016/S0082-0784(06)80378-4.

[232] Zhu W, Li X, Peng J, Wang Z, Sun R, Zhang L, et al. Study on the combustion

behaviours of two high-volatile coal particle streams with high-speed OH-PLIF. Fuel 2020;265:116956. https://doi.org/10.1016/j.fuel.2019.116956.

[233] Farazi S, Attili A, Kang S, Pitsch H. Numerical study of coal particle ignition in air and oxy-atmosphere. Proc Combust Inst 2019;37:2867–74. https://doi.org/10.1016/j.proci.2018.07.002.

[234] Muto M, Yuasa K, Kurose R. Numerical simulation of ignition in pulverized coal combustion with detailed chemical reaction mechanism. Fuel 2017;190:136–44. https://doi.org/10.1016/j.fuel.2016.11.029.

[235] Li T, Schiemann M, Köser J, Dreizler A, Böhm B. Experimental investigations of single particle and particle group combustion in a laminar flow reactor using simultaneous volumetric OH-LIF imaging and diffuse backlight-illumination. Renew Sustain Energy Rev 2021;136. https://doi.org/10.1016/j.rser.2020.110377.

[236] Awasthi A, Kuerten JGM, Geurts BJ. Direct Numerical Simulation of biomass pyrolysis and combustion with gas phase reactions. J Phys Conf Ser 2016;745:1–8. https://doi.org/10.1088/1742-6596/745/3/032119.